Dynamic Polymer Hydrogels through Reversible Thiol Conjugate Addition Crosslinks

Fan, B.

DOI
10.4233/uuid:f4dac086-ca05-4c49-acc2-748dcc4fcd42

Publication date
2021

Document Version
Final published version

Citation (APA)
Fan, B. (2021). *Dynamic Polymer Hydrogels through Reversible Thiol Conjugate Addition Crosslinks*. [Dissertation (TU Delft), Delft University of Technology]. https://doi.org/10.4233/uuid:f4dac086-ca05-4c49-acc2-748dcc4fcd42

Dynamic Polymer Hydrogels through Reversible Thiol Conjugate Addition Crosslinks

Dissertation

for the purpose of obtaining the degree of doctor

at Delft University of Technology

by the authority of the Rector Magnificus, Prof.dr.ir. T.H.J.J. van der Hagen

Chair of the Board for Doctorates

to be defended publicly on

Tuesday 6 July 2021 at 17:30 o'clock

by

Bowen FAN

Master of Engineering in Chemical Engineering and Technology,

China University of Mining and Technology, China

born in Jining, China

This dissertation has been approved by the promotors.

Composition of the doctoral committee:

Rector Magnificus,	chairperson
Dr. R. Eelkema	Delft University of Technology, promotor
Prof. dr. J.H. van Esch	Delft University of Technology, promotor

Independent members:

Prof. dr. J. Chalker	Flinders University, Australia
Dr. S.I. van Kasteren	Leiden University
Dr. J.P.A. Heuts	Eindhoven University of Technology
Prof. dr. S. Otto	University of Groningen
Prof. dr. E.A. Pidko	Delft University of Technology
Prof. dr. A. Urakawa	Delft University of Technology, reserve member

The work described in this thesis was carried out in the Advanced Soft Matter (ASM) group at Delft University of Technology, Faculty of Applied Science. This research was funded by China Scholarship Council (CSC) and a consolidator grant from the European Research Council (ERC).

Cover design: Bowen Fan and Bohang Wu

Printed by Ipskmp Printing, Enschede

Table of Content

Chapter 1

Introduction

1.1 Hydrogel: from permanent to transient

Hydrogels are water-rich three-dimensional networks formed by crosslinked hydrophilic polymers, or fibers self-assembled from small molecules. Due to the similarity to living tissues, hydrogels have drawn great attention in many applications, especially in biomedical settings. The soft, flexible and mechanically tunable nature of hydrogels gives them the ability to mimic the biological extracellular matrix (ECM) environment to regulate cell behavior in tissue engineering, or act as drug vehicles in controlled drug delivery.[1–6]

Conventional synthetic hydrogels formed by permanent crosslinks between polymer chains can have a large stability and durability, but also show static behavior as, once synthesized, these hydrogels are permanently stable, can't be remolded or broken down, and lack in responsive properties like self-healing or structural adaptation to changes in their environment. However, dynamic or interactive hydrogels may play an important role in many advanced applications. For instance, the ECM shows spatiotemporal dynamic interaction with cells to regulate cell fate and behavior, which cannot be achieved using traditional static hydrogels.[7–9] Controlled drug release, biosensors and soft robotics also require temporal responsive behavior of hydrogels, such as temporal change in crosslink density and gel-sol transitions.[10,11]

Stimuli-responsive hydrogels are a type of smart materials that can change their properties in reaction to external stimuli (e.g. pH, light, temperature and chemical signals).[12–14] Dynamic covalent hydrogels are a classical example of a hydrogel that can respond to stimuli with a change in their crosslink density or topology, leading to many fascinating dynamic behaviors, such as network remolding and gel-sol transitions. However, such hydrogels are formed at or near thermodynamic equilibrium, resulting in the fact that these materials are highly stable once the stimulus is removed, making it generally not possible to revert back to their initial state in an autonomous fashion.[15–17] Figure 1.1a shows an general example of a hydrogel that can respond to external stimuli with formation and removal of crosslinks. Stimulus 1 drives the conversion of precursors to crosslinkers that in turn crosslink polymer chains to form a hydrogel. However, these crosslinks are only stable until stimulus 2 is added to the system to trigger crosslink breaking, followed by the collapse of hydrogel. The formation and breaking of crosslinks require the sequential application of two external stimuli, which means that such hydrogels do not show autonomous transient formation behavior.

Some network materials in living organisms (e.g. microtubules and actin filaments) are formed away from thermodynamic equilibrium, and need an influx of chemical energy (fuel) to be maintained.[18,19] Such materials show transient stability and properties which can be controlled by fuel gradients, catalysis and feedback loops, leading to complex dynamics, such as self-healing, autonomous adaptive response and collective behavior. It would be interesting and useful to use synthetic methods to develop fuel-driven transiently formed hydrogels, endowing such materials with autonomous dynamic and temporal programmable life-like properties. An example of out-of-equilibrium fuel-driven transient formation of hydrogels is shown in Figure 1.1b. Stimulus 2 is a species which is already present in the operating environment, and no crosslinking will take place at thermodynamic equilibrium. Addition of fuel (stimulus 1) drives the production of unstable out of equilibrium crosslinks, leading to the formation of a hydrogel. In the meantime, the crosslinks of the hydrogel will be broken by stimulus 2, present in the environment. Once the fuel concentration is too low, the

hydrogel will start to collapse. Such novel hydrogels are in high demand in many biomedical applications, like mimicking the spatiotemporal dynamic ECM environment to regulate cell behavior, controlled release of pharmaceuticals, temporal wound healing dressings and to temporally block channels such as arteries.

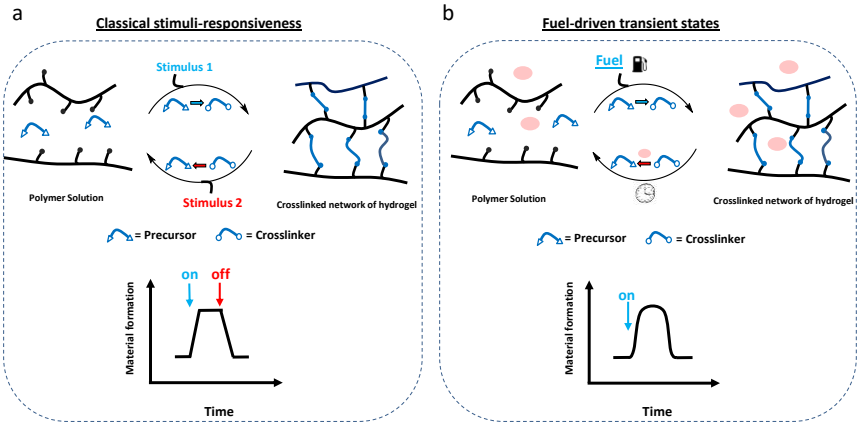

Figure 1.1 Comparison of stimuli-responsive formation of crosslinked hydrogel and fuel-driven transient formation of crosslinked hydrogel. (a) The original system contains polymer chains and precursors. External stimulus 1 is able to promote the conversion of precursors in polymer solution to crosslinkers. The crosslinkers connect the polymer chains to a crosslinked network of hydrogel. External stimulus 2 is able to drive the crosslinkers back to the initial precursors, followed by the breaking of the crosslinks of hydrogel. This system requires two signals, “on” by stimulus 1 to trigger the formation of material, and “off” by stimulus 2 to trigger the deformation of material. (b) The original system contains polymer chains, precursors and prestored stimulus 2. Addition of fuel drives the conversion of precursors to the crosslinkers, followed by a formation of hydrogel. The prestored stimulus 2 will induce the crosslinker back to precursor and the collapse of hydrogel over time. The transient formation of material in this system can be driven by addition of fuel (“on”).

1.2 Fuel-driven transient formation of hydrogels

In the past decade, an increasing number of fuel-driven transient systems has been reported including molecular motors[20,21], self-replicating systems[22,23], supramolecular polymerization[24–26], polymer aggregation[27], and fuel-controlled chemical reactivity and assembly of macrocycles.[28,29] Besides the examples above, different types of fuel-driven transient hydrogels have also been successfully developed in many research groups.

The pioneering example reported by van Esch, Eelkema and coworkers shows the fuel-driven transient formation of supramolecular hydrogels by self-assembly of small synthetic molecules (dibenzoyl-L-cystine, DBC) (Figure 1.2a).[33,34] DBC is a water-soluble precursor and cannot assemble to fibers due to its two anionic carboxylate groups. A carboxylate alkylation between DBC and a methylating agent (dimethyl sulfate, DMS, as a fuel) generates the uncharged methyl ester product, inducing the assembly of the ester products into fibers that subsequently form a supramolecular gel. Since such methyl esters are thermodynamically unstable in aqueous conditions, a spontaneous hydrolysis of the methyl ester product to the initial precursor will drive the disassembly of the fibers. Once the fuel

was fully consumed, the hydrolysis reaction will be dominant in the system, resulting in the collapse of the hydrogel. The lifetime, self-recovery behavior and mechanic properties of these hydrogels can be regulated through the kinetics of the reactions involved. For instance, changing the concentration of fuel or the pH of the system is able to alter the rate of activation and deactivation reactions, thereby modifying the lifetime of these hydrogels.

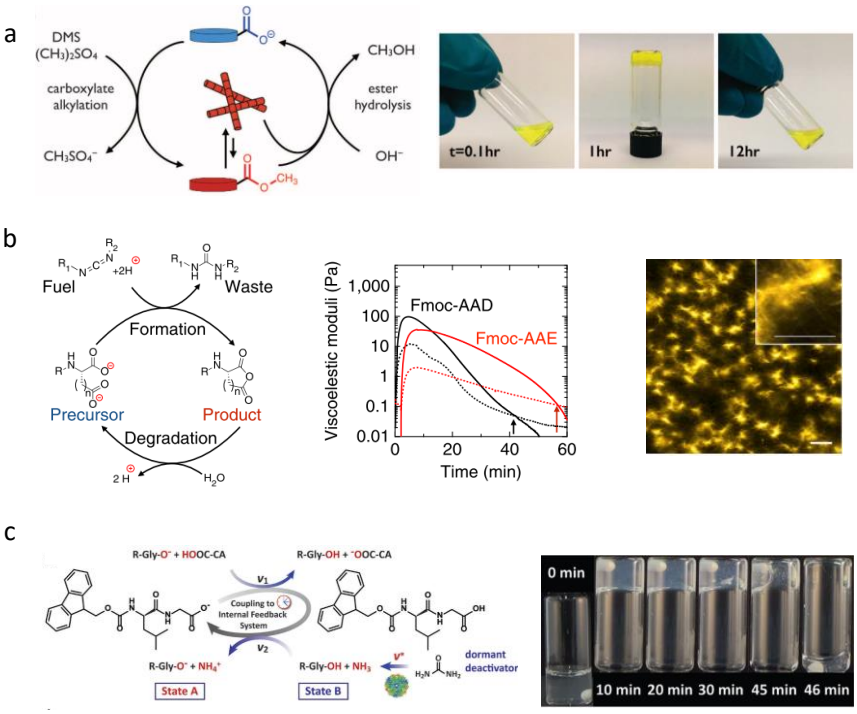

Figure 1.2 Fuel-driven transient formation of hydrogels (a) Schematic of dimethyl sulfate driven self-assembly of dibenzoyl-L-cystine into fibers (left) and photographs of transient hydrogel formation (right). (b) Schematic of a chemical reaction network, showing the EDC-driven transient formation of uncharged anhydride (left), rheological time sweeps of gels formed by Fmoc-AAD and Fmoc-AAE (middle) and confocal microscopy of fiber formation from Fmoc-AAD driven by EDC (right). (c) Schematic of transient formation of building blocks, Fmoc-Leu-Gly-OH, driven by a fuel combining an acidic buffer and urea (left) and photographs of temporal controlled formation of hydrogel (right). Reproduced from reference. [30–32]

Another example of transient hydrogel formation was reported by Boekhoven and coworkers (Figure 1.2b).[31] An initially water-soluble fluorenylmethyloxycarbonyl (Fmoc) protected amino acid can be converted to an uncharged anhydride product by using the common coupling agent 1-ethyl-3-(3-dimethylaminopropyl) carbodiimide (EDC). The loss of two anionic charges upon the activation reaction drives assembly into fibers, that in turn formed a supramolecular hydrogel. Similar to the previous system, spontaneous hydrolysis of the unstable anhydride product took place in aqueous buffer. The lifetime of gels could be tuned by the nature of precursors (Fmoc-AAD or Fmoc-AAE) and the concentration of fuel added.

Walther and coworkers developed a lifetime-defined hydrogel by coupling a fuel-driven transient jump of pH to self-assembly of building blocks (Figure 1.2c).[32,35] The fuel is composed of urea as a dormant deactivator and acidic buffer as promotor. A quick drop of pH by addition of acidic buffer as fuel induced the self-assembly of the precursors (Fmoc-Leu-Gly-OH) to a hydrogel. While slow conversion of urea to NH_3 by catalysis of prestored urease increased the pH of system back to the initial value, thereby leading the disassembly of hydrogel. The lifetime of such transient hydrogels can be tuned from minutes to days by changing the ratio of fuel components. This fuel-driven transient hydrogel has been used for fluidic guidance, burst release and self-erasing.

Ulijn and coworkers reported the transient formation of hydrogels driven by a peptide coupling between a dipeptide fuel (aspartame) and different amino acid amides as precursors.[36] The hydrolysis of aspartame by α-chymotrypsin promotes the generation of the tripeptide hydrogelator, followed by forming a hydrogel. In the meantime, hydrolysis of gelator is taking place with a lower rate. Over time the fuel is consumed, hydrolysis of tripeptide to precursor results in the collapse of hydrogels.

As is clear from examples above, the fuel-driven activation and the spontaneous deactivation are two essential factors to construct a fuel-driven transient system. The activation and deactivation can be achieved by fuel-driven chemical reaction networks (CRNs).[37–40] Such networks consist of at least two chemical reactions, capable of the formation and deconstruction of the activated building blocks (e.g. methyl ester in Figure 1.2a, cyclic anhydride in Figure 1.2b and protonated dipeptide in Figure 1.2c). The formation of the activated products is driven by the irreversible consumption of fuels. The activated product is unstable under the operating reaction conditions, and spontaneously reacts with some species that are already present in environment (e.g. H_2O, O_2 or H^+) to the initial precursors. The concentration of the activated product is dependent on the rate of activation and deactivation reactions. Therefore, the continuous influx of fuel is required to maintain a certain concentration of product.

Besides CRNs above using in fuel-driven formation of hydrogels, another two redox-mediated CRNs have been applied in transient self-assembly of building blocks to supramolecular hydrogels. However, most previous fuel-driven transient formation of hydrogels is based on supramolecular interactions. It is difficult to predict control over crosslink density in supramolecular hydrogels, hindering their further application. So far only few fuel-driven transient covalently crosslinked hydrogels have been reported, all of them using a previously developed CRN (EDC driven transient ester formation). It would be of great interest if we can design a novel fuel driven CRN which is able to be coupled to the formation of covalently crosslinked hydrogels.

1.3 Self-healing hydrogels

Self-healing hydrogels are a type of dynamic material with the inherent ability to automatically repair when damaged. Compared to conventional static hydrogels, self-healing hydrogels are capable of maintaining their structural integrity after injection, which endow such materials with some potential in biomedical applications, such as in wound healing dressings, tissue engineering and drug delivery.[41–43] In addition, self-healing hydrogels are able to prolong their lifetimes and retain long term reliability and durability for some implant applications due to their quick recovery upon the inevitable defects that arise during

operations.[44–46] Figure 1.3a shows applications of self-healing hydrogels in stem cell based therapy.[46–48] Traditional delivery of stem cells to the disease areas shows poor treatment efficiency. Such problems can be solved by the incorporation of stem cells into self-healing hydrogels, which are carriers to deliver stem cells to the target tissue. The reconnecting of broken hydrogels after injection avoids abrupt release of cells. Besides the delivery of stem cells, self-healing hydrogels have been used successfully as drug and vaccine carriers.[49,50] In addition, due to the conductive nature of hydrogels, self-healing hydrogels are good candidates for the emerging field of cyborganics, bioacutators and injectable bioelectronics (Figure 1.3b).[46,51]

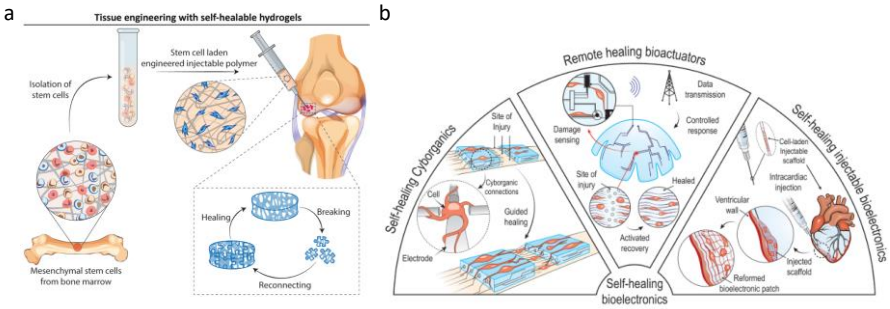

Figure 1.3 Examples of applications of self-healing hydrogels in tissue engineering and bioelectronics. (a) Schematic of delivery of stem cell to target tissue by self-healing hydrogels. (b) The potential applications of self-healing hydrogels in bioelectronics field. Reproduced from reference.[46]

Typically, the self-healing properties of hydrogels stem from noncovalent interactions[52,53] and dynamic covalent bonds (DCBs).[54,55] Still, the weak mechanical properties of physical hydrogels and often harsh condition for the operating process of DCBs hinders the application of many self-healing hydrogels. It is therefore useful to investigate new DCBs to use in the construction of self-healing hydrogels.

1.4 Reversible thiol Michael addition

The thiol Michael addition is a reaction between a thiol and an electron deficient olefin. Since such reaction is able to proceed efficiently under mild physiological aqueous conditions, it has been widely used in biology and polymer science, such as protein modification, the formation of antibody-drug conjugates and the synthesis of sequence-defined oligomers.[56–59] Typically, thiol Michael addition is considered as an irreversible click reaction under ambient conditions. However, in the past decade, some reversible thiol conjugate additions have been explored, showing their potential for application in materials science.

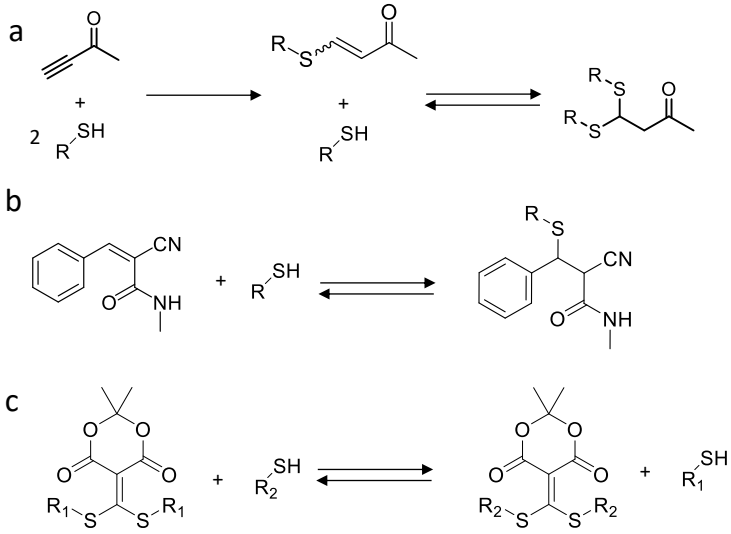

Figure 1.4 Examples of reversible thiol Michael additions. (a) The thiol double conjugate addition to alkynones: the first thiol addition is irreversible, generating a β-sulfido enone. The second thiol addition to the formed enone is reversible, generating a dynamic bond. (b) Reversible thiol Michael addition to benzalcyanoacetamides. (c) Thiol-exchange through reversible thiol Michael addition to a Meldrum's acid derivative.

The thiol-alkyne Michael addition is a conjugate addition of a thiol to an electron deficient alkyne. This reaction can typically take place in an efficient, rapid fashion under mild aqueous or organic conditions. Although it has been reported for many applications, such as polymerization, the formation of hydrogels for cell encapsulation and degradable elastomer-like polymers,[60–62] the addition of a thiol to an alkynoic ester is an irreversible process, lacking the dynamic nature needed for the development of some smart materials. Anslyn and coworkers reported a reversible thiol-alkynone Michael addition between a thiol and a β-sulfido-α,β-unsaturated carbonyl (the thiol-alkynone single adduct) (Figure 1.4a).[63] They found that a reversible, rapid exchange of thiols took place in a mixture of thiols, thiol-alkynone single adduct and thiol-alkynone double adduct in organic and aqueous media. This dynamic thiol-alkynone double addition has also been used in many applications, such as dynamic combinational libraries, cleavage methods in peptide modification and adaptable dynamic covalent polymer networks.[64–66] Besides alkynones, benzalcyanoacetamides are another class of Michael acceptors that show dynamic exchange of thiols in a reversible Michael addition (Figure 1.4b).[67–69] This reversible thiol addition has found some application like self-healing hydrogels, healable polymer networks and dynamic reaction-induced phase separation. More recently, another example of reversible thiol addition was reported in the preparation of a hyperbranched polythioether.[70,71] This study found that the addition between two thiols and dimethyl acetylenedicarboxylate is also a reversible reaction.

In 2016, Anslyn and coworkers reported a new reversible thiol conjugated addition by coupling and decoupling thiols via a Meldrum's acid derivative as the Michael acceptor (Figure 1.4c).[72] In this dynamic system, the thiol-conjugated product can not only exchange

thiols but also release the original thiol upon the addition of dithiothreitol (DTT) in aqueous and organic conditions. These dynamic coupling and decoupling reactions have found some application, for instance, optical sensing, vitrimers and degradable hydrogels.[73–76]

1.5 Outline of the thesis

This thesis describes the experimental development of new dynamic hydrogels based on reversible thiol conjugate additions. Redox-controlled hydrogels and self-healing injectable hydrogels have been achieved by introducing reversible thiol conjugate additions to crosslink polymers, leading to hydrogel formation. The overall objective in this thesis was to develop a new fuel-driven transient polymeric hydrogel formation system. Although this final aim was not entirely met, we developed several important concepts along the way, which are described in Chapters 2-5.

Chapter 2 describes a new chemical reaction network for fuel-driven transient formation of covalent S-C bonds, based on redox-controlled conjugate addition and elimination. We found that the formation and breaking of covalent bonds in the reaction cycle can be realized in separate reactions, but side reactions hindered the operation in full cycle. If such problems would be solved, this CRN could have potential to be used to form fuel-driven polymer materials.

Chapter 3 investigates the formation of a self-healing injectable hydrogel by introducing dynamic thiol-alkynone double addition crosslinks in a polymer network. Such dynamic hydrogels show self-healing and shear thinning properties, confirmed by rheological measurements, macroscopic self-healing, and injection tests. Good cytocompatibility of these hydrogels opens an opportunity for future biomedical applications such as tissue engineering and drug delivery.

Chapter 4 describes a redox-controlled reversible thiol-alkynone double addition. First, we created a redox-responsive hydrogel by using such reversible addition for the formation of crosslinks in hydrogels. Second, based on this thiol-alkynone double addition, we developed a fuel-driven transient formation of thiol-alkynone double adduct on small molecules.

Chapter 5 explores coupling and decoupling reactions of thiols to an azanorbornadiene bromo sulfone. A self-healing hydrogel can be formed by using azanorbornadiene bromo sulfone to couple two thiol groups together. Such hydrogels are also degradable, trigged by glutathione. Glutathione-triggered dye release experiments suggest this self-healing hydrogel is a potential carrier of drugs, cells or vaccines for biomedical applications.

1.6 Reference

(1) Tong, Z.; Jin, L.; Oliveira, J. M.; Reis, R. L.; Zhong, Q.; Mao, Z.; Gao, C. Adaptable Hydrogel with Reversible Linkages for Regenerative Medicine: Dynamic Mechanical Microenvironment for Cells. *Bioact. Mater.* **2021**, *6*, 1375–1387.

(2) Seliktar, D. Designing Cell-Compatible Hydrogels for Biomedical Applications. *Science* **2012**, *336*, 1124–1128.

(3) Caliari, S. R.; Burdick, J. A. A Practical Guide to Hydrogels for Cell Culture. *Nat. Methods* **2016**, *13*, 405–414.

(4) Discher, D. E.; Mooney, D. J.; Zandstra, P. W. Growth Factors, Matrices, and Forces Combine and Control Stem Cells. *Science* **2009**, *324*, 1673–1677.

(5) Khademhosseini, A.; Langer, R. Microengineered Hydrogels for Tissue Engineering. *Biomaterials* **2007**, *28*, 5087–5092.

(6) Slaughter, B. V.; Khurshid, S. S.; Fisher, O. Z.; Khademhosseini, A.; Peppas, N. A. Hydrogels in Regenerative Medicine. *Adv. Mater.* **2009**, *21*, 3307–3329.

(7) Ooi, H. W.; Hafeez, S.; Van Blitterswijk, C. A.; Moroni, L.; Baker, M. B. Hydrogels That Listen to Cells: A Review of Cell-Responsive Strategies in Biomaterial Design for Tissue Regeneration. *Mater. Horizons* **2017**, *4*, 1020–1040.

(8) Rosales, A. M.; Anseth, K. S. The Design of Reversible Hydrogels to Capture Extracellular Matrix Dynamics. *Nat. Rev. Mater.* **2016**, *1*, 1–15.

(9) Tang, S.; Richardson, B. M.; Anseth, K. S. Dynamic Covalent Hydrogels as Biomaterials to Mimic the Viscoelasticity of Soft Tissues. *Prog. Mater. Sci.* **2020**, No.100738.

(10) Zhang, Y. S.; Khademhosseini, A. Advances in Engineering Hydrogels. *Science* **2017**, *356*, eaaf3627.

(11) Brown, T. E.; Anseth, K. S. Spatiotemporal Hydrogel Biomaterials for Regenerative Medicine. *Chem. Soc. Rev.* **2017**, *46*, 6532–6552.

(12) Stuart, M. A. C.; Huck, W. T. S.; Genzer, J.; Müller, M.; Ober, C.; Stamm, M.; Sukhorukov, G. B.; Szleifer, I.; Tsukruk, V. V.; Urban, M.; Winnik, F.; Zauscher, S.; Luzinov, I.; Minko, S. Emerging Applications of Stimuli-Responsive Polymer Materials. *Nat. Mater.* **2010**, *9*, 101–113.

(13) Shi, Q.; Liu, H.; Tang, D.; Li, Y.; Li, X. J.; Xu, F. Bioactuators Based on Stimulus-Responsive Hydrogels and Their Emerging Biomedical Applications. *NPG Asia Mater.* **2019**, *11*, 64.

(14) Ulijn, R. V.; Bibi, N.; Jayawarna, V.; Thornton, P. D.; Todd, S. J.; Mart, R. J.; Smith, A. M.; Gough, J. E. Bioresponsive Hydrogels. *Mater. Today* **2007**, *10*, 40–48.

(15) Fischer, P. Vision Statement: Interactive Materials—Drivers of Future Robotic Systems. *Adv. Mater.* **2020**, *32*, 1–4.

(16) Walther, A. Viewpoint: From Responsive to Adaptive and Interactive Materials and Materials Systems: A Roadmap. *Adv. Mater.* **2020**, *32*, 1–10.

(17) Burdick, J. A.; Murphy, W. L. Moving from Static to Dynamic Complexity in Hydrogel Design. *Nat. Commun.* **2012**, *3*, 1–8.

(18) Needleman, D.; Dogic, Z. Active Matter at the Interface between Materials Science and Cell Biology. *Nat. Rev. Mater.* **2017**, *2,* 17048.

(19) Kurchan, J. In and out of Equilibrium. *Nature* **2005**, *433*, 222–225.

(20) Eelkema, R.; Pollard, M. M.; Vicario, J.; Katsonis, N.; Ramon, B. S.; Bastiaansen, C. W. M.; Broer, D. J.; Feringa, B. L. Nanomotor Rotates Microscale Objects. *Nature* **2006**, *440*, 163.

(21) Wilson, M. R.; Solà, J.; Carlone, A.; Goldup, S. M.; Lebrasseur, N.; Leigh, D. A. An Autonomous Chemically Fuelled Small-Molecule Motor. *Nature* **2016**, *534*, 235–240.

(22) Colomer, I.; Morrow, S. M.; Fletcher, S. P. A Transient Self-Assembling Self-Replicator. *Nat. Commun.* **2018**, *9*, 2239.

(23) Morrow, S. M.; Colomer, I.; Fletcher, S. P. A Chemically Fuelled Self-Replicator. *Nat. Commun.* **2019**, *10*, 1011.

(24) Sorrenti, A.; Leira-Iglesias, J.; Sato, A.; Hermans, T. M. Non-Equilibrium Steady States in Supramolecular Polymerization. *Nat. Commun.* **2017**, *8*, 1–8.

(25) Leira-Iglesias, J.; Sorrenti, A.; Sato, A.; Dunne, P. A.; Hermans, T. M. Supramolecular Pathway Selection of Perylenediimides Mediated by Chemical Fuels. *Chem. Commun.* **2016**, *52*, 9009–9012.

(26) Heinen, L.; Walther, A. Programmable Dynamic Steady States in ATP-Driven Nonequilibrium DNA Systems. *Sci. Adv.* **2019**, *5*, eaaw0590.

(27) Helm, M. P.; Wang, C.; Fan, B.; Macchione, M.; Mendes, E.; Eelkema, R. Organocatalytic Control over a Fuel-Driven Transient-Esterification Network. *Angew. Chem. Int. Ed* **2020**, *132*, 20785–20792.

(28) Maiti, S.; Fortunati, I.; Ferrante, C.; Scrimin, P.; Prins, L. J. Dissipative Self-Assembly of Vesicular Nanoreactors. *Nat. Chem.* **2016**, *8*, 725–731.

(29) Hossain, M. M.; Atkinson, J. L.; Hartley, C. S. Dissipative Assembly of Macrocycles Comprising Multiple Transient Bonds. *Angew. Chem. Int. Ed.* **2020**, *59*, 13807–13813.

(30) Boekhoven, J.; Hendriksen, W. E.; Koper, G. J.; Eelkema, R.; van Esch, J. H. Transient Assembly of Active Materials Fueled by a Chemical Reaction. *Science* **2015**, *349*, 1075–1079.

(31) Tena-Solsona, M.; Rieß, B.; Grötsch, R. K.; Löhrer, F. C.; Wanzke, C.; Käsdorf, B.; Bausch, A. R.; Müller-Buschbaum, P.; Lieleg, O.; Boekhoven, J. Non-Equilibrium Dissipative Supramolecular Materials with a Tunable Lifetime. *Nat. Commun.* **2017**, *8*, 1–8.

(32) Heuser, T.; Weyandt, E.; Walther, A. Biocatalytic Feedback-Driven Temporal Programming of Self-Regulating Peptide Hydrogels. *Angew. Chem. Int. Ed.* **2015**, *54*, 13258–13262.

(33) Boekhoven, J.; Brizard, A. M.; Kowlgi, K. N.; Koper, G. J. M.; Eelkema, R.; van Esch, J. H. Dissipative Self-Assembly of a Molecular Gelator by Using a Chemical Fuel. *Angew. Chem. Int. Ed.* **2010**, *49*, 4825–4828.

(34) Boekhoven, J.; Hendriksen, W. E.; Koper, G. J. M.; Eelkema, R.; Esch, J. H. Van. Transient Self-Assembly of Active Materials Fueled by a Chemical Reaction. *Science* **2015**, *349*, 1075.

(35) Heuser, T.; Steppert, A.-K.; Lopez, C. M.; Zhu, B.; Walther, A.; Molano Lopez, C.; Zhu, B.; Walther, A. Generic Concept to Program the Time Domain of Self-Assemblies with a Self-Regulation Mechanism. *Nanoletters* **2015**, *15*, 2213–2219.

(36) Pappas, C. G.; Sasselli, I. R.; Ulijn, R. V. Biocatalytic Pathway Selection in Transient Tripeptide Nanostructures. *Angew. Chem. Int. Ed.* **2015**, *54*, 8119–8123.

(37) Singh, N.; Formon, G. J. M.; De Piccoli, S.; Hermans, T. M. Devising Synthetic Reaction Cycles for Dissipative Nonequilibrium Self-Assembly. *Adv. Mater.* **2020**, *32*, 1906834.

(38) Rieß, B.; Grötsch, R. K.; Boekhoven, J. The Design of Dissipative Molecular Assemblies Driven by Chemical Reaction Cycles. *Chem* **2020**, *6*, 552–578.

(39) van Rossum, S. A. P.; Tena-Solsona, M.; van Esch, J. H.; Eelkema, R.; Boekhoven, J. Dissipative Out-of-Equilibrium Assembly of Man-Made Supramolecular Materials. *Chem. Soc. Rev.* **2017**. *46*, 5519−5535

(40) Leng, Z. J.; Peng, F.; Hao, X. Chemical-Fuel-Driven Assembly in Macromolecular Science: Recent Advances and Challenges. *Chempluschem* **2020**, *85*, 1190–1199.

(41) Tu, Y.; Chen, N.; Li, C.; Liu, H.; Zhu, R.; Chen, S.; Xiao, Q.; Liu, J.; Ramakrishna, S.; He, L. Advances in Injectable Self-Healing Biomedical Hydrogels. *Acta Biomater.* **2019**, *90*, 1–20.

(42) Li, J.; Mooney, D. J. Designing Hydrogels for Controlled Drug Delivery. *Nat. Rev. Mater.* **2016**, *1*, 1-17.

(43) Taylor, D. L.; in het Panhuis, M. Self-Healing Hydrogels. *Adv. Mater.* **2016**, *28*, 9060–9093.

(44) Phadke, A.; Zhang, C.; Arman, B.; Hsu, C.-C.; Mashelkar, R. A.; Lele, A. K.; Tauber, M. J.; Arya, G.; Varghese, S. Rapid Self-Healing Hydrogels. *Proc. Natl. Acad. Sci.* **2012**, *109*, 4383–4388.

(45) Jeon, I.; Cui, J.; Illeperuma, W. R. K.; Aizenberg, J.; Vlassak, J. J. Extremely Stretchable and Fast Self-Healing Hydrogels. *Adv. Mater.* **2016**, *28*, 4678−4683.

(46) Talebian, S.; Mehrali, M.; Taebnia, N.; Pennisi, C. P.; Kadumudi, F. B.; Foroughi, J.; Hasany, M.; Nikkhah, M.; Akbari, M.; Orive, G.; Dolatshahi-Pirouz, A. Self-Healing Hydrogels: The Next Paradigm Shift in Tissue Engineering? *Adv. Sci.* **2019**, *1801664*.

(47) Tseng, T. C.; Tao, L.; Hsieh, F. Y.; Wei, Y.; Chiu, I. M.; Hsu, S. H. An Injectable, Self-Healing Hydrogel to Repair the Central Nervous System. *Adv. Mater.* **2015**, *27*, 3518–3524.

(48) Han, L.; Lu, X.; Wang, M.; Gan, D.; Deng, W.; Wang, K.; Fang, L.; Liu, K.; Chan, C. W.; Tang, Y.; Weng, L. T.; Yuan, H. A Mussel-Inspired Conductive, Self-Adhesive, and Self-Healable Tough Hydrogel as Cell Stimulators and Implantable Bioelectronics. *Small* **2017**, *13*, 1–9.

(49) Roth, G. A.; Gale, E. C.; Alcantara-Hernandez, M.; Luo, W.; Axpe, E.; Verma, R.; Yin, Q.; Yu, A. C.; Hernandez, H. L.; Maikawa, C. L.; Smith, A. A. A.; Davis, M. M.; Pulendran, B.; Idoyaga, J.; Appel, E. A. Injectable Hydrogels for Sustained Codelivery of Subunit Vaccines Enhance Humoral Immunity. *ACS Cent. Sci.* **2020**, *6*, 1800–1812.

(50) Roth, G. A.; Saouaf, O. M.; Smith, A. A. A.; Gale, E. C.; Hernández, M. A.; Idoyaga, J.; Appel, E. A. Prolonged Codelivery of Hemagglutinin and a TLR7/8 Agonist in a Supramolecular Polymer–Nanoparticle Hydrogel Enhances Potency and Breadth of Influenza Vaccination. *ACS Biomater. Sci. Eng.* **2021**. https://doi.org/10.1021/acsbiomaterials.0c01496

(51) Chen, J.; Peng, Q.; Thundat, T.; Zeng, H. Stretchable, Injectable, and Self-Healing Conductive Hydrogel Enabled by Multiple Hydrogen Bonding toward Wearable Electronics. *Chem. Mater.* **2019**, *31*, 4553–4563.

(52) Appel, E. A.; Tibbitt, M. W.; Webber, M. J.; Mattix, B. A.; Veiseh, O.; Langer, R. Self-Assembled Hydrogels Utilizing Polymer-Nanoparticle Interactions. *Nat. Commun.* **2015**, *6*. No. 6295

(53) Liu, Y.; Hsu, S. Synthesis and Biomedical Applications of Self-Healing Hydrogels. *Front. Chem.* **2018**, *6*, 1–10.

(54) Wang, W.; Xiang, L.; Gong, L.; Hu, W.; Huang, W.; Chen, Y.; Asha, A. B.; Srinivas, S.; Chen, L.; Narain, R.; Zeng, H. Injectable, Self-Healing Hydrogel with Tunable Optical, Mechanical, and Antimicrobial Properties. *Chem. Mater.* **2019**, *31*, 2366–2376.

(55) Scheutz, G. M.; Lessard, J. J.; Sims, M. B.; Sumerlin, B. S. Adaptable Crosslinks in Polymeric Materials: Resolving the Intersection of Thermoplastics and Thermosets. *J. Am. Chem. Soc.* **2019**, *141*, 16181–16196.

(56) Mutlu, H.; Ceper, E. B.; Li, X.; Yang, J.; Dong, W.; Ozmen, M. M.; Theato, P. Sulfur Chemistry in Polymer and Materials Science. *Macromol. Rapid Commun.* **2019**, *40*, 1–51.

(57) Lowe, A. B. Thiol-Yne 'Click'/Coupling Chemistry and Recent Applications in Polymer and Materials Synthesis and Modification. *Polymer.* **2014**, *55*, 5517–5549.

(58) Lopus, M. Antibody-DM1 Conjugates as Cancer Therapeutics. *Cancer Lett.* **2011**, *307*, 113–118.

(59) Nair, D. P.; Podgórski, M.; Chatani, S.; Gong, T.; Xi, W.; Fenoli, C. R.; Bowman, C. N. The Thiol-Michael Addition Click Reaction: A Powerful and Widely Used Tool in Materials Chemistry. *Chem. Mater.* **2014**, *26*, 724–744.

(60) Truong, V. X.; Dove, A. P. Organocatalytic, Regioselective Nucleophilic "Click" Addition of Thiols to Propiolic Acid Esters for Polymer-Polymer Coupling. *Angew. Chem. Int. Ed.* **2013**, *52*, 4132–4136.

(61) Macdougall, L. J.; Pérez-Madrigal, M. M.; Arno, M. C.; Dove, A. P. Nonswelling Thiol-Yne Cross-Linked Hydrogel Materials as Cytocompatible Soft Tissue Scaffolds. *Biomacromolecules* **2018**, *19*, 1378–1388.

(62) Wandel, M. B.; Bell, C. A.; Yu, J.; Arno, M. C.; Dreger, N. Z.; Hsu, Y.-H.; Pitto-Barry, A.; Worch, J. C.; Dove, A. P.; Becker, M. L. Concomitant Control of Mechanical Properties and Degradation in Resorbable Elastomer-like Materials Using Stereochemistry and Stoichiometry for Soft Tissue Engineering. *Nat. Commun.* **2021**, *12*, 1–13.

(63) Joshi, G.; Anslyn, E. V. Dynamic Thiol Exchange with β-Sulfido-α,β-Unsaturated Carbonyl Compounds and Dithianes. *Org. Lett.* **2012**, *14*, 4714–4717.

(64) Shiu, H. Y.; Chan, T. C.; Ho, C. M.; Liu, Y.; Wong, M. K.; Che, C. M. Electron-Deficient Alkynes as Cleavable Reagents for the Modification of Cysteine-Containlng Peptides in Aqueous Medium. *Chem. - A Eur. J.* **2009**, *15*, 3839–3850.

(65) Van Herck, N.; Maes, D.; Unal, K.; Guerre, M.; Winne, J. M.; Prez, F. E. Du. Covalent Adaptable Networks with Tunable Exchange Rates Based on Reversible Thiol-Yne Cross-Linking. *Angew. Chem. Int. Ed.* ***2019,*** *9,* 3609-3617.

(66) Matysiak, B. M.; Nowak, P.; Cvrtila, I.; Pappas, C.; Liu, B.; Komaromy, D.; Otto, S. Antiparallel Dynamic Covalent Chemistries. *J. Am. Chem. Soc.* **2017***, 139,* 6744-6751.

(67) Zhong, Y.; Xu, Y.; Anslyn, E. V. Studies of Reversible Conjugate Additions. *European J. Org. Chem.* **2013**, *2013*, 5017–5021.

(68) Zhang, B.; Digby, Z. A.; Flum, J. A.; Chakma, P.; Saul, J. M.; Sparks, J. L.; Konkolewicz, D. Dynamic Thiol-Michael Chemistry for Thermoresponsive Rehealable and Malleable Networks. *Macromolecules* ***2016****, 49, 6871–6878.*

(69) Fitzsimons, T. M.; Oentoro, F.; Shanbhag, T. V.; Anslyn, E. V.; Rosales, A. M. Preferential Control of Forward Reaction Kinetics in Hydrogels Crosslinked with Reversible Conjugate Additions. *Macromolecules* **2020**, *53*, 3738–3746.

(70) Daglar, O.; Gungor, B.; Guric, G.; Gunay, U. S.; Hizal, G.; Tunca, U.; Durmaz, H. Rapid Hyperbranched Polythioether Synthesis Through Thiol-Michael Addition Reaction. *J. Polym. Sci.* **2020**, *58*, 824–830.

(71) Daglar, O.; Luleburgaz, S.; Baysak, E.; Gunay, U. S.; Hizal, G.; Tunca, U. Nucleophilic Thiol-Yne Reaction in Macromolecular Engineering : From Synthesis to Applications. *Eur. Polym. J.* **2020**, *137*, 109926.

(72) Diehl, K. L.; Kolesnichenko, I. V.; Robotham, S. A.; Bachman, J. L.; Zhong, Y.; Brodbelt, J. S.; Anslyn, E. V. Click and Chemically Triggered Declick Reactions through Reversible Amine and Thiol Coupling via a Conjugate Acceptor. *Nat. Chem.* **2016**, *8*, 968–973.

(73) Sun, X.; Anslyn, E. V. An Auto-Inductive Cascade for the Optical Sensing of Thiols in Aqueous Media: Application in the Detection of a VX Nerve Agent Mimic. *Angew. Chem. Int. Ed.* **2017**, *56*, 9522–9526.

(74) Ishibashi, J. S. A.; Kalow, J. A. Vitrimeric Silicone Elastomers Enabled by Dynamic Meldrum's Acid-Derived Cross-Links. *ACS Macro Lett.* **2018**, *7*, 482–486.

(75) Sun, X.; Chwatko, M.; Lee, D.; Reuther, J. F.; Lynd, N. A.; Anslyn, E. V; Sun, X.; Chwatko, M.; Lee, D.; Bachman, J. L.; Reuther, J. F. Chemically-Triggered Synthesis, Remodeling , and Degradation of Soft Materials. *J. Am. Chem. Soc.* **2020**. *142,* 3913-3922.

(76) El-Zaatari, B. M., Ishibashi, J. S., & Kalow, J. A. Cross-Linker Control of Vitrimer Flow. *Polym. Chem.* **2020**. *11,* 5339-5345.

Chapter 2

A fuel-driven chemical reaction network based on conjugate addition and elimination chemistry

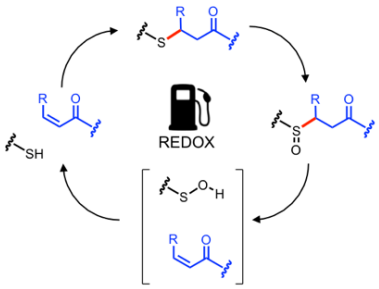

Abstract: Fuel-driven chemical reaction networks provide an opportunity to develop chemical systems that operate out-of-equilibrium. There remains a need to design and develop new fuel-driven chemical reaction networks capable of repeated operation using simple and benign chemistry. Here, we propose a new chemical reaction network for fuel-driven transient formation of covalent bonds, based on redox-controlled conjugate addition and elimination chemistry. By investigating the separate reactions making up the cycle, we find that the bond formation, breaking and regeneration processes can be realized. At present, substantial side reactivity prevents achieving repeated operation of a full cycle in a single system. If such obstacles would be overcome, this chemical reaction network could be a valuable addition to the toolbox for out-of-equilibrium systems chemistry.

This chapter is mainly based on:
B. Fan, Y. Men, S. A. P. Rossum, G. Li, R. Eelkema, "A Fuel Driven Chemical Reaction Network Based on Conjugate Addition and Elimination Chemistry" *ChemSystemsChem* **2020**, *2*, 2–5.

2.1 Introduction

Within systems chemistry there is a need for new fuel-driven chemical reaction networks as they will allow powering and out of equilibrium operation of chemical systems. Inspired by the functional behavior seen in living systems, fuel-driven chemical reaction networks have been used in many exciting examples, including oscillators[1–4], self-replicating systems[5–7], fuel-driven transient hydrogel formation[8,9], polymerization[10], fuel-controlled chemical reactivity[11], and fuel-driven molecular motion[12]. At the base of many of these discoveries are chemical reaction networks where a fuel can reversibly and thereby temporarily change the properties of a chemical building block. Fuel-driven chemical reaction networks capable of repeated operation are rare and in some cases have problems in terms of biocompatibility, harsh chemistry or irreversible side reactivity.[13] Therefore, there remains a need to design and develop novel fuel-driven chemical reaction networks. Fuel-driven transient material formation is a promising application of chemical reaction networks. Most examples of fuel-driven systems focus on non-covalent assembly of supramolecular materials.[13] It would also be interesting to develop a new fuel-driven reaction cycle that enables formation and breakdown of covalent bonds, for instance as crosslinks in a polymer material. As such, it would allow transient adjustment of the mechanical properties or porosity of soft materials. An essential part in the design of such a fuel-dependent polymeric material is that the reaction network contains both the bond forming and breaking processes. Here, we propose a novel fuel-driven chemical reaction network based on redox-controlled conjugate addition and elimination chemistry. We tested this cycle using several model reactions. Although we were able to demonstrate several individual steps in the cycle and observed some signs of operation of the full cycle, we were not able to demonstrate a full cycle in one pot, most likely due to substantial side reactivity of some of the cycle intermediates.

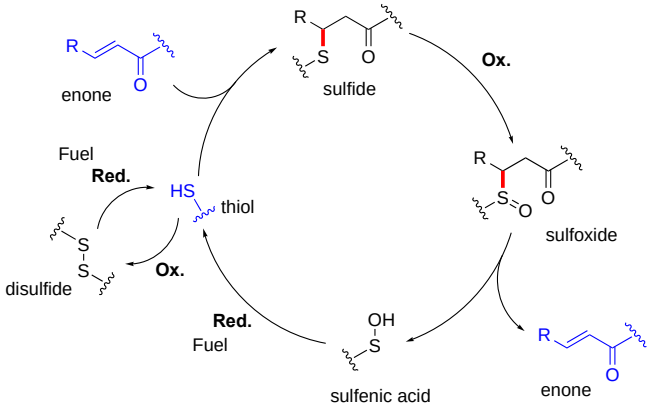

Figure 2.1. Proposed reductant-driven covalent bond formation in a conjugate addition chemical reaction network. The cycle starts when a disulfide is reduced by a reductant to a thiol. Then the thiol reacts with an enone to a sulfide adduct, which is subsequently oxidized to a sulfoxide by the oxidant. The elimination of the sulfoxide will release the enone and sulfenic acid, which can be reduced back to the thiol, closing the cycle. The substrates of the conjugate addition (the thiol and enone) are depicted in blue. The transiently formed covalent S-C bond is depicted in red. Ox. indicates oxidant, Red. indicates reductant.

To realize a chemical reaction network with the desired effects, the reactions of the network have to fulfil a complex set of requirements: 1) run at ambient conditions on acceptable time scales; 2) be selective to the desired bond forming and breaking reactions; 3) form an unstable bond during the cycle; 4) regenerate the original bond formation precursor after a full cycle; 5) have only limited off-cycle reactivity of the fuel. Based on the above requirements, we here propose a new fuel-driven chemical reaction network.

The conjugate addition of a thiol to an electron deficient olefin (an enone) was chosen as the bond forming reaction. First, a thiol will be liberated by reduction of a disulfide using a reducing agent as fuel. This thiol reacts with an enone in a conjugate addition, to form a sulfide adduct, which can be further oxidized to a sulfoxide using an oxidizing agent. Elimination of a sulfoxide is prone to occur using base or under heating, regenerating the enone double bond.[14,15] The sulfenic acid elimination product can then react with a reducing agent to regenerate the thiol and close the cycle (**Figure 2.1**). Overall, the reductant acts as the fuel driving this cycle to transiently produce the sulfide addition product, which constitutes bond formation. Oxidation will lead to destabilization and elimination of the sulfide adduct, constituting bond breaking.

2.2 Results and Discussion

Before testing this fuel-driven cycle, some possible pitfalls associated to the chemistry in this cycle should be noted. Firstly, the oxidation of the sulfide to a sulfoxide requires a relatively strong oxidizing agent.[16,17] The presence of such an oxidant may also lead to irreversible epoxidation or dihydroxylation of the enone double bond[18] causing the removal of substrate from the cycle. To avoid this potential side-reaction, maleimide was selected as the first enone in our cycle because it is less prone to oxidation.[19,20] Based on literature procedures, we selected dichloromethane as solvent for the reaction network.[14,15] Secondly, the reductants and oxidants should be chosen carefully as they might react with each other in non-productive side reactions. If these side reactions outcompete the reaction cycle, the desired covalent bond will not be generated during operation of the cycle.

To gain insights in the operation of the cycle, the reaction network was split to four individual parts that were investigated separately. At each step the final products were isolated and applied as the reactant in the next reaction. Only after ensuring that every reaction step can take place under the same conditions, with high selectivity and high yield of the desired product, a sustainable cycle can be achieved. Then afterward, all reactions can be put in one pot to test the feasibility of this fuel driven cycle.

The conjugate addition reaction, as the mainstay of the network, was tested first. Catalyzed by triethylamine (10 mol%), thiophenol **2** reacts with *N*-phenylmaleimide **1** to give the sulfide product **3** at a nearly quantitative yield at room temperature within a few minutes. The isolated product **3** (**Figure S2.1**, **Figure S2.2**) was used as the starting material in the following oxidation step.

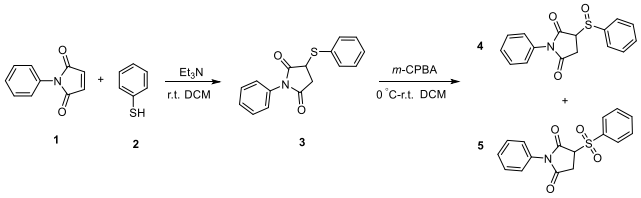

Figure 2.2. The conjugate addition of thiophenol **2** with *N*-phenylmaleimide **1** and the subsequent oxidation of **3** by *m*-CPBA.

The selective oxidation of sulfide **3** to sulfoxide **4** turned out to be a challenge.[21,22] Meta-chloroperoxybenzoic acid (*m*-CPBA), as one of the most common and efficient oxidants for the oxidation of sulfides in DCM, was first selected for this reaction step.[19,20] The ^{1}H NMR, ^{1}H-^{1}H COSY and ^{1}H-^{13}C HSQC and LC-MS spectra (**Figure S2.3, Figure S2.5**, **Figure S2.6**, **Figure S2.14**) show that the resulting mixture contains the desired sulfoxide **4** (~41 mol%), the over-oxidized sulfone **5** (~27 mol%), unreacted sulfide **3** (~25 mol%) and maleimide **1** (~7 mol%). The presence of maleimide **1** may be caused by the spontaneous elimination of sulfoxide or sulfone during workup after oxidation. The poor selectivity and low conversion in this oxidation indicate that *m*-CPBA is not an ideal oxidant in this cycle. Alternatively, hydrogen peroxide was also tested as an oxidant. H_2O_2 is a less strong oxidant compared to *m*-CPBA. The rate of oxidation by hydrogen peroxide may be enhanced using a vanadium catalyst that consists of $VO(acac)_2$ and a β-amino alcohol-derived Schiff base ligand.[23,24] Unfortunately, the ^{1}H NMR yields of **4** were ~7% after 6 days without catalyst and ~13% after 16 h when catalyzed by the vanadium-Schiff base complex catalyst. Sulfone **5** was also observed in both oxidation by only H_2O_2 and by H_2O_2 with the catalyst (**Figure S2.8**, **Figure S2.10**).

The next step in the cycle was the elimination of the sulfoxide to regenerate the enone. We tested this reaction on an inseparable mixture of sulfoxide **4** (~70 mol%), sulfone **5** (~29 mol%) and maleimide **1** (~1 mol%) (**Figure S2.11**), generated in the previous oxidation step.

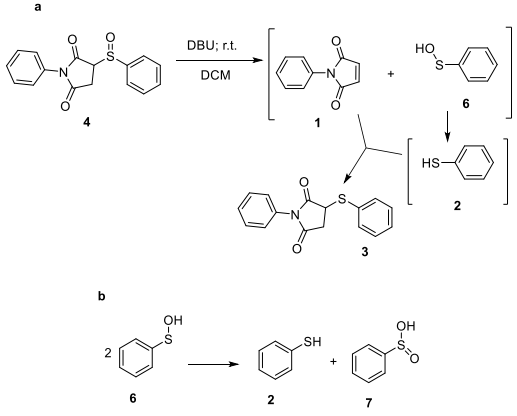

Figure 2.3. (a) Proposed elimination of sulfoxide **4** (b) Proposed disproportionation of sulfenic acid **6** to give thiophenol **2** and sulfinic acid **7**. The compounds in the brackets (maleimide **1**, sulfenic acid **6** and thiol **2**) indicate that they could be the intermediates which were not detected during characterization).

The elimination tests were aimed at establishing whether the sulfoxide product could be converted into the enone and thiol or disulfide, so that the cycle can continue. This experiment was monitored using ^{1}H NMR. The reaction was performed in DCM at room temperature with a 0.1 molar equivalent of the same base in the conjugate addition (triethylamine). However, no conversion of the oxidized mixture, or generation of maleimide **1** or sulfide **3** was observed. We then switched to 0.1 equivalent of the strong base 1,8-diazabicyclo[5.4.0]undec-7-ene (DBU). Figure 2.4a shows the ^{1}H NMR spectrum for the starting materials of elimination. The spectrum shows peaks of sulfoxide **4** (2.60 and 3.99 ppm) and sulfone **5** (3.01 and 4.71 ppm), as well as a minor contribution (~1 mol%) from maleimide **1** at 6.86 ppm. Addition of DBU resulted in the disappearance of sulfoxide **4** and sulfone **5**. Surprisingly, after elimination no characteristic protons of maleimide **1** were present in the ^{1}H NMR spectrum but protons of addition product sulfide **3** (2.92 ppm and 4.16 ppm) were observed with a conversion of 17% (**Figure 2.4b**). Also, several protons from unidentified by-products can be seen in the spectrum. (**Figure S2.11**). A possible explanation for the presence of sulfide **3** here is that a conjugate addition occurred between elimination product maleimide **1** and thiophenol **2**. The latter may have formed from the disproportionation of sulfenic acid **6** as the another product of elimination (**Figure 2.3a** and **2.3b**). Sulfenic acids are inherently unstable and are prone to disproportionate to thiols and sulfinic acids (**Figure 2.3b**).[25–27] Although the final reaction did not yield the starting point maleimide and thiol, it does afford the adduct of maleimide and thiol. This result suggests that in principle it is possible to achieve the proposed chemical reaction network. In the original network, we proposed using a reductant to reduce the sulfenic acid to a thiol. Currently, this reaction is achieved by disproportionation instead of using an external reductant.

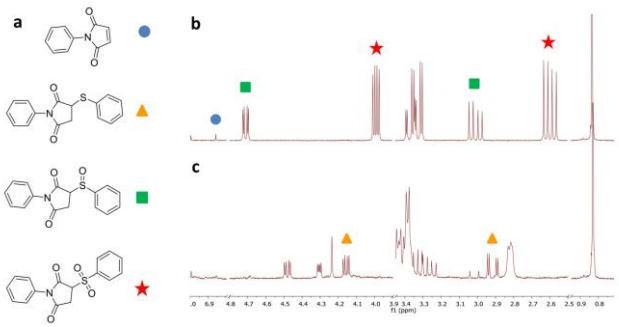

Figure 2.4. (a) The compounds during the elimination and their schematic representation. ^{1}H NMR spectra showing the characteristic protons of (b) the starting mixture for elimination: maleimide **1** (blue circle), sulfoxide **4** (green square) and sulfone **5** (red star); (c) sulfide **3** (yellow triangle) after the elimination.

Nevertheless, several problems still exist regarding the elimination step. The first problem is inefficient elimination evident upon quantitatively analyzing the elimination conversion. We used ^{1}H NMR to follow the reaction and used methyltriphenylsilane as internal standard. The results show that all maleimide **1**, sulfoxide **4** and sulfone **5** were consumed completely after elimination, but to yield only 17 mol% sulfide **3**. The unidentified by-product peaks in NMR indicate that several side-reactions have happened during this experiment (**Figure S2.12**). Such by-product formation results in a substantial reduction of substrate incapable of

participating in the cycle. Another reason of the low conversion to sulfide **3** might be that a substantial part of the starting compound thiol is converted to sulfinic acid **7** either by over-oxidation to sulfone and subsequent elimination, or by disproportionation of sulfenic acid **6** (**Scheme S2.1**; **Figure 2.3b**). The reduction of sulfinic acid back to thiol is nearly impossible so that it irreversibly removes a large portion of the starting substance thiol from the cycle.[28,29] A second problem is that it is difficult to investigate the reduction of sulfenic acid **6** to thiol **2**. As laid out in the original cycle, the reduction of sulfenic acid also needs to be tested as an essential path back to the thiol (**Figure 2.1**). Sulfenic acids are highly reactive molecules that are very difficult to isolate or even detect.[30] Therefore, we used the elimination of sulfoxide **4** and sulfone **5** by DBU to generate sulfenic acid in situ, followed by reduction using added triphenylphosphine (PPh_3) without intermediate purification. The mixture was stirred overnight at room temperature, after which it was analyzed by ^{1}H NMR (**Figure S2.13**). However, the ^{1}H NMR spectrum after reaction with PPh_3 indicated that the yield of sulfide **3** does not show a significant change (decreased ~1% within measurement error) and several more unidentified by-products appeared. At this point, it is difficult to say whether PPh_3 can reduce sulfenic acid, but PPh_3 does not promote formation of more sulfide **3**.

In summary, we have designed a new chemical reaction network for transient formation of covalent bonds, based on redox-controlled conjugate addition and elimination chemistry. We investigated the separate reactions making up the cycle starting at conjugate addition of thiophenol to *N*-phenylmaleimide. The conjugate addition product was used in subsequent oxidation and elimination steps, affording the conjugate addition product without observing the enone product (**Figure 2.5**). The bond formation, breakage and regeneration processes were successfully realized in separate reaction tests. Still, there are many obstacles to be overcome before this fuel-driven bond formation chemical reaction network can be applied as a continuous cycle. First of all, no external reductant was applied in this cycle. Under the current conditions, the observed sulfide formation may have originated from disproportionation of

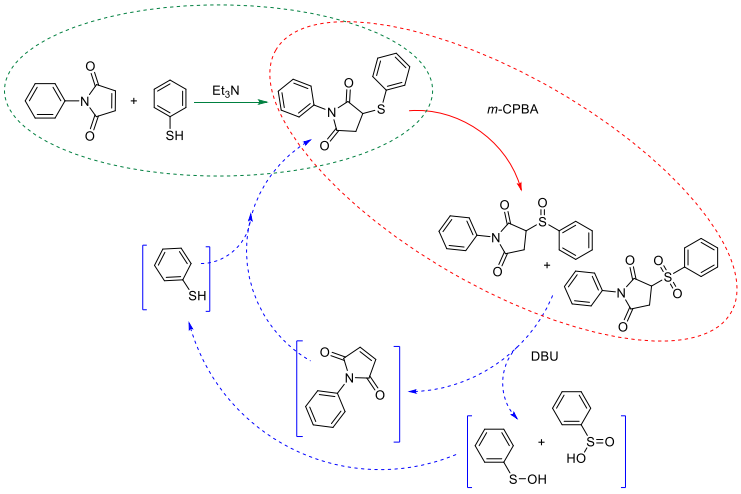

Figure 2.5. The conjugate addition chemical reaction network tested as separate reactions. The green arrow and dashed frame indicate the addition; the red arrow and dashed frame indicate the oxidation; the blue arrows indicate the elimination and subsequent sulfide formation. The brackets indicate that those compounds were not detected directly but their transient formation is implicated by the formation of sulfide **3**.

sulfenic acid leading to thiol formation and subsequent conjugate addition. Here, disproportionation also leads to removal of some of the thiol starting material from the cycle, in the form of sulfinic acid. Second, too many side reactions lead to a low yield of the desired products. Over-oxidation of sulfide **3** by *m*-CPBA, side reactions of sulfenic acid and the possible disproportionation of sulfenic acid result in the irreversible formation of many undesired substances, limiting the efficiency and continuous operation of the cycle. Next, although *m*-CPBA was able to oxidize the sulfide to a sulfoxide, its strong oxidizing ability may cause problems when in the same system as a reducing agent. There, a mild oxidant is desired to achieve selective oxidation to the sulfoxide and to run the full cycle with all components in the system at the same time. Finally, we proposed a coupled cycle of thiol oxidation and disulfide reduction as part of the initial chemical reaction network (**Figure 2.1**). We did not test this coupled network as part of the presented results, but it is worthwhile to discuss it here. The thiol-disulfide redox pair reactions have to operate at similar timescales as the conjugate addition-elimination reaction cycle. If the thiol-disulfide cycle is much faster than the major cycle, the majority of oxidant and reductant will be consumed unproductively. If the thiol-disulfide cycle is much slower, it will not supply enough thiol to the conjugate addition-elimination cycle. This part should be taken into account in future investigations.

2.3 Conclusion

On the whole, this fuel driven chemical reaction network provides an opportunity to achieve transient bond and material formation far from equilibrium. Experiments on separate parts of the cycle indicate that this cycle may work but at present several problems prevent running a full cycle continuously in a single system.

2.4 Reference

(1) Pogodaev, A. A.; Wong, A. S. Y.; Huck, W. T. S. Photochemical Control over Oscillations in Chemical Reaction Networks. *J. Am. Chem. Soc.* **2017**, *139*, 15296–15299.

(2) Semenov, S. N.; Kraft, L. J.; Ainla, A.; Zhao, M.; Baghbanzadeh, M.; Campbell, V. E.; Kang, K.; Fox, J. M.; Whitesides, G. M. Autocatalytic, Bistable, Oscillatory Networks of Biologically Relevant Organic Reactions. *Nature* **2016**, *537*, 656–660.

(3) Semenov, S. N.; Wong, A. S. Y.; Van Der Made, R. M.; Postma, S. G. J.; Groen, J.; Van Roekel, H. W. H.; De Greef, T. F. A.; Huck, W. T. S. Rational Design of Functional and Tunable Oscillating Enzymatic Networks. *Nat. Chem.* **2015**, *7*, 160–165.

(4) Leira-Iglesias, J.; Tassoni, A.; Adachi, T.; Stich, M.; Hermans, T. M. Oscillations, Travelling Fronts and Patterns in a Supramolecular System. *Nat. Nanotechnol.* **2018**, *13*, 1021–1027.

(5) Colomb-Delsuc, M.; Mattia, E.; Sadownik, J. W.; Otto, S. Exponential Self-Replication Enabled through a Fibre Elongation/Breakage Mechanism. *Nat. Commun.* **2015**, *6*, 1–7.

(6) Colomer, I.; Morrow, S. M.; Fletcher, S. P. A Transient Self-Assembling Self-Replicator. *Nat. Commun.* **2018**, *9*, 2239.

(7) Morrow, S. M.; Colomer, I.; Fletcher, S. P. A Chemically Fuelled Self-Replicator. *Nat. Commun.* **2019**, *10*, 1011.

(8) Boekhoven, J.; Brizard, A. M.; Kowlgi, K. N.; Koper, G. J.; Eelkema, R.; van Esch, J. H. Dissipative Self-Assembly of a Molecular Gelator by Using a Chemical Fuel. *Angew Chem Int Ed Engl* **2010**, *49*, 4825–4828.

(9) Boekhoven, J.; Hendriksen, W. E.; Koper, G. J. M.; Eelkema, R.; Esch, J. H. Van. Transient Self-Assembly of Active Materials Fueled by a Chemical Reaction. *Science (80-.).* **2015**, *349*, 1075.

(10) Jain, A.; Dhiman, S.; Dhayani, A.; Vemula, P. K.; George, S. J. Chemical Fuel-Driven Living and Transient Supramolecular Polymerization. *Nat. Commun.* **2019**, *10*, 1–9.

(11) Maiti, S.; Fortunati, I.; Ferrante, C.; Scrimin, P.; Prins, L. J. Dissipative Self-Assembly of Vesicular Nanoreactors. *Nat. Chem.* **2016**, *8*, 725–731.

(12) Wilson, M. R.; Solà, J.; Carlone, A.; Goldup, S. M.; Lebrasseur, N.; Leigh, D. A. An Autonomous Chemically Fuelled Small-Molecule Motor. *Nature* **2016**, *534*, 235–240.

(13) van Rossum, S. A. P.; Tena-Solsona, M.; van Esch, J. H.; Eelkema, R.; Boekhoven, J. Dissipative Out-of-Equilibrium Assembly of Man-Made Supramolecular Materials. *Chem. Soc. Rev.* **2017**,*46,* 5519-5535.

(14) Ponton, J.; Helquist, P.; Conrad, P. C.; Fuchs, P. L. Six-Membered-Ring Annulation via a Conjugate Addition-Alkylation Sequence Using Functionalized Aryllithium Reagents and Vinyl Sulfones. *J. Org. Chem.* **1981**, *46*, 118–122.

(15) Auvray, P.; Knochel, P.; Normant, J. F. Preparation and Nucleophilic Substitution of (e)-1-Bromo-2-Phenylsulfonyl-2-Alkenes and 3-Acetoxy-2-Phenylsulfonyl-1-Alkenes. *Tetrahedron* **1988**, *44*, 6095–6106.

(16) Sato, K.; Hyodo, M.; Aoki, M.; Zheng, X. Q.; Noyori, R. Oxidation of Sulfides to Sulfoxides and Sulfones with 30% Hydrogen Peroxide under Organic Solvent- and Halogen-Free Conditions. *Tetrahedron* **2001**, *57*, 2469–2476.

(17) Gayakwad, E. M.; Patel, K. P.; Shankarling, G. S. Sodium Sulfate-Hydrogen Peroxide-Sodium Chloride Adduct: Selective Protocol for the Oxidative Bromination, Iodination and Temperature Dependent Oxidation of Sulfides to Sulfoxides and Sulfones. *New J. Chem.* **2019**, *43*, 6001–6009.

(18) Srour, H.; Le Maux, P.; Chevance, S.; Simonneaux, G. Metal-Catalyzed Asymmetric Sulfoxidation, Epoxidation and Hydroxylation by Hydrogen Peroxide. *Coord. Chem. Rev.* **2013**, *257*, 3030–3050.

(19) Denancé, M.; Banaszak, E.; Samadi, M. An Expeditious Synthesis of Natural and Unnatural Disubstituted Maleic Anhydrides. *Tetrahedron Lett.* **2006**, *47*, 7409–7411.

(20) Arai, Y.; Matsui, M.; Fujii, A.; Kontani, T.; Ohno, T.; Koizumi, T.; Shiro, M. Asymmetric Diels–Alder Reaction of Optically Active α-(2-Exo-Hydroxy-10-Bornyl)Sulfinylmaleimides and Its Application to Optically Active 5-Functionalised Pyrrolines via Retro-Diels–Alder Reaction. *J. Chem. Soc., Perkin Trans. 1* **1994**, No. 1, 25–39.

(21) Baig, N.; Madduluri, V. K.; Sah, A. K. Selective Oxidation of Organic Sulfides to Sulfoxides Using Sugar Derived Cis-Dioxo Molybdenum(vi) Complexes: Kinetic and Mechanistic Studies. *RSC Adv.* **2016**, *6*, 28015–28022.

(22) Kirihara, M.; Yamamoto, J.; Noguchi, T.; Hirai, Y. Selective Synthesis of Sulfoxides and Sulfones by Tantalum(V) Catalyzed Oxidation of Sulfides with 30% Hydrogen Peroxide. *Tetrahedron Lett.* **2009**, *50*, 1180–1183.

(23) Bolm, C.; Bienewald, F. Asymmetric Sulfide Oxidation with Vanadium Catalysts and H2O2. *Angew. Chem. Int. Ed.* **2004***, 34*, 2640–2642.

(24) Wu, Y.; Mao, F.; Meng, F.; Li, X. Enantioselective Vanadium-Catalyzed Oxidation of 1,3-Dithianes from Aldehydes and Ketones Using β-Amino Alcohol Derived Schiff Base Ligands. *Adv. Synth. Catal.* **2011**, *353*, 1707–1712.

(25) Goto, K.; Holler, M.; Okazaki, R. Synthesis, Structure, and Reactions of a Sulfenic Acid Bearing a Novel Bowl-Type Substituent: The First Synthesis of a Stable Sulfenic Acid by Direct Oxidation of a Thiol. *J Am Chem Soc* **1997**, *119*, 1460–1461.

(26) O'Donnell, J. S.; Schwan, A. L. *Generation, Structure and Reactions of Sulfenic Acid Anions*; **2004**; Vol. 25.

(27) Pan, J.; Carroll, K. S. Light-Mediated Sulfenic Acid Generation from Photocaged Cysteine Sulfoxide. *Org. Lett.* **2015**, *17*, 6014–6017.

(28) Groitl, B.; Jakob, U. Thiol-Based Redox Switches. *Biochim. Biophys. Acta - Proteins Proteomics* **2014**, *1844*, 1335–1343.

(29) Van Bergen, L. A. H.; Roos, G.; De Proft, F. From Thiol to Sulfonic Acid: Modeling the Oxidation Pathway of Protein Thiols by Hydrogen Peroxide. *J. Phys. Chem. A* **2014**, *118*, 6078–6084.

(30) Alcock, L. J.; Oliveira, B. L.; Deery, M. J.; Pukala, T. L.; Perkins, M. V.; Bernardes, G. J. L.; Chalker, J. M. Norbornene Probes for the Detection of Cysteine Sulfenic Acid in Cells. *ACS chemical biology*, **2019**,*14*, 594-598.

2.5 Supplementary information

2.5.1 Materials and methods

NMR spectra were recorded on an Agilent-400 MR DD2 (399.7 MHz for ^{1}H and 100.5 MHz for ^{13}C) at 298 K. HPLC-MS analysis was performed on a Shimadzu Liquid Chromatograph Mass Spectrometer, LCMS-2010, and LC-8A pump with a diode array detector SPD-M20. All compounds and solvents were used as received without further purification. The technical solvents were purchased from VWR and the reagent grade solvents were purchased from Sigma Aldrich. N-Phenylmaleimide was purchased from Fluorochem. Meta-chloroperoxybenzoic acid (*m*-CPBA), 1,8-diazabicyclo(5.4.0)undec-7-ene (DBU), vanadyl acetylacetonate ($VO(acac)_2$), methyltriphenylsilane were purchased from Sigma Aldrich. Trimethylchlorosilane was purchased from TCI Europe. Thiophenol was purchased from Acros.

2.5.2. Synthetic/Reaction test procedures

Synthesis of sulfide 3

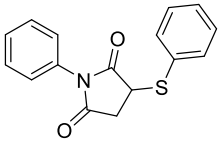

3

To a solution of the *N*-phenylmaleimide (150 mg, 0.866 mmol) in DCM (10 mL) thiophenol (95.4 mg, 0.87 mmol) was added, followed by 4 drops of triethylamine. The mixture was stirred for 4 hours at room temperature. The resulting mixture was washed with water, then the aqueous layer was extracted with DCM. The combined organic layers were dried over anhydrous $MgSO_4$, and the solvent was evaporated in vacuo. Sulfide product 3 was obtained as a white powder (230 mg, 0.812 mmol, 93.8% yield). ^{1}H NMR (399.7 MHz, $CDCl_3$) δ 7.60-7.58 (m, 2H), 7.47-7.34 (m, 6H), 7.08-7.04 (m, 2H), 4.16 (dd, *J*= 5.6, 4.0 Hz, 1H), 3.34 (dd, *J*=9.6, 9.2 Hz, 1H), 2.92 (dd, *J*=14.8, 4.0 Hz, 1H). ^{13}C NMR (100.5 MHz, 298 K in $CDCl_3$) δ 174.48, 173.48, 135.10, 131.52, 129.80, 129.69, 129.51, 129.15, 128.80, 126.34, 44.14, 36.41. (ESI Neg.) m/z: 282.1 $[(M-H^+)^-]$ (calculated for $C_{16}H_{13}NO_2S$ M/z=283.35).

The oxidation of 3 by *m*-CPBA

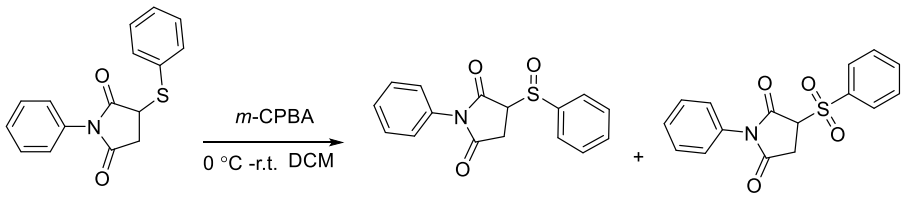

3 **4** **5**

To a stirred solution of **3** (200 mg, 0.706 mmol) in DCM (10 mL) was added *m*-CPBA (121.79 mg, 0.706 mmol) in DCM (10 mL) at 0 °C portion wise in 10 min. The reaction mixture was stirred at this temperature for 30 min then warmed up to room temperature and stirred for 4 hours. Afterwards, the reaction was diluted with DCM (8 mL) and washed with 5 wt% aqueous Na_2SO_3 solution, then the aqueous layer was extracted with DCM. The combined organic layers were dried over anhydrous $MgSO_4$, and the solvent was evaporated in vacuo. The yellow powder crude mixture product (oxidation product **S_1**) (146 mg, contains 25 mol% sulfide **3**, 41 mol% sulfoxide **4**, 27 mol% sulfone **5** and 7 mol% maleimide **1**) was characterized by ^{1}H NMR, ^{13}C NMR, ^{1}H-^{1}H COSY, ^{1}H-^{13}C HSQC and LC-MS without separation (**Figure S2.3**, **Figure S2.4**, **Figure S2.5**, **Figure S2.6**, **Figure S2.14**).

Further purification of oxidation product **S_1** was performed by flash silica gel column chromatography (Ethyl acetate/DCM = 1/5). The white powder mixture product (oxidation product **S_2**) (122 mg, contains 70 mol% sulfoxide **4**, 29 mol% sulfone **5** and 1 mol% maleimide **1**) was characterized by ^{1}H NMR (**Figure S2.7**).

The oxidation of 3 by H_2O_2

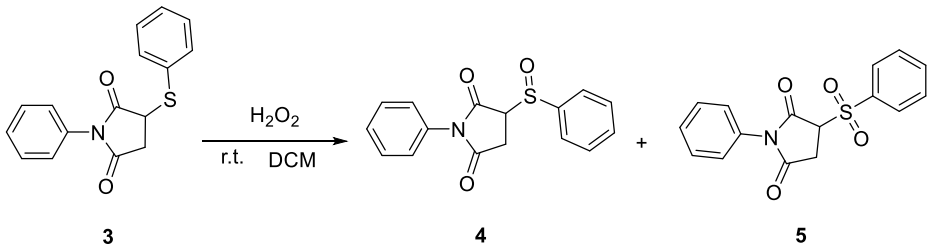

3 **4** **5**

To a solution of **3** (80 mg, 0.28 mmol) in DCM (10 mL) was added H_2O_2 (30% aq., 0.013 mL, 0.424 mmol). The reaction mixture was stirred at room temperature and was monitored by TLC. After 6 days, the reaction was diluted with DCM (8 mL) and washed with 5 wt% aqueous Na_2SO_3 solution to remove excess H_2O_2. Then the aqueous layer was extracted with DCM, the combined organic layers were dried over anhydrous $MgSO_4$, and the solvent was evaporated in vacuo. The white powder product (61.2 mg, contains 85 mol% sulfide **3**, 7 mol% sulfoxide **4**, 4 mol% sulfone **5** and 3 mol% maleimide **1**) was characterized by ^{1}H NMR (**Figure S2.8**).

The oxidation of 3 by H_2O_2 with a vanadium-Schiff base complex catalyst

According to a publication about the oxidation of sulfides by hydrogen peroxide using vanadium catalysts[1], we synthesized the ligand as described in reference [1] (**Figure S2.9**) and tested it for the oxidation of sulfide **3**.

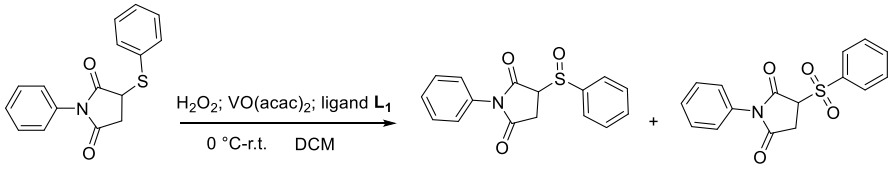

3 **4** **5**

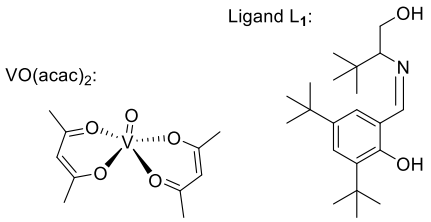

To a solution of $VO(acac)_2$ (9.36 mg, 0.0353 mmol) in DCM (5 mL), ligand L_1 (17.66 mg, 0.0529 mmol) was added at room temperature. The mixture was stirred for 10 min and then sulfide **3** (100 mg, 0.353 mmol) was added. Afterwards, the solution was stirred for another 5 min and then cooled to 0 °C. Next, H_2O_2 (30% aq., 0.424 mmol, 0.013 mL) was slowly added. The mixture was stirred at room temperature for 16 h. Next the reaction was diluted with DCM (8 mL) and washed with 5 wt% aqueous Na_2SO_3 solution. Then the aqueous layer was extracted with DCM, the combined organic layers were dried over anhydrous $MgSO_4$, and the solvent was evaporated in vacuo. The yellow powder product (77 mg, contains 66 mol% sulfide **3**, 13 mol% sulfoxide **4**, 14 mol% sulfone **5** and 7 mol% maleimide **1**) was characterized by ^{1}H NMR (**Figure S2.10**).

The elimination of the oxidation product S_2 with DBU and attempted reduction by PPh_3

Oxidation product **S_2** (40 mg) and methyltriphenylsilane (11.89 mg, 0.130 mmol) as the internal standard were dissolved in DCM (20 mL). The ^{1}H NMR of this solution is reported in Figure S2.11 and Table S2.1. To the DCM solution, DBU (1.97 mg, 0.0130 mmol, 0.1 molar equivalent to oxidation product **S_2**) was added. The solution was stirred for 2 h at room temperature. Then 2 mL of the elimination solution was taken as the elimination product sample. The solvent of this 2 mL solution was removed by evaporator under vacuum and processed to report the ^{1}H NMR (**Figure S2.12**). PPh_3 (34.09 mg, 0.130 mmol) was added into the elimination solution with stirring at room temperature. The mixture was stirred overnight. Then 2 mL solution of mixture was processed to remove solvent and studied by ^{1}H NMR (**Figure S2.13**).

2.5.3. Supplementary schemes, figures and tables

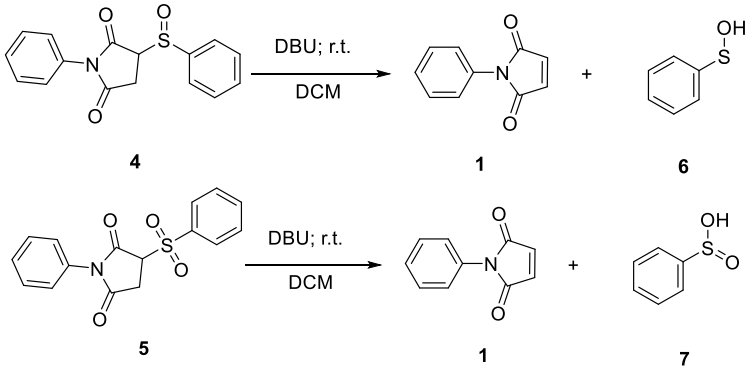

Scheme S2.1. Schematic of the elimination of the oxidation product $\mathbf{S_2}$

Table S2.1. The mmol percentage of each component before and after elimination

Compound number	**3**	**4**	**1**	**5**
Before elimination*	-	70%	29%	1%
After elimination**	17%	-	-	-
Addition of PPh_3	16%			

* the percentage of each component before elimination calculated by ^{1}HNMR

** the yield of **3** after elimination calculated by ^{1}H-NMR. Methyltriphenylsilane was used as an internal standard. It was added into the elimination substrate DCM solution before elimination. In the ^{1}H-NMR spectrum, the methyl group of the methyltriphenylsilane (0.83 ppm, Figure 2.4, Figure S2.11, Figure S2.12) was kept integrating as the same value before and after elimination. The yield of sulfide **3** can be calculated based on this value.

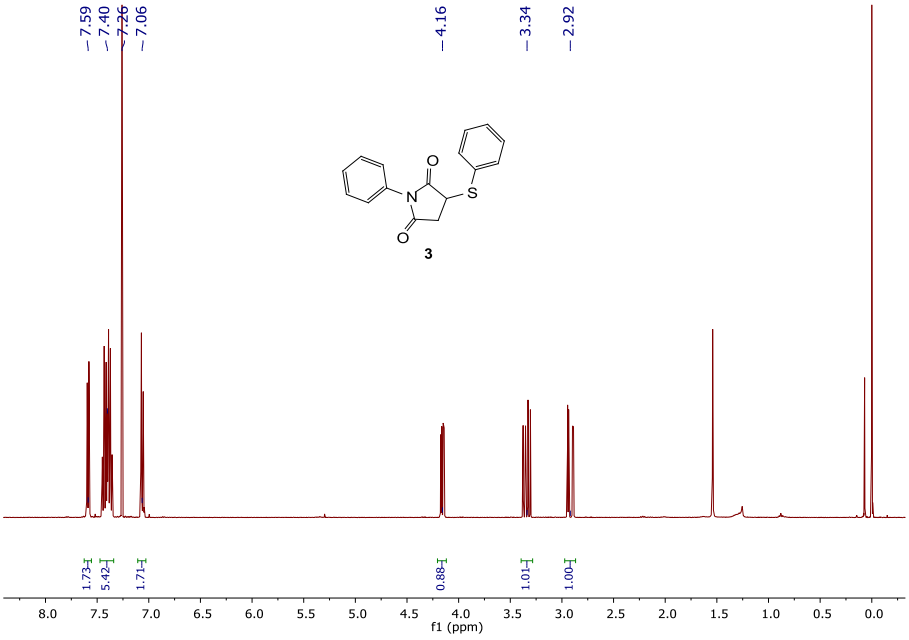

Figure S2.1. ^{1}H NMR (399.7 MHz, 298 K in $CDCl_3$) spectrum of **3**.

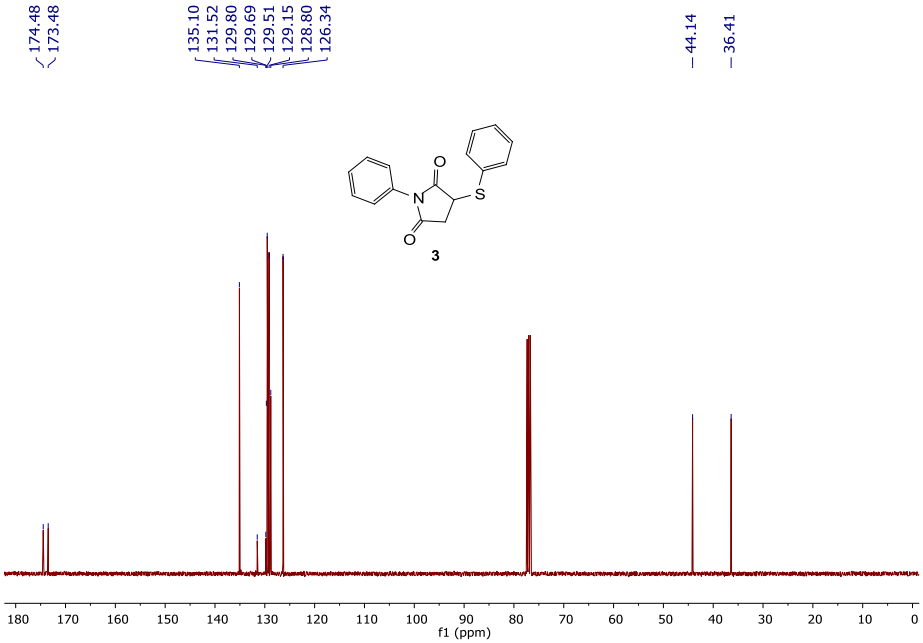

Figure S2.2. ^{13}C NMR (100.5 MHz, 298 K in $CDCl_3$) spectrum of **3.**

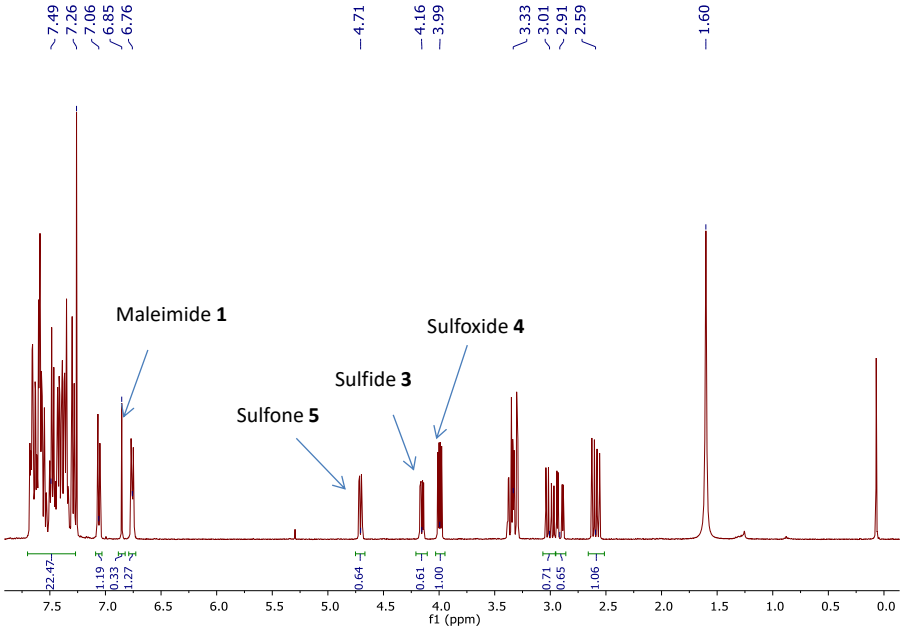

Figure S2.3. ^{1}H NMR (399.7 MHz, 298 K in $CDCl_3$) spectrum of the oxidation product $\mathbf{S_1}$.

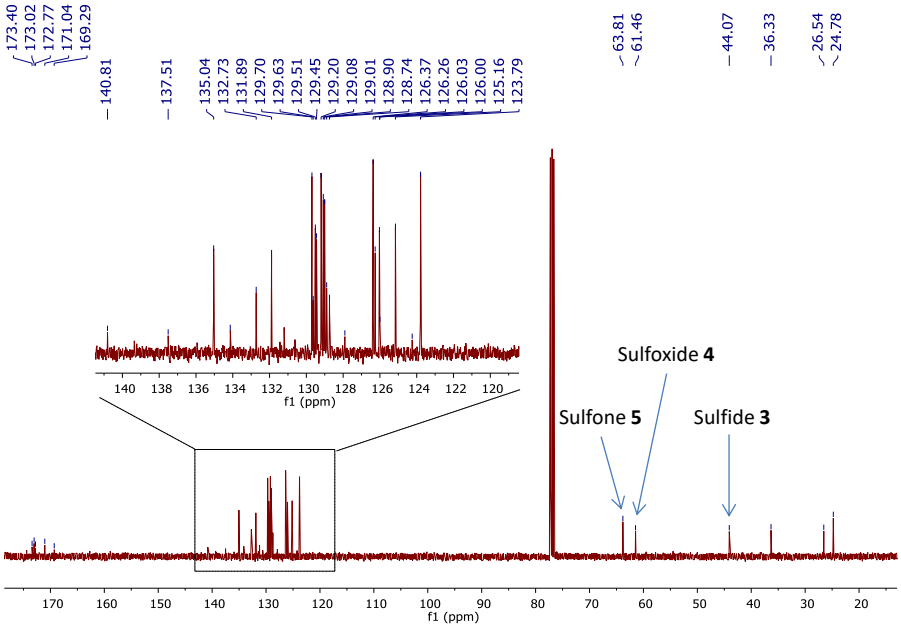

Figure S2.4. ^{13}C NMR (100.5 MHz, 298 K in $CDCl_3$) spectrum of the oxidation product **S**$_1$.

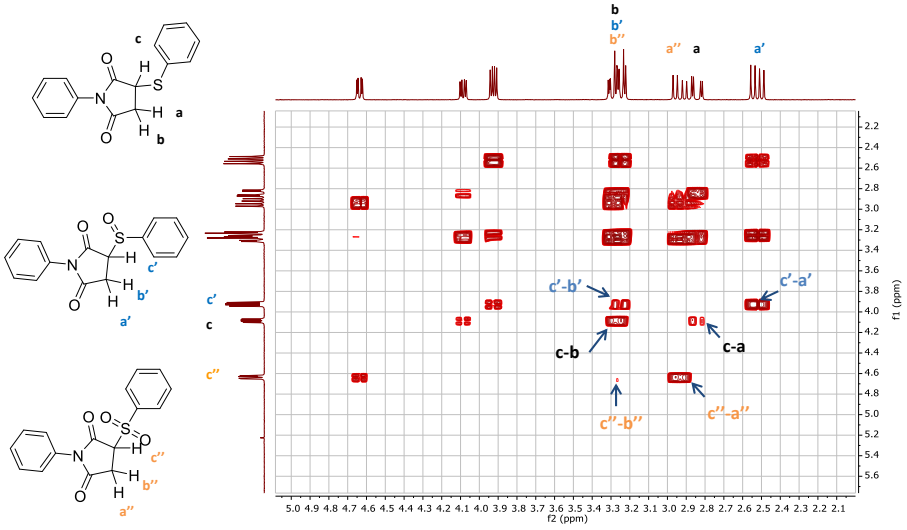

Figure S2.5. ^{1}H-^{1}H COSY at 298 K in $CDCl_3$ spectrum of the aliphatic region of the oxidation product **S**$_1$.

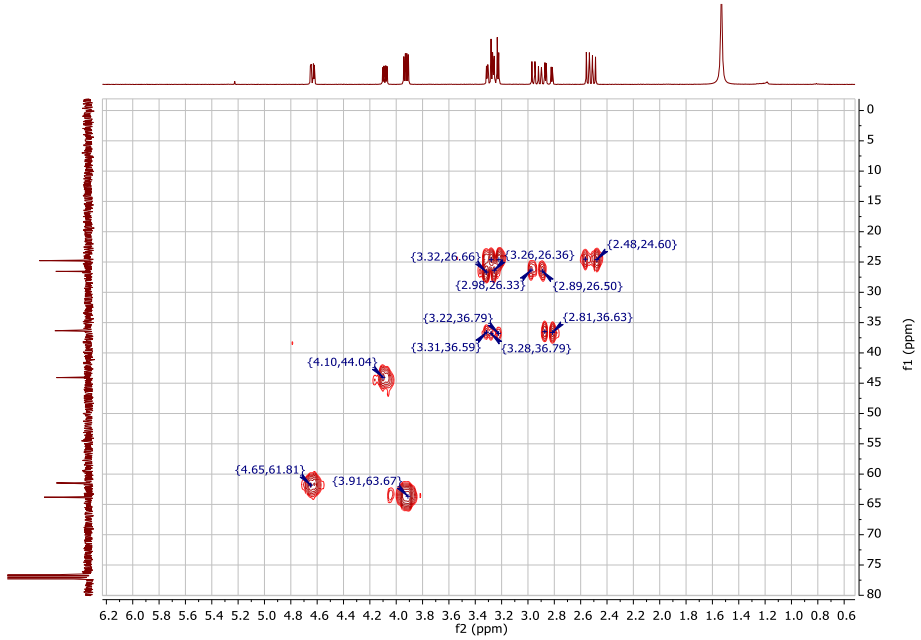

Figure S2.6. ^{1}H-^{13}C HSQC at 298 K in $CDCl_3$ spectrum of the aliphatic region of the oxidation product $\mathbf{S_1}$.

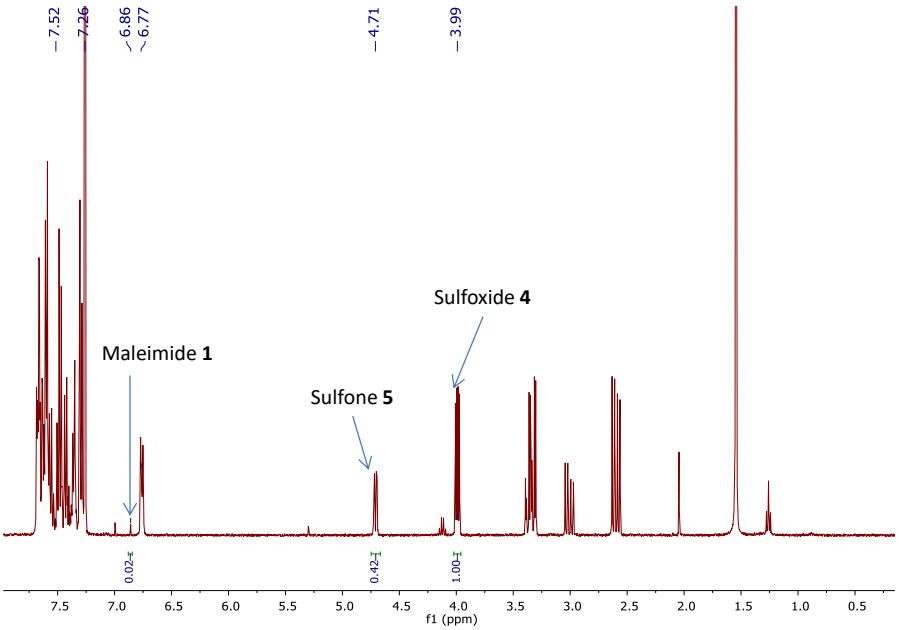

Figure S2.7. ^{1}H NMR (399.7 MHz, 298 K in $CDCl_3$) spectrum of oxidation product **S_2**.

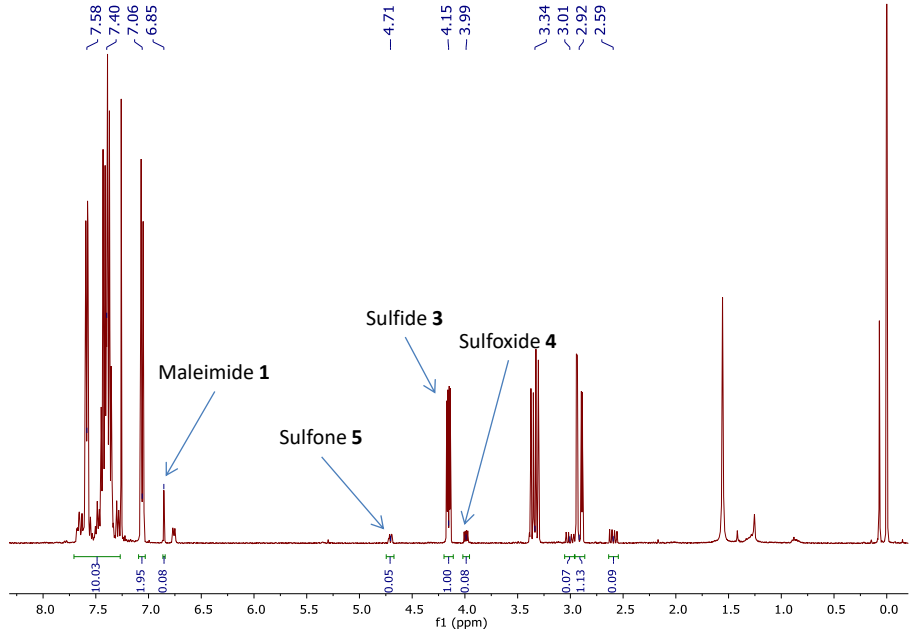

Figure S2.8. ^{1}H NMR (399.7 MHz, 298 K in $CDCl_3$) spectrum of product mixture after oxidation by H_2O_2.

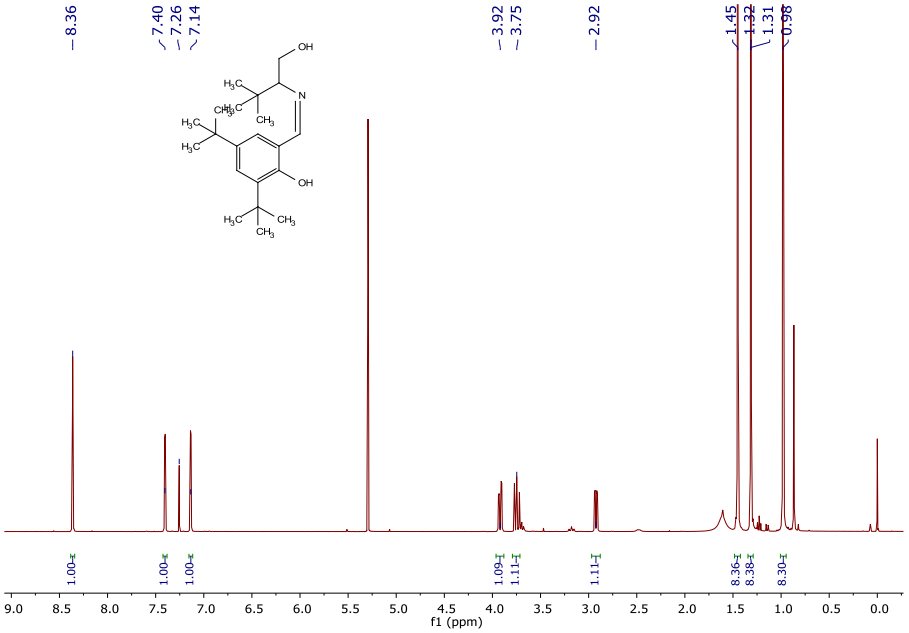

Figure S2.9. ^{1}H NMR (399.7 MHz, 298 K in $CDCl_3$) spectrum of ligand **1**.

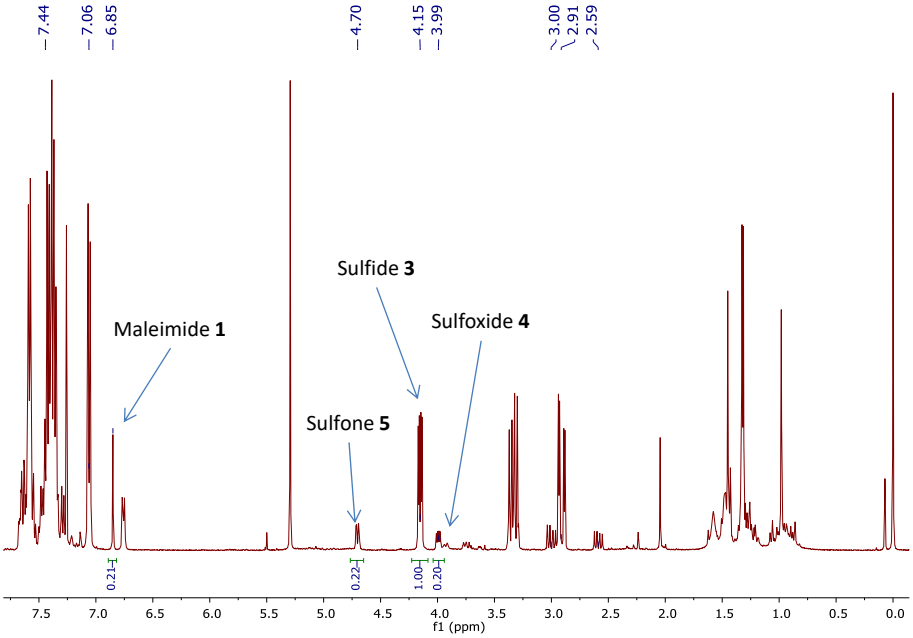

Figure S2.10. ^{1}H NMR (399.7 MHz, 298 K in $CDCl_3$) spectrum of product mixture after oxidation by H_2O_2 with vanadium complex catalyst.

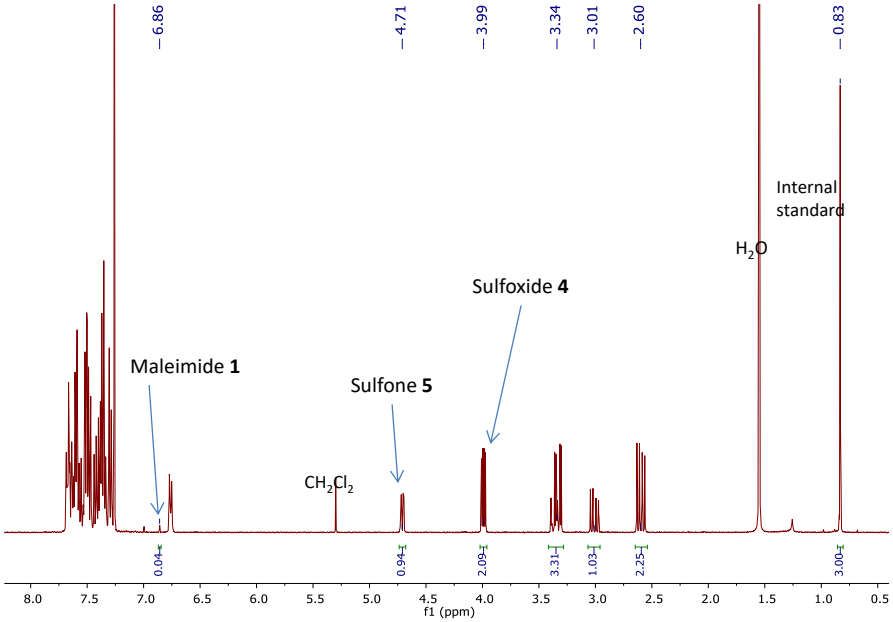

Figure S2.11. ^{1}H NMR (399.7 MHz, 298 K in $CDCl_3$) spectrum of the elimination substrate sample before elimination with DBU.

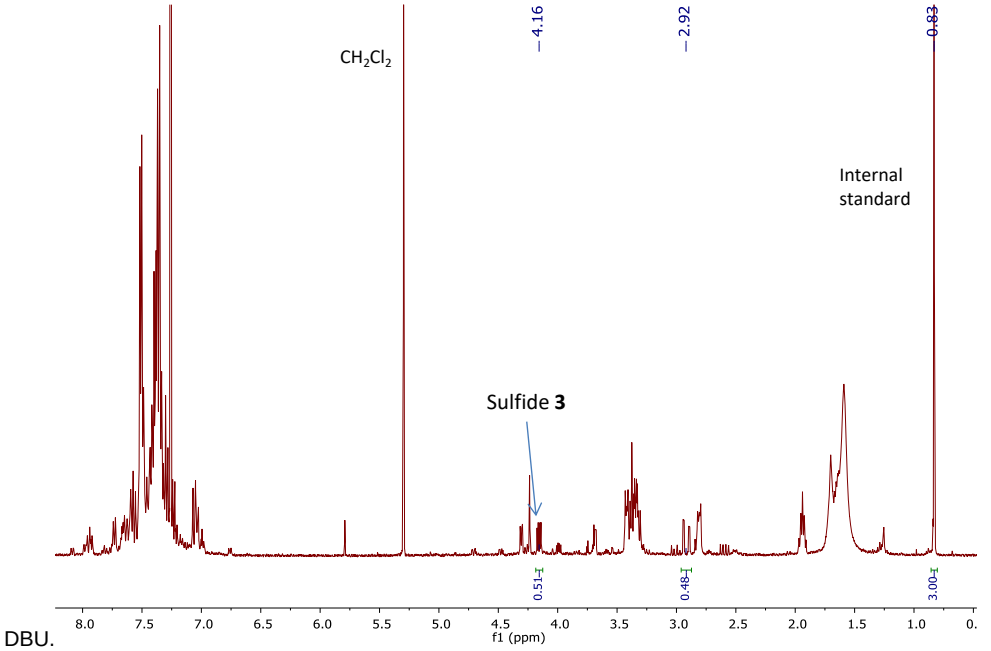

Figure S2.12. ^{1}H NMR (399.7 MHz, 298 K in $CDCl_3$) spectrum of the elimination product sample after elimination with DBU.

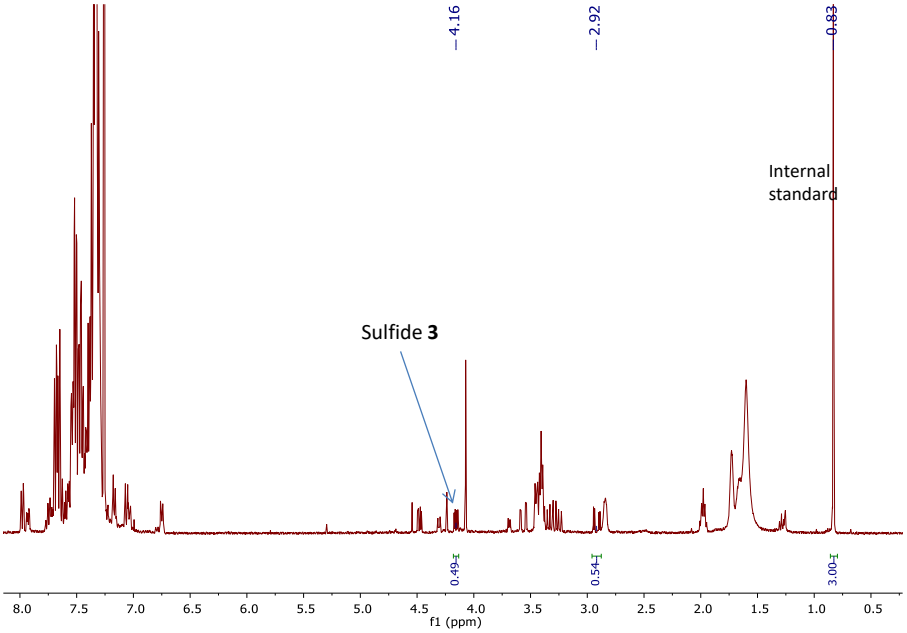

Figure S2.13. ^{1}H NMR (399.7 MHz, 298 K in $CDCl_3$) spectrum of the product mixture after addition of PPh_3 to elimination product mixture.

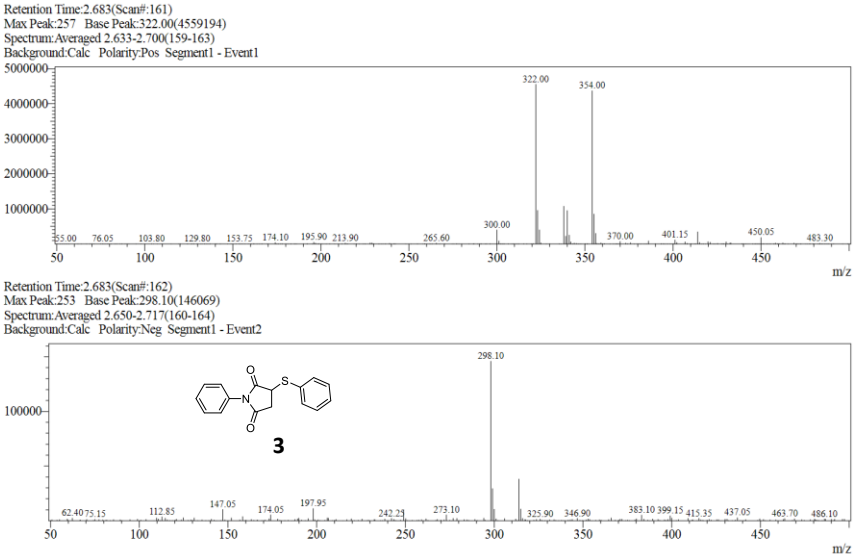

Figure S2.13. Mass spectrum of the sulfide **3**.

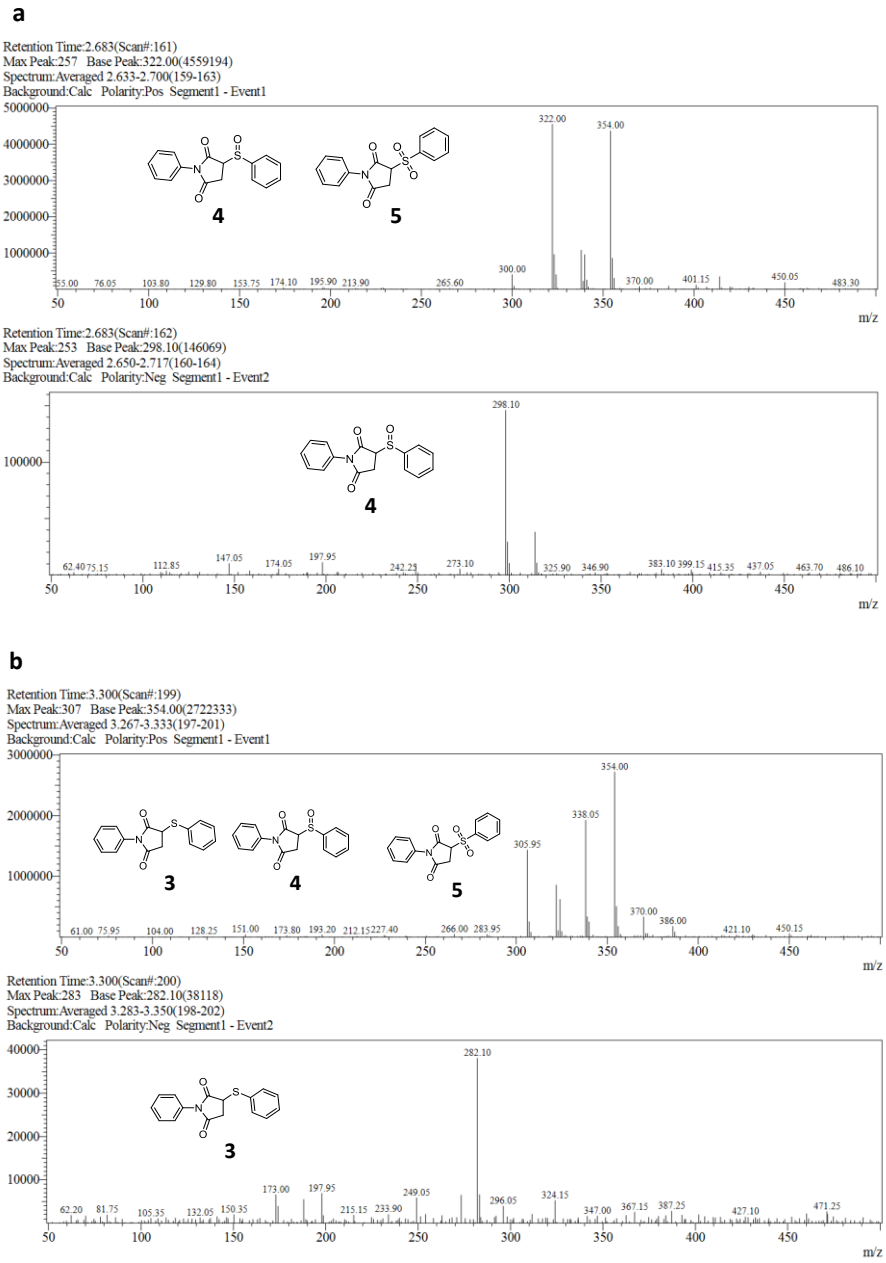

Figure S2.14. Mass spectrum of the product mixture after oxidation of **3** by *m*-CPBA without separation. a) Retention time 2.683 min, Sulfoxide **4** ((ESI Pos.) m/z: 322.0 [(M+Na^+)$^-$] (expected m/z = 322.34), (ESI Neg.) m/z: 298.10 [(M-H^+)$^-$] (expected m/z = 298.34)), sulfone **5** ((ESI Pos.) m/z: 354.0 [(M+K^+)$^-$] (expected m/z = 354.34))

b) Retention time 3.300 min, Sulfide **3** ((ESI Pos.) m/z: 305.65 $[(M+Na^+)^-]$ (expected m/z = 306.34), (ESI Neg.) m/z: 282.10 $[(M-H^+)^-]$ (expected m/z = 282.34)), Sulfoxide **4** ((ESI Pos.) m/z: 338.0 $[(M+K^+)^-]$ (expected m/z = 338.34)), sulfone **5** ((ESI Pos.) m/z: 354.0 $[(M+K^+)^-]$ (expected m/z = 354.34)).

Supplementary references

(1) Y. Wu, F. Mao, F. Meng, X. Li, "Enantioselective Vanadium-Catalyzed Oxidation of 1, 3-Dithianes from Aldehydes and Ketones using β-Amino Alcohol Derived Schiff Base Ligands." *Adv. Synth. Catal.* **2011**, *353*, 1707–1712.

Chapter 3

Self-healing Injectable Polymer Hydrogel via Dynamic Thiol-alkynone Double Addition Crosslinks

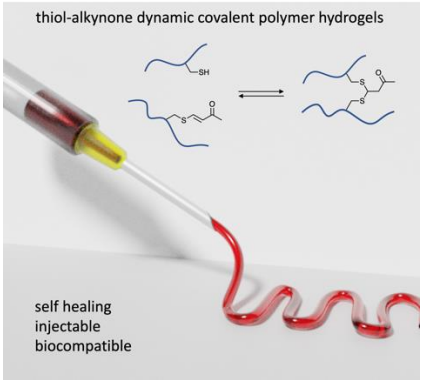

Abstract: Introduction of dynamic thiol-alkynone double addition crosslinks in a polymer network enable the formation of a self-healing injectable polymer hydrogel. A 4-arm polyethylene glycol (PEG) tetra-thiol star polymer is crosslinked by a small molecule alkynone via the thiol-alkynone double adduct, to generate a hydrogel network under ambient aqueous conditions (buffer pH=7.4 or 8.2, room temperature). The mechanical properties of these hydrogels can be easily tuned by varying the concentration of polymer precursors. Through the dynamic thiol-alkynone double addition crosslink, these hydrogels are self-healing and shear thinning, as demonstrated by rheological measurements, macroscopic self-healing and injection tests. These hydrogels can be injected through a 20G syringe needle and recover after extrusion. In addition, good cytocompatibility of these hydrogels is confirmed by cytotoxicity test. This work shows the application of the thiol-alkynone double addition dynamic covalent chemistry in the straightforward preparation of self-healing injectable hydrogels, which may find future biomedical applications such as tissue engineering and drug delivery.

This chapter is mainly based on:
B. Fan, K. Zhang, Q. Liu, R. Eelkema, "Self-Healing Injectable Polymer Hydrogel via Dynamic Thiol-Alkynone Double Addition Cross-Links" *ACS Macro Lett.* **2020**, *9*, 776–780.

3.1 Introduction

Polymer hydrogels are soft materials with many properties similar to those of biological tissue, leading to current and future applications as biomedical materials, for instance in tissue engineering, wound dressing and drug delivery.[1–3] Where conventional hydrogels have a static, permanent network structure, dynamic or reversible, responsive hydrogels have recently attracted attention for application in the biomedical field, as well as in soft robotics.[4] As a prime example of dynamic materials, self-healing injectable hydrogels show fascinating properties such as autonomous healing after damage and maintaining viscoelastic integrity after injection. These properties are highly important for biomedical applications such as minimally invasive implantation of cells and drug delivery vehicles.[5–7] Currently, there are two general approaches to generate the dynamic interactions between hydrogel fibers or polymer chains for constructing self-healing injectable hydrogels: noncovalent bonds (e.g., hydrogen bonds, ionic bonds, host-guest interactions)[8,9] and dynamic covalent bonds (e.g., boronic ester, Schiff base and disulfide bonds).[10–14] So far, a few examples of self-healing injectable hydrogels based on dynamic covalent bonds (DCBs) have been developed as well as applied in for example the repair of the central nervous system,[15] or the delivery of an antitumor drug.[14] However, there are currently only a few types of dynamic covalent chemistry that meet the requirements for constructing self-healing injectable hydrogels. On one hand, some dynamic covalent bonds are only reversible under harsh conditions, impeding their application in hydrogels. For example, Diels-Alder reactions are generally only reversible at high temperatures,[16] hydrazone formation and exchange requires an acidic environment.[17] On the other hand, although some DCBs can used in self-healing hydrogels, too complicated synthetic procedures for precursors or prepolymers may limit their application.[11–14] Therefore, dynamic covalent chemistry that operates under ambient conditions while allowing simple hydrogel preparation procedures would be a valuable extension of the toolbox of reversible chemistry needed for the development of responsive hydrogel materials, as demonstrated here in the construction of a self-healing injectable hydrogel.

The reversible thiol-alkynone double conjugate addition is a recently developed dynamic covalent bond forming reaction, that now starts to find its way into some applications. Anslyn and coworkers investigated β-dithiane carbonyls (the thiol-alkynone double adduct) and β-sulfido-α,β-unsaturated carbonyls (the thiol-alkynone single adduct), demonstrating the reversibility of the thiol-alkynone double addition on small molecules.[18] Based on this chemistry, applications such as dynamic combinational libraries, cleavage methods in peptide modification and adaptable dynamic covalent polymer networks [19–21] were reported in recent years. Previous studies[20] found that the first addition between a thiol and a conjugated alkynone is an irreversible reaction, but the second step, the addition between the single adduct and a second thiol, is a reversible reaction (**Figure 3.1a**). Although the thiol-alkyne single addition has been applied in formation of hydrogel and polymer materials,[22–24] so far there is no example of using the thiol-alkynone double addition as a reversible bond to tailor the properties of hydrogel materials. Other dynamic thiol-Michael approaches based on thiol−acrylate and thiol-benzalcyanoacetate additions have been applied in the construction of thermo-responsive polymer materials.[25–28] Here, we propose the use of the thiol-alkynone double addition to construct a dynamic crosslinked hydrogel network from a 4-arm polyethylene glycol (PEG) tetra-thiol star polymer and a small molecule alkynone as a cross linker (**Figure 3.1b**). Rather than complicated synthesis of

precursors, two commercially available materials are used directly to generate hydrogels at ambient conditions. The mechanical properties of the obtained hydrogels can be easily tuned by varying the concentrations of the network components. These hydrogels are self-healing, shear thinning and can be injected through a medical syringe needle after which they spontaneously reform a gel. Importantly, such hydrogels exhibit dynamic viscoelastic behavior and biocompatibility, showing great potential in biomedical applications.

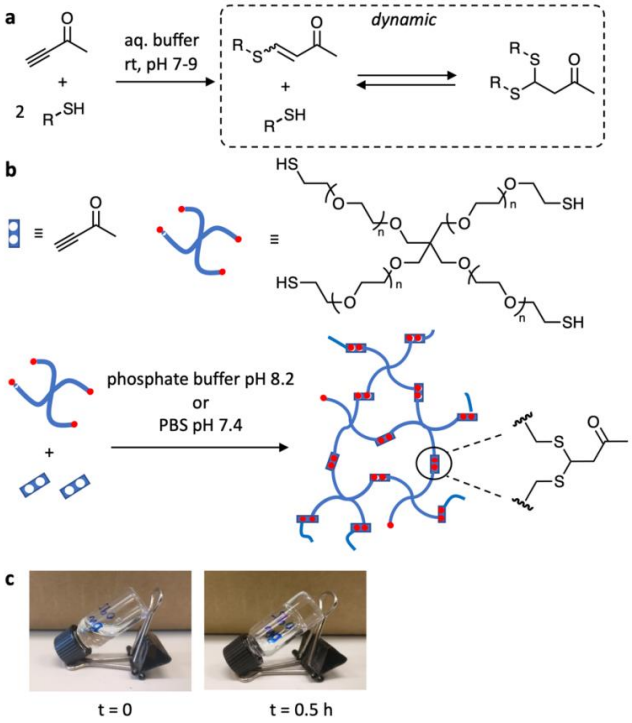

Figure 3.1. Gelation mechanism based on thiol-alkynone double conjugate addition. **a)** The thiol-alkynone double conjugate addition: the first thiol addition is irreversible, generating a β-sulfido enone. The second thiol addition to the formed enone is reversible, generating a dynamic bond. **b)** Schematic presentation of hydrogel formation via thiol-alkynone double addition, by crosslinking a tetra thiol star polymer with the alkynone. **c)** A solution of thiol polymer and alkynone in PB8.2, at the start of the gelling process (left) and after 0.5 hour (right), when a transparent gel has formed.

3.2 Results and Discussion

First, we used a reaction between low molecular weight model compounds to probe the feasibility of this reaction in mild aqueous conditions. 3-Butyn-2-one (as alkynone) reacted with two equivalents 2-mercaptoethanol to generate the mercaptoethanol-alkynone double adduct with 95% conversion after 1 hour in sodium phosphate buffer (100 mM phosphate, pH=8.2; 'PB8.2') at room temperature (**Figure S3.1**). We also tested the dynamic nature of the thiol-alkynone double addition by adding another small molecule thiol (sodium 2-mercaptoethanesulfonate) into the mercaptoethanol-alkynone double adduct PB8.2 solution.

We observed generation of the new thiol-alkynone double adduct and release of mercaptoethanol over the course of 5 hours, monitored by ^{1}H NMR, suggesting that the system was undergoing dynamic exchange in PB8.2 at room temperature (**Figure S3.3**). Then, using the same conditions, we investigated the use of a high molecular weight tetrathiol star polymer with 3-butyn-2-one as a low molecular weight crosslinker. Upon simply mixing 3-butyn-2-one PB8.2 solution (0.39 µL in 100 µL, 50 mM) and 4-arm PEG thiol PB8.2 solution (25 mg polymer (Mw = 10 kDa, Đ ≤ 1.05) in 150 µL, 16.7 wt%) in a 1:2 molar ratio of alkynone and thiol groups at room temperature, the storage modulus (G') surpassed the loss modulus (G") ~30 minutes after mixing the two solutions, indicating the formation of a hydrogel **(Figure 3.2a)**. This process resulted in the formation of a transparent, colorless hydrogel with a G' of 3.9*10^{3} Pa and tan δ (G"/G') of 4.0*10^{-3} (10 wt% network content). We also determined the progress of single and double addition product formation in the hydrogel, in relation to gel formation, using ^{1}H NMR spectroscopy and the tube-inversion method. ^{1}H NMR showed the disappearance of alkynone together with the appearance and decrease of single adduct followed by the appearance and increase of double adduct on a timescale of minutes (single adduct) to hours (double adduct). **(Figure S3.4 and S3.5)** Gelation coincided with the conversion to the double adduct (the crosslink) surpassing ~60%.

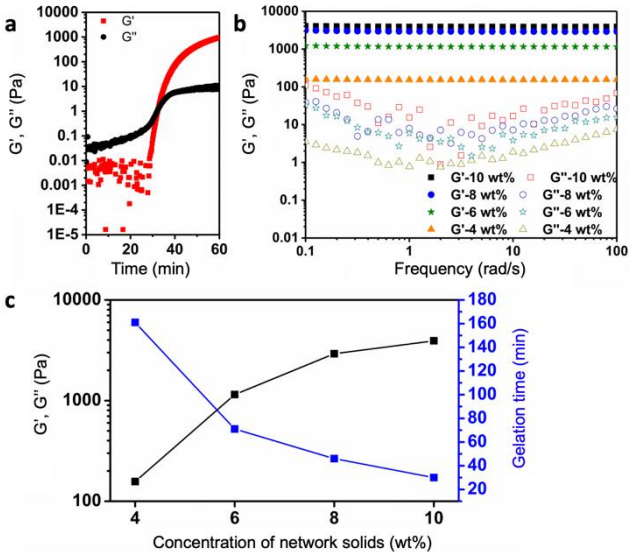

Figure 3.2. Rheological properties of hydrogels. **a)** Time sweep measurement of the gelation process of a 10 wt% hydrogel (γ = 1%, ω = 1 Hz, 25 °C). **b)** Frequency sweeps of the hydrogels with 4 wt%, 6 wt%, 8 wt% and 10 wt% solid concentration (γ = 1%, ω = 0.1-100 rad/s, 25 °C). c) The storage moduli (G') and gelation time of hydrogels with solid concentration 4 wt%, 6 wt%, 8 wt% and 10 wt%.

To investigate the influence of alkynone cross-linker on hydrogel formation we performed experiments varying the molar ratio of alkynone and thiol group (2:1, 1:1, 1:4, 1:8) (**Table S3.1**). The vial-inversion method and rheological time sweep measurements were used for checking hydrogel formation and gelation time. At 2:1 and 1:1 alkynone:thiol ratios no hydrogel formation is observed, the mixtures remain liquid. Under these conditions, the excess of alkynone limits the reaction to the formation of the single addition product, which

does not function as a crosslink in the material. At 1:4 and 1:8 alkynone:thiol ratios hydrogels did form, albeit on slightly longer time scales (~50 min and ~90 min, respectively) and lower final storage modulus ($2.1*10^3$ Pa and $1.2*10^3$ Pa, respectively) than the 1:2 hydrogel (**Figure S3.6**). The low alkynone content likely leads to slower crosslinking and fewer crosslinks formed, causing longer gelation times and gels with a lower final G'. In the following experiments, we set the ratio of alkynone and thiol groups to 1:2 to ensure efficient crosslinking in these hydrogels.

The influence of polymer content on the gelation and mechanical properties of these hydrogels was studied by rheological time and frequency sweep experiments on hydrogels with varying solid concentration (4 - 10 wt%) (**Figure S3.7 and Figure 3.2b**). From Figure 3.2b it can be seen that for all hydrogels, G' remained constant between 0.1-100 rad/s oscillatory frequency and was always larger than G", which indicates elastic behavior and a gel-like state of the samples. The gelation time and mechanical properties of these hydrogels show a dependence on polymer concentration. G' increases from $1.6*10^2$ Pa for the 4 wt% hydrogel to $3.9*10^3$ Pa for the 10 wt% hydrogel and gelation times decrease from ~160 min for the 4 wt% hydrogel to ~30 min for the 10 wt% hydrogel (**Figure 3.2c**). Facile control over mechanical properties of hydrogels is desired for various tissue engineering and in vivo hydrogel applications, where a match in mechanical strength between hydrogel and tissue is required.[29]

As phosphate buffered saline (PBS) is more relevant to physiological conditions, we also tested a 10 wt% hydrogel formed in PBS (100 mM, pH=7.4, 'PBS7.4') for rheological behavior (**Figure S3.8**). Hydrogel formation in PBS (Gel-PBS7.4) takes 6.5 hours which is much longer than the 0.5 hour gelation time in PB8.2 (Gel-PB8.2). The long gelation time in PBS7.4 may hinder application for cell encapsulation. However, the final storage modulus observed for the 10 wt% hydrogel formed in PB8.2 ($G'=3.9*10^3$ Pa) is similar to that of the hydrogel formed in PBS ($G'=3.8*10^3$ Pa), indicating a similar crosslink density. The origin of the difference in gelation rate in different buffer conditions was studied using small molecule model tests. The rate of double addition between small molecules 3-butyn-2-one (1 eq.) and 2-mercaptoethanol (2 eq.) in PB8.2 and PBS7.4 were monitored by ^{1}H-NMR (**Scheme S3.4, Figure S3.9-S3.11**), which showed that the equilibration time of double addition in PBS7.4 (~4 hours) is much slower than in PB8.2 (~1 hour). Still, in both cases a similar final conversion to double adduct was observed (~95%). PB8.2 and PBS7.4 differ in pH and salt concentration. According to a previous report, the rate of thiol-alkynone double addition increases with pH,[20] which explains the increased rate of gelation in PB8.2.

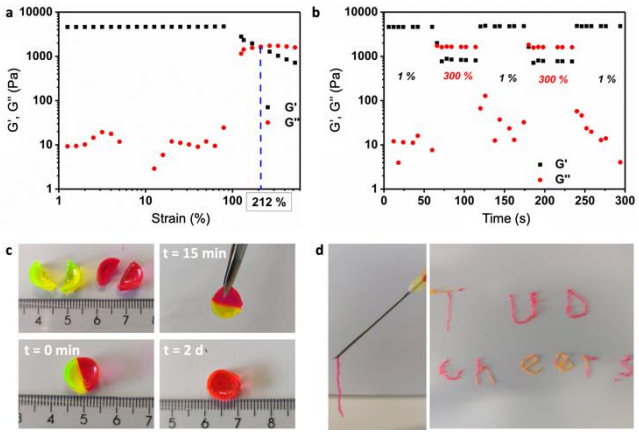

Figure 3.3. Self-healing and injectable properties of hydrogels. **a)** Strain sweep of 10 wt% Gel-PB8.2. **b)** step strain measurement of 10 wt% Gel-PB8.2, strain is switched from 1% to 300% to 1%, for two cycles. **c)** macroscopic self-healing of 10 wt% Gel-PB8.2 (thickness: 4 mm; diameter: 9 mm). Two gel cylinders were made, each containing a dye (The yellow dye is fluorescein, the red dye is rhodamine B, both are incorporated in the gel by mixing them into the gelling solution). Both were cut in half using a scalpel, and then one half of each was pressed together with the other color gel. After 15 minutes, the two parts had adhered and could hold their own weight. After two days, the dyes diffused into the opposite piece and the crack visually disappeared. **d)** Gel injection: immediate gel formation upon hand-pressing an 8 wt% Gel-PB8.2 through a 20G needle, leading to a 0.6±0.2 mm diameter strip-shaped hydrogel. Fluorescein and rhodamine B dyes are added to the gel for visualization. The extruded Gel-PB8.2 allowed printing stable structures, in this case words with feature sizes on the mm scale.

We investigated the response of these hydrogels to mechanical failure. Initially, a rheological strain sweep was measured on the 10 wt% Gel-PB8.2 to determine the critical strain value to disrupt the hydrogel network and induce a gel-sol transition. As can be seen in **Figure 3.3a**, G' starts to decrease substantially when a strain over 80 % is applied, showing the beginning of the nonlinear viscoelastic region. There is a crossover point of G' and G" at the critical strain value of 212%. Next, a step strain measurement was performed on PB8.2 hydrogels, starting at 1% strain, then going to 300% strain and back to 1% strain, with for each value a 1 minute interval of constant strain. As illustrated by **Figure 3.3b**, when the hydrogel was subjected to 300% strain, G' dropped from $3.9*10^3$ Pa to $8*10^2$ Pa. tan δ (G"/G') became >1, suggesting the collapse of the hydrogel network and conversion to a viscous fluid state. Return to 1% strain led to a quick recovery of the initial G' value and a tan δ < 1, which means the hydrogel network recovered immediately. Next, we performed a macroscopic self-healing test by reconnecting two pieces of hydrogel (**Figure 3.3c and Figure S3.14**). Two disk shape hydrogels were stained with either fluorescein (yellow) or rhodamine B (red). Both were cut into equal halves using a scalpel. Two different color pieces were then pressed together at the side of the cut. After 15 min, the two pieces had reconnected and the integrated hydrogel could be lifted by a tweezer, bearing its own weight. After ~10 hours, the dyes diffused into the opposite piece, indicating the formation of a continuous gel structure. The crack visually disappeared over the course of two days. The

self-healing properties of a 10 wt% Gel-PBS7.4 were also investigated by step strain measurement and macroscopic self-healing experiments (**Figure S3.12** and **S3.15**). There, we observed macroscopic self-healing of cut gels as well as quick recovery after applying a 300% strain. Two notable differences were that even at 300% strain, tan δ remained <1 and the gel recovered to only 88% of the initial G' after removing the strain.

Rheological viscosity-shear rate flow step measurements showed that these hydrogels are shear-thinning (**Figure S3.13**). The viscosity of a 10 w/v% hydrogel (Gel-PB8.2) decreased with increasing shear rate, from $5.0*10^3$ Pa·s at 0.1 s^{-1} to $0.13*10^3$ Pa·s at 80 s^{-1}. When a large shear stress is applied, the viscosity of a hydrogel will decrease and the hydrogel should show viscous flow through a needle. A 10 w/v% hydrogel formed in PB8.2 was unable to pass through a 20G needle (0.9 mm diameter, sufficiently narrow for subcutaneous injections) probably due to its highly dense, crosslinked network. However, an 8 w/v% hydrogel formed in PB8.2 and a 10 w/v % hydrogel formed in PBS7.4 can both be successfully injected through a 20G syringe needle (**Figure 3.3d and Figure S3.15**). The extruded hydrogel instantly recovers upon exiting the needle, as at that point the shear stress is removed. We demonstrated gel injection and recovery by writing letters made from 8% Gel-PB8.2 passed through a 20G needle. In principle, this property of these hydrogels should also allow future 3D-printing to construct structured gel materials.[30]

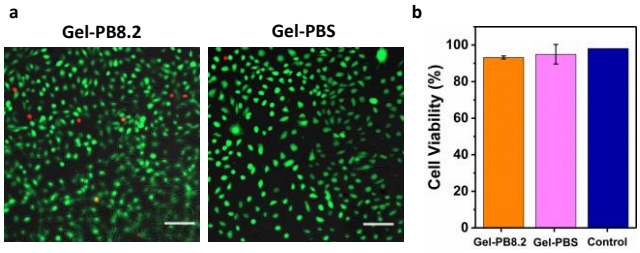

Figure 3.4. Biocompatibility of hydrogels. **a)** Fluorescence microscopy images of NIH/3T3 cells after live/dead assay with calcein AM (green, live cells) and propidium iodide (red, dead cells). The cells were incubated together with Gel-PB8.2 (left) and Gel-PBS7.4 (right) around 48 h. Scale bar = 100 µm. **b)** Cell viability of NIH/3T3 cells after incubating with Gel-PB8.2, Gel-PBS7.4 and without hydrogel (control experiment). Error bars indicate the s.d. of three independent experiments.

The cytotoxicity of 10 wt% Gel-PB8.2 and Gel-PBS7.4 was evaluated using the live/dead staining assay with NIH/3T3 cells (mouse fibroblast cells). The cells were loaded on a piece of hydrogel and co-cultured in the cell culture media at 37 °C in 5%/95% CO_2/Air atmosphere. After incubating of 48 h, the cell viability was checked. As shown in Figure 3.4a and 3.4b, the cell viability in the control experiment was around 98%, and only slightly lower viability was observed in both Gel-PB8.2 (93%) and Gel-PBS7.4 (94%). It indicates that the thiol-alkynone double addition hydrogels exhibit a good biocompatibility.

3.3 Conclusion

In conclusion, we have developed a novel self-healing injectable hydrogel based on dynamic thiol-alkynone double addition chemistry. The thiol-alkynone double addition reaction enables facile synthesis of dynamic polymer hydrogels. The mechanical properties and gelation times are easily tuned by changing the concentration of polymer precursors during

hydrogel preparation. Furthermore, the dynamic thiol-alkynone double addition endows shear-thinning and self-healing properties to these hydrogels, confirmed by rheological measurements and macroscopic self-healing and injection tests. As a result, these gels can be injected through a 20G needle, to afford stable gel objects upon extrusion. A 48 hour cytotoxicity test confirmed a good biocompatibility of these hydrogels. In all, these self-healing, injectable hydrogels show promising potential in biomedical applications such as tissue engineering and drug delivery.

3.4 Reference

(1) Zhang, Y. S.; Khademhosseini, A. Advances in Engineering Hydrogels. *Science.* ***2017****, 356, 3627.*

(2) Talebian, S.; Mehrali, M.; Taebnia, N.; Pennisi, C. P.; Kadumudi, F. B.; Foroughi, J.; Hasany, M.; Nikkhah, M.; Akbari, M.; Orive, G.; Dolatshahi-Pirouz, A. Self-Healing Hydrogels: The Next Paradigm Shift in Tissue Engineering? *Adv. Sci.* **2019**, *1801664*.

(3) Li, J.; Mooney, D. J. Designing Hydrogels for Controlled Drug Delivery. *Nat. Rev. Mater.* ***2016****, 1, 1-17.*

(4) Eelkema, Rienk, and A. P. Pros and Cons: Supramolecular or Macromolecular: What Is Best for Functional Hydrogels with Advanced Properties? *Adv. Mater.* **2020**, 201906012.

(5) Tu, Y.; Chen, N.; Li, C.; Liu, H.; Zhu, R.; Chen, S.; Xiao, Q.; Liu, J.; Ramakrishna, S.; He, L. Advances in Injectable Self-Healing Biomedical Hydrogels. *Acta Biomater.* **2019**, *90*, 1–20.

(6) Lu, H. D.; Charati, M. B.; Kim, I. L.; Burdick, J. A. Injectable Shear-Thinning Hydrogels Engineered with a Self-Assembling Dock-and-Lock Mechanism. *Biomaterials*. **2012**, *33*, 2145–2153.

(7) Wei, Z.; Yang, J. H.; Zhou, J.; Xu, F.; Zrínyi, M.; Dussault, P. H.; Osada, Y.; Chen, Y. M. Self-Healing Gels Based on Constitutional Dynamic Chemistry and Their Potential Applications. *Chem. Soc. Rev.* **2014**, *43*, 8114–8131.

(8) Phadke, A.; Zhang, C.; Arman, B.; Hsu, C.-C.; Mashelkar, R. A.; Lele, A. K.; Tauber, M. J.; Arya, G.; Varghese, S. Rapid Self-Healing Hydrogels. *Proc. Natl. Acad. Sci.* **2012**, *109*, 4383–4388.

(9) Taylor, D. L.; in het Panhuis, M. Self-Healing Hydrogels. *Adv. Mater.* **2016**, *28*, 9060–9093.

(10) Scheutz, G. M.; Lessard, J. J.; Sims, M. B.; Sumerlin, B. S. Adaptable Crosslinks in Polymeric Materials: Resolving the Intersection of Thermoplastics and Thermosets. *J. Am. Chem. Soc.* **2019**, *141*, 16181–16196.

(11) Yesilyurt, V.; Webber, M. J.; Appel, E. A.; Godwin, C.; Langer, R.; Anderson, D. G. Injectable Self-Healing Glucose-Responsive Hydrogels with PH-Regulated Mechanical Properties. *Adv. Mater.* **2016**, *28* (1), 86–91.

(12) Wu, D.; Wang, W.; Diaz-Dussan, D.; Peng, Y. Y.; Chen, Y.; Narain, R.; Hall, D. G. In Situ Forming, Dual-Crosslink Network, Self-Healing Hydrogel Enabled by a Bioorthogonal Nopoldiol-Benzoxaborolate Click Reaction with a Wide PH Range. *Chem. Mater.* **2019**, *31*, 4092-4102.

(13) Wang, W.; Xiang, L.; Gong, L.; Hu, W.; Huang, W.; Chen, Y.; Asha, A. B.; Srinivas, S.; Chen, L.; Narain, R.; Zeng, H. Injectable, Self-Healing Hydrogel with Tunable Optical, Mechanical, and Antimicrobial Properties. *Chem. Mater.* **2019**, *31*, 2366–2376.

(14) Li, Y.; Yang, L.; Zeng, Y.; Wu, Y.; Wei, Y.; Tao, L. Self-Healing Hydrogel with a Double Dynamic Network Comprising Imine and Borate Ester Linkages. *Chem. Mater.* **2019**, *31*, 5576-5583.

(15) Tseng, T. C.; Tao, L.; Hsieh, F. Y.; Wei, Y.; Chiu, I. M.; Hsu, S. H. An Injectable, Self-Healing Hydrogel to Repair the Central Nervous System. *Adv. Mater.* **2015**, *27*, 3518–3524.

(16) Adzima, B. J.; Kloxin, C. J.; Bowman, C. N. Externally Triggered Healing of a Thermoreversible Covalent Network via Self-Limited Hysteresis Heating. *Adv. Mater.* **2010**, *22*, 2784–2787.

(17) Tan, K. L.; Jacobsen, E. N. Indium-Mediated Asymmetric Allylation of Acylhydrazones Using a Chiral Urea Catalyst. *Angew. Chem. Int. Ed.* **2007**, *46*, 1315–1317.

(18) Joshi, G.; Anslyn, E. V. Dynamic Thiol Exchange with β-Sulfido-α,β-Unsaturated Carbonyl Compounds and Dithianes. *Org. Lett.* **2012**, *14*, 4714–4717.

(19) Matysiak, B. M.; Nowak, P.; Cvrtila, I.; Pappas, C.; Liu, B.; Komaromy, D.; Otto, S. Antiparallel Dynamic Covalent Chemistries. *J. Am. Chem. Soc.* **2017**, *139*, 6744-6751.

(20) Shiu, H. Y.; Chan, T. C.; Ho, C. M.; Liu, Y.; Wong, M. K.; Che, C. M. Electron-Deficient Alkynes as Cleavable Reagents for the Modification of Cysteine-Containing Peptides in Aqueous Medium. *Chem. Eur. J.* ***2009****, 15, 3839–3850.*

(21) Van Herck, N.; Maes, D.; Unal, K.; Guerre, M.; Winne, J. M.; Prez, F. E. Du. Covalent Adaptable Networks with Tunable Exchange Rates Based on Reversible Thiol-Yne Cross-Linking. *Angew. Chem. Int. Ed.* **2019,** *9*, 3609-3617.

(22) Truong, V. X.; Dove, A. P. Organocatalytic, Regioselective Nucleophilic “Click” Addition of Thiols to Propiolic Acid Esters for Polymer-Polymer Coupling. *Angew. Chem. Int. Ed.* **2013**, *52*, 4132–4136.

(23) Macdougall, L. J.; Pérez-Madrigal, M. M.; Arno, M. C.; Dove, A. P. Nonswelling Thiol-Yne Cross-Linked Hydrogel Materials as Cytocompatible Soft Tissue Scaffolds. *Biomacromolecules* **2018**, *19*, 1378–1388.

(24) Macdougall, L. J.; Truong, V. X.; Dove, A. P. Efficient in Situ Nucleophilic Thiol-Yne Click Chemistry for the Synthesis of Strong Hydrogel Materials with Tunable Properties. *ACS Macro Lett.* **2017**, *6*, 93–97.

(25) Zhang, B.; Digby, Z. A.; Flum, J. A.; Chakma, P.; Saul, J. M.; Sparks, J. L.; Konkolewicz, D. Dynamic Thiol-Michael Chemistry for Thermoresponsive Rehealable and Malleable Networks. *Macromolecules* **2016**, *49*, 6871–6878.

(26) Kuhl, N.; Geitner, R.; Bose, R. K.; Bode, S.; Dietzek, B.; Schmitt, M.; Popp, J.; Garcia, S. J.; van der Zwaag, S.; Schubert, U. S.; Hager, M. D. Self-Healing Polymer Networks Based on Reversible Michael Addition Reactions. *Macromol. Chem. Phys.* **2016**, *217*, 2541–2550.

(27) El-Zaatari, B. M., Ishibashi, J. S., & Kalow, J. A. Cross-Linker Control of Vitrimer Flow. *Polym. Chem.* **2020**, DOI: 10.1039/d0py00233j

(28) Herbert, K. M.; Getty, P. T.; Dolinski, N. D.; Hertzog, J. E.; Jong, D. De; Lettow, J. H.; Romulus, J.; Onorato, J. W.; Foster, E. M.; Rowan, S. J. Dynamic Reaction-Induced Phase Separation in Tunable, Adaptive Covalent Networks. *Chem. Sci.* **2020**, DOI: 10.1039/d0sc00605j.

(29) Discher, D. E.; Mooney, D. J.; Zandstra, P. W. Growth Factors, Matrices, and Forces Combine and Control Stem Cells. *Science* **2009**, *324*, 1673–1677.

(30) Truby, R. L.; Lewis, J. A. Printing Soft Matter in Three Dimensions. *Nature* **2016**, *540*, 371–378.

3.5 Supplementary information

3.5.1. Materials and Measurements

NMR spectra were recorded on an Agilent-400 MR DD2 (399.7 MHz for ^{1}H and 100.5 MHz for ^{13}C) at 298 K. The rheological measurements were performed using a rheometer (AR G2, TA instruments) equipped with a steel plate-and-plate geometry of 40 mm in diameter and equipped with hexadecane trap. Cell viability were obtained by Andor Inverted Microscope (Zeiss, ×20 air objective). Thiol terminated 4-arm poly(ethylene glycol) (PEG10k-4-SH, Mw = 10 000, PDI ≤ 1.05) was purchased from JenKem Technology (USA). 3-Butyn-2-one was purchased from Fluorochem ltd. 2-Mercaptoethanol, sodium 2-mercaptoethanesulfonate, phosphate buffered saline, Dulbecco's phosphate-buffered saline (DPBS), Calcein AM, Fluorescein，Rhodamine B and Dulbecco's modified eagle medium (DMEM), fetal bovine serum (FBS), penicillin/streptomycin (Pen-Strep) were purchased from Sigma Aldrich. Propidium iodide (PI) was purchased from Thermo Fisher Scientific Inc. NIH/3T3 cell (mouse fibroblast cells) culture line was obtained from American Type Culture Collection. Deuterium Oxide (D_2O) was purchased from Euriso-top. Hexadecane was purchased from VWR International BV. All chemicals were analytical grade and used without further purification.

3.5.2. Experimental Methods

Dynamic exchange of thiol-alkynone double addition products

First, the double addition between 2-mercaptoethanol (thiol#1) and 3-butyn-2-one was followed by ^{1}H NMR. 2-Mercaptoethanol (6.2 µL, 0.088 mmol) and 3-butyn-2-one (3.4 µL, 0.044 mmol) were dissolved in a 1 mL solution of phosphate buffer solution (100 mM, pH=8.2; 'PB8.2') including 4 drops of D_2O. Sodium trimethylsilylpropanesulfonate (1 mg) was added as the internal standard. The ^{1}H NMR spectrum was obtained after 1-hour reaction time. Then, the double addition between sodium 2-mercaptoethanesulfonate (thiol#2) and 3-butyn-2-one was followed by ^{1}H NMR using the same procedure as described above. The ^{1}H NMR spectrum was obtained after 4 hours reaction time. Next, the thiol#1-alkynone double adduct was prepared as describe above. Sodium 2-mercaptoethanesulfonate (7.23 mg, 0.044 mmol) was added into the thiol#1-alkynone double adduct in PB8.2 at room temperature. The dynamic exchange was monitored by ^{1}H NMR.

Preparation of Thiol-alkynone double addition hydrogel

The thiol-alkynone double addition hydrogel was prepared by a mixing procedure. 4-arm PEG thiol (25 mg) was dissolved in 150 µL PB8.2 as PEG-thiol solution. 3-butyn-2-one (3.9 µL, 'alkynone') was dissolved in 1 mL PB8.2 as alkynone solution. A transparent colorless hydrogel was obtained by mixing 150 µL PEG-thiol solution (25 mg polymer in 150 µL, 16.7 wt%) and 100 µL alkynone solution (0.39 µL in 100 µL, 50 mM) in a glass vial at room temperature. Starting from these amounts, the total solid concentration is 10 wt % and the ratio of alkynone to thiol groups is 1:2.

Monitoring of single addition and double addition products during hydrogel formation

4-arm PEG thiol (60 mg) was dissolved in 140 µL PB8.2 and 10 µL D_2O ('PEG-thiol solution'). 3-butyn-2-one (9 µL) was dissolved in 950 mL PB8.2 and 50 µL D_2O ('alkynone solution'). 150 µL PEG-thiol solution and 100 µL alkynone solution were mixed in an NMR tube at room temperature. Sodium trimethylsilylpropanesulfonate (1 mg) was added as the internal standard. The reaction during hydrogel formation was monitored by ^1H NMR at room temperature. The hydrogel formation was tested by the tube-inversion method after each NMR measurement.

Gelation test: variation of alkynone/thiol ratio

The same amount of 4-arm PEG thiol PB8.2 solutions (25 mg in 150 µL, 16.7 wt%) was mixed with 100 µL alkynone PB8.2 solutions containing varying amount of alkynone (1.57 µL, 0.78 µL, 0.20 µL and 0.01 µL) to prepare alkynone-thiol pre-gel solutions (alkynone: thiol group= 2:1; 1:1; 1:4; 1:8). Gelation and gelation time were tested by vial-inversion method rheological experiments. The vial is a 12 mm diameter, 32 mm high glass vial. The hydrogel formation was checked by reverting vial every half hour in first 2 hour, then every 2 hours in next 10 hours, then every half day in next 1.5 days. If no hydrogel formed after 2 days, we concluded there is no hydrogel formation under this ratio condition. Once the hydrogels under certain ratios were able to form, the rheological time sweeps of those hydrogels were conducted using the procedures described in 2.6. The total solid content was set as 10 wt %.

Preparation of Thiol-alkynone double addition hydrogel with varying solid concentration

Similar to hydrogels containing 10 wt% solid concentration, we also prepared hydrogels with 2 wt%, 4 wt%, 6 wt%, 8 wt% solid concentration using the same procedure. The ratio of alkynone and thiol group is 1:2 in all cases. Gelation and gelation time were tested by vial-inversion method and rheological experiments.

Preparation of Thiol-alkynone double addition hydrogel in PBS7.4

Gels were prepared using the same preparation procedure as before, except using phosphate buffered saline solution (100 mM, pH=7.4, prepared by dissolving a commercial PBS tablet in 200 mL distilled water, 'PBS7.4') instead of PB8.2.

Model Reactions

The aim of small molecular model reactions is to study the gelation mechanism in two different condition of PB8.2 and PBS7.4. The rate of double additions between 2-mercaptoethanol and 3-butyn-2-one were followed by ^1H NMR. 2-Mercaptoethanol (6.2 µL, 0.088 mmol) and 3-butyn-2-one (3.4 µL, 0.044 mmol) were dissolved in a 1 mL solution of PB8.2 including 4 drops of D_2O. Sodium trimethylsilylpropanesulfonate (1 mg) was added as the internal standard. The rate of formation of double adduct in PB8.2 between 2-mercaptoethanol and 3-butyn-2-one was monitored by ^1H-NMR. The small molecular model reaction in PBS7.4 was carried out as described above.

Rheological measurements of hydrogels

Thiol-alkynone double addition hydrogels were prepared as described above, at the different solid concentrations (4 wt %, 6 wt %, 8 wt %, 10 wt%) in PB8.2 and 10 wt% in PBS7.4. After

mixing PEG thiol solution and alkynone solution, 0.7 mL of the sample was positioned on the rheometer plate. Time sweep measurements were performed at fix strain (γ = 1%) and frequency (ω =6.28 rad/s = 1 Hz). Frequency sweep measurements were performed from 0.1 to 100 rad/s at fix strain (γ = 1%). All frequency sweeps were measured after storage modulus (G') reached equilibrium state. All measurements were performed in the linear viscoelastic region. The modulus of hydrogels was measured under strain sweep from 1 to 600% at a fixed frequency (ω = 6.28 rad/s). Continuous step strain measurements were measured at fixed frequency (ω = 6.28 rad/s). Oscillatory strains were switched from 1% strain to subsequent 300% strain with 1 minute for every strain period. The viscosity of hydrogels was measured under flow step as a function of shear rate from 0.1 /s to 80 /s to study the shear thinning behavior of the hydrogel.

Macroscopic Self-healing and Injectable Test of Hydrogels

Two pieces of disk-shaped hydrogel (thickness: 4 mm; diameter: 9 mm) were prepared as described above stained by rhodamine B (red dye) and fluorescein (yellow dye). Both hydrogels were cut into two equal pieces. Then two piece of different color hydrogels were brought together and kept in a moist environment for 15 mins. Healing of the hydrogel was checked by lifting the combined gel using tweezers. Afterwards, this healed hydrogel was cut to 4 equal pieces using a scalpel. Then a piece of hydrogels was put in a syringe (1 mL volume; 0.5 inner diameter) using a tweezer and syringe plunger, and subsequently injected through a 20G needle using manual force.

Cell Cytotoxicity

Thiol-alkynone double addition hydrogels were prepared as described above at 10 wt% in PB8.2 and PBS7.4. The hydrogel sample was cut to a ~1 mm layer of square shape (4 x 3 mm) and transferred into a sterile 8-well cell culture plate. The hydrogels of Gel-PB8.2 and Gel-PBS7.4 were sterilized with 70% ethanol (2 times), DPBS (5 times) and cell culture media (3 times). The cell culture media was made with DMEM supplemented 10% (v/v) FBS and 0.5% (v/v) Pen-Strep. Cells were cultured in 25 cm^2 tissue culture flasks and immersed in 5 mL cell culture media. Cells were washed with 3 mL DPBS, trypsinized and centrifuged. Afterwards the cells were resuspended in 3 mL cell culture media. Then the cells were added in the 8-well cell culture plate containing the hydrogel samples and incubated for 48 h. Cell viability was checked by the Live/Dead Cell Double Staining Kit with Calcein AM and propidium iodide (PI). After removing the cell culture media, the integrate pieced of hydrogel cannot be found under microscope, indicating that the hydrogel had dissolved in the medium over the period of incubation. Then 200 µL calcein AM solution (2 µM, DPBS) was added into the culture plate and incubated for 10 minutes, followed by adding 200 µL PI solution (12 µM, DPBS). After 5 minutes, the samples were placed under the fluorescence microscope and imaged by double two excitation wavelengths of 490 and 535 nm channels. In alive cells the nonfluorescent calcein AM is converted to a green-fluorescent calcein ($\lambda_{ex}/\lambda_{em}$: 490/515 nm) after acetoxymethyl ester hydrolysis by intracellular esterases. PI only permeates dead cells leading to red fluorescence ($\lambda_{ex}/\lambda_{em}$: 535/617 nm).

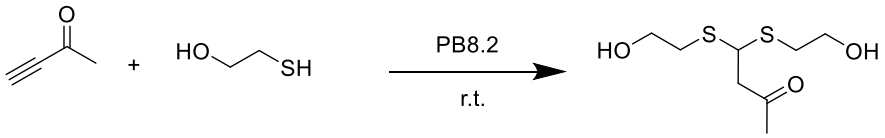

Scheme S3.1. Small molecule test of thiol-alkynone double reaction between 3-butyn-2-one and 2-mercaptoethanol in sodium phosphate buffer (100 mM, pH=8.2) at room temperature.

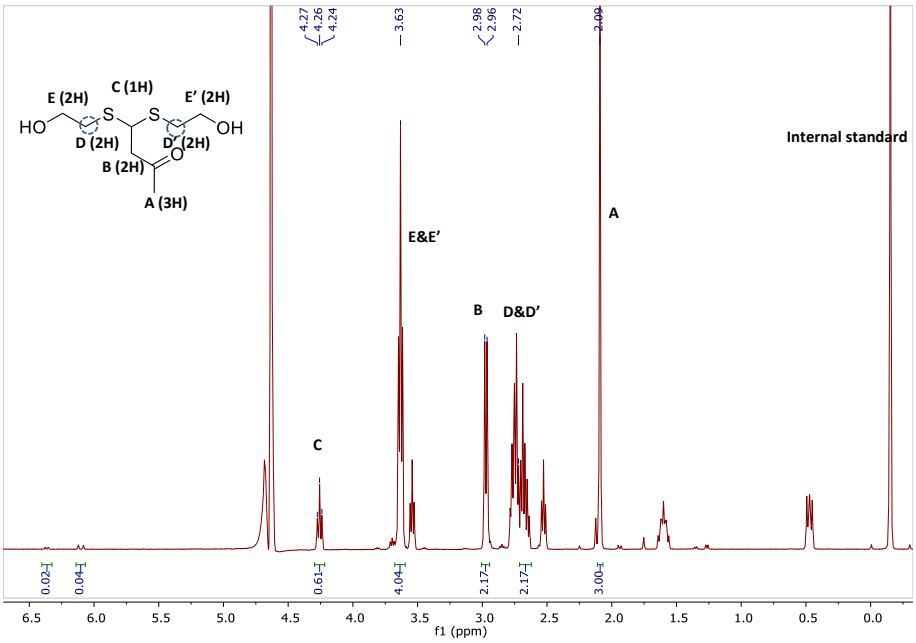

Figure S3.1. ^{1}H-NMR (399.7 MHz, 298 K in D_2O/ PB8.2, 4 drops of D_2O in 1 mL PB8.2) spectrum of thiol-alkynone double reaction between 3-butyn-2-one and 2-mercaptoethanol. 2-Mercaptoethanol (3 mg, 0.044 mmol) and 3-butyn-2-one (6.2 µL, 0.088 mmol) were dissolved in a 1 mL solution of PB8.2 including 4 drops of D_2O. The spectrum was obtained after 1hour reaction time.

.

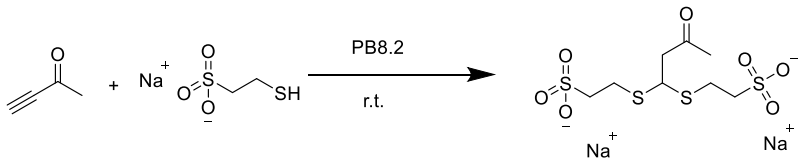

Scheme S3.2. Small molecule test of thiol-alkynone double reaction between 3-butyn-2-one and sodium 2-mercaptoethanesulfonate in sodium phosphate buffer (100 mM, pH=8.2) at room temperature.

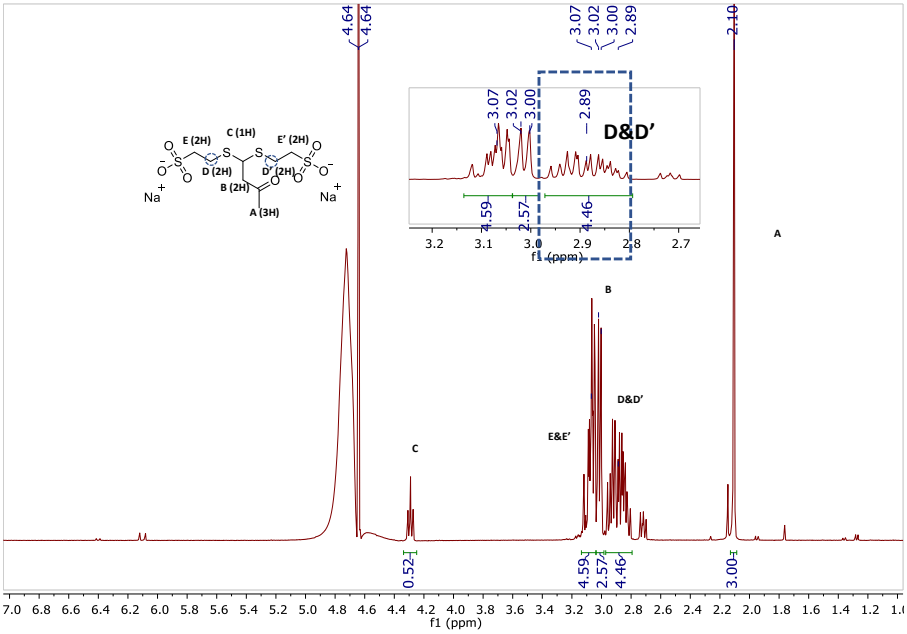

Figure S3.2. ^{1}H-NMR (399.7 MHz, 298 K in D_2O/ PB8.2, 4 drops of D_2O in 1 mL PB8.2) spectrum of thiol-alkynone double reaction between 3-butyn-2-one and sodium 2-mercaptoethanesulfonate. Sodium 2-mercaptoethanesulfonate (14.46 mg, 0.088 mmol) and 3-butyn-2-one (3 mg, 0.044 mmol) were dissolved in a 1 mL solution of PB8.2 including 4 drops of D_2O. The spectrum was obtained after 4 hours reaction time.

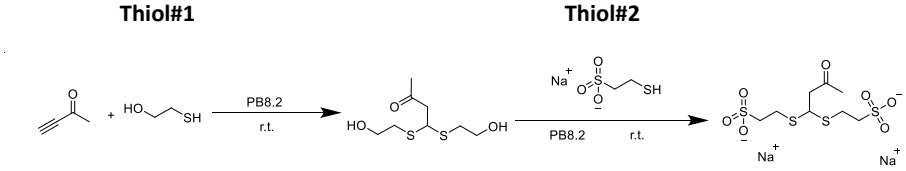

Scheme S3.3. Small molecule test of dynamic exchange between thiol#1-alkynone double adduct sodium 2-mercaptoethanesulfonate in sodium phosphate buffer (100 mM, pH=8.2) at room temperature. Besides the double 2-mercaptoethanesulfonate addition product, there is likely also formation of a mixed thiol double addition product.

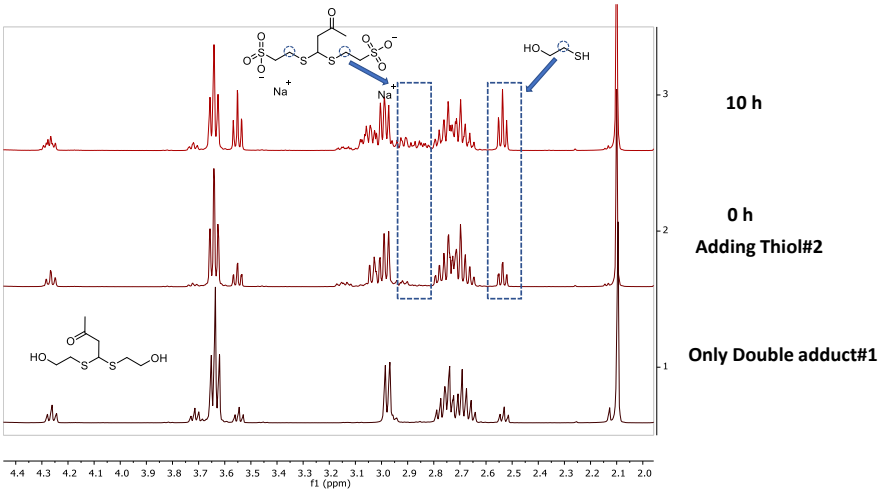

Figure S3.3. ^{1}H-NMR (399.7 MHz, 298 K in D_2O / PB8.2, 4 drops of D_2O in 1 mL PB8.2) monitoring of dynamic exchange between thiol#1-alkynone double adduct and sodium 2-mercaptoethanesulfonate (thiol#2) in sodium phosphate buffer (100 mM, pH=8.2) at room temperature.

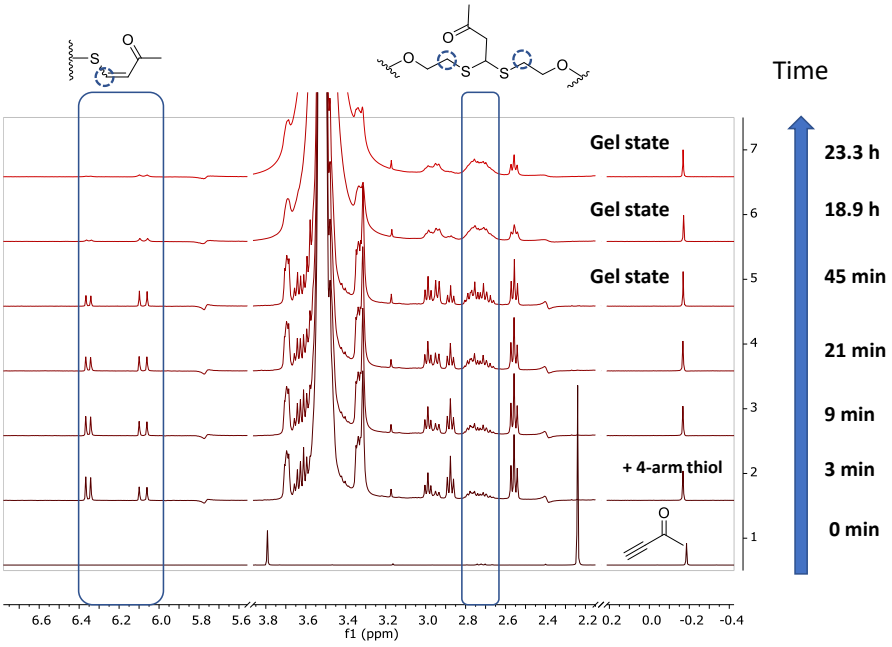

Figure S3.4. ^{1}H-NMR (399.7 MHz, 298 K in D_2O / PB8.2, 15 µL D_2O in 585 µL PB8.2) monitoring of single addition and double addition during thiol-alkynone double addition hydrogel formation between 3-butyn-2-one and 4-arm PEG thiol.

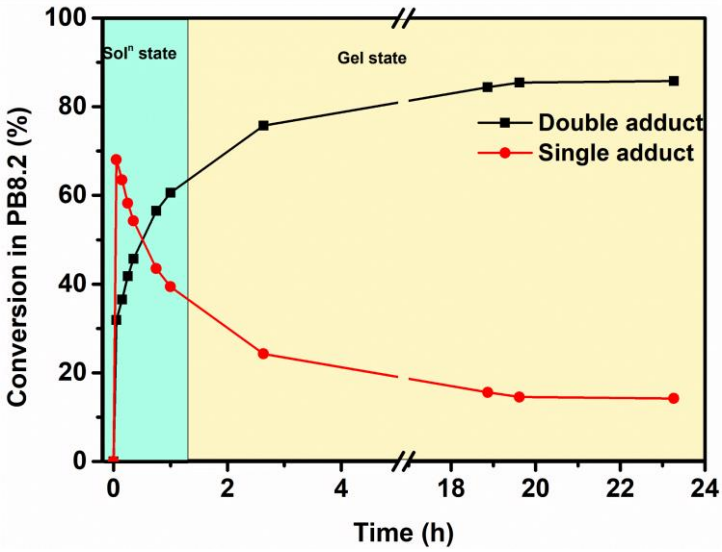

Figure S3.5. The conversion of double adduct and single adduct during thiol-alkynone double addition hydrogel formation between 3-butyn-2-one and 4-arm PEG thiol. The conversion of single adduct is calculated based on the integration of the alkene protons of the single adducts by ^{1}H NMR. The conversion of double adduct is calculated based on the integration of the methylene group of the double adduct by ^{1}H NMR. The methyl signal of sodium trimethylsilylpropanesulfonate was set as the internal standard. The cyan area in the graph indicates that the sample is in solution state. The yellow area indicates that the sample is in the hydrogel state.

Table S3.1. Gelation test with varying molar ratio of alkynone and thiol group (2:1; 1:1; 1:2; 1:4; 1:8). All experiments are run at 10% solid content and in PB8.2.

	Ratio of alkynone and thiol group				
Alkynone	1	1	1	1	2
Thiol group	8	4	2	1	1
Gelation Time*	~90 min	~50 min	~30 min	ng**	ng**

* Gelation time is defined as the time it takes to reach the gel point (G'=G") as measured by rheology.

**: no gel, i.e. no hydrogel is observed after two days reaction time, checked by vial-inversion method.

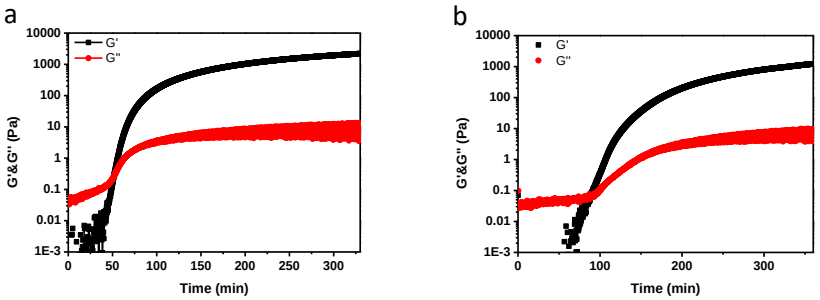

Figure S3.6. Time sweep measurements of the gelation process of a) hydrogel at 1:4 alkynone: thiol ratio; b) hydrogel at 1:8 alkynone: thiol ratio (γ = 1%, ω = 1 Hz, 25 °C)

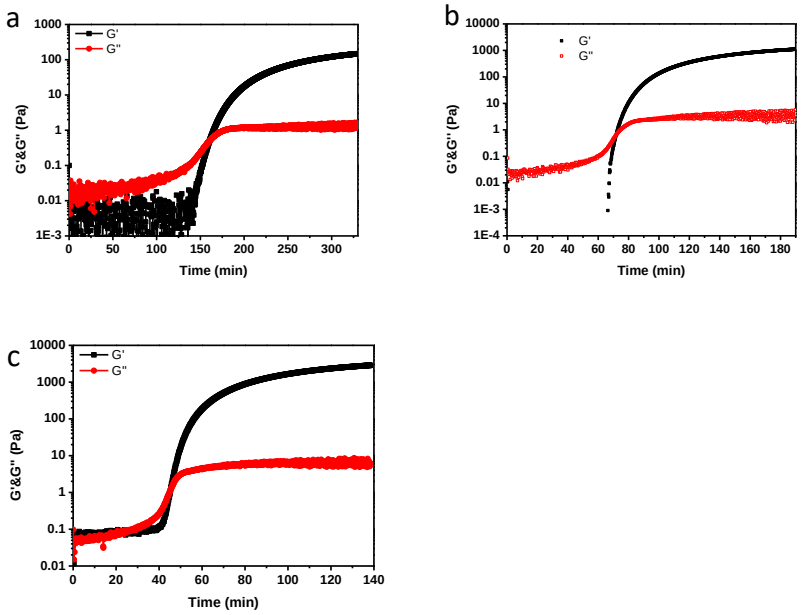

Figure S3.7. Time sweep measurements of the gelation process of a) 8 wt% hydrogel; b) 6 wt% hydrogel c) 4 wt% hydrogel (γ = 1%, ω = 1 Hz, 25 °C)

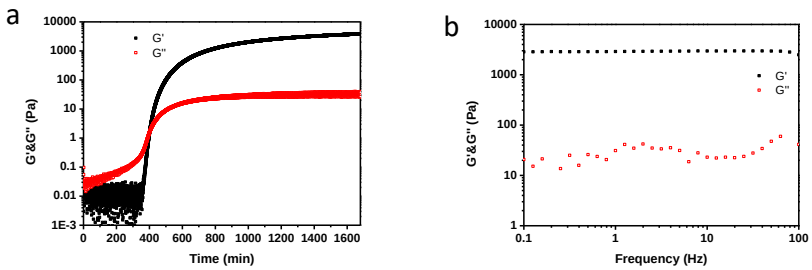

Figure S3.8. a) Time sweep measurement of the gelation process of 10 wt% hydrogel formed in PBS7.4 (γ = 1%, ω = 1 Hz, 25 ºC). b) Frequency sweep measurement of 10 wt% hydrogel formed in PBS7.4 (γ = 1%, ω = 0.1-100 Hz, 25 ºC).

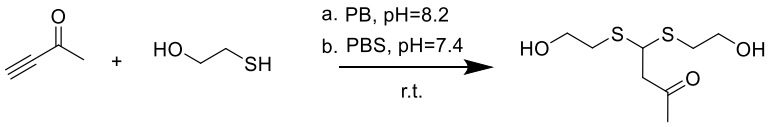

Scheme S3.4. Small molecular test of thiol-alkynone double reaction between 3-butyn-2-one and 2-mercaptoethanol in PB8.2 or PBS7.4 at room temperature.

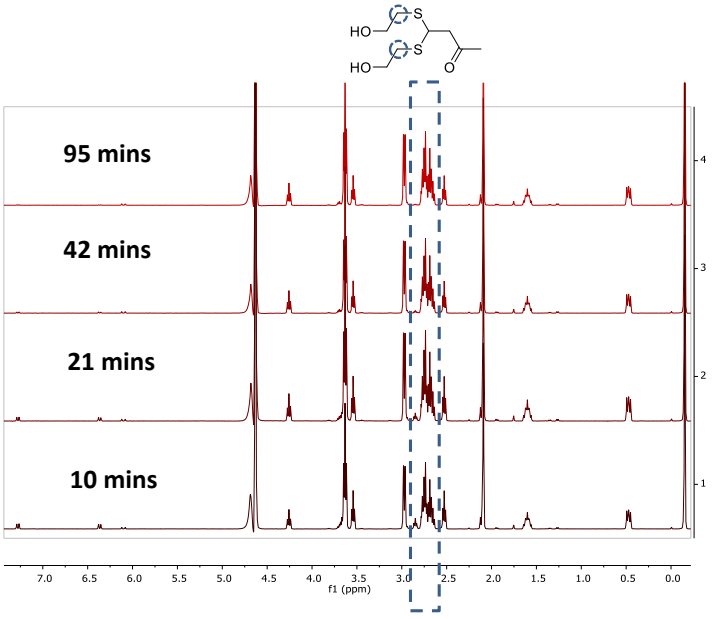

Figure S3.9. ^{1}H-NMR (399.7 MHz, 298 K in D_2O / PB8.2, 4 drops of D_2O in 1 mL PB8.2) monitoring of thiol-alkynone double reaction between 3-butyn-2-one and 2-mercaptoethanol in PB8.2.

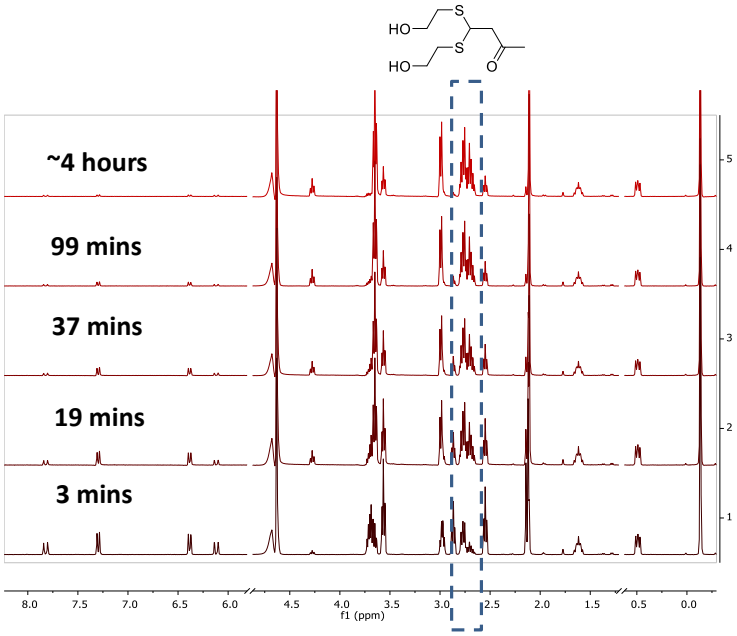

Figure S3.10. ^{1}H-NMR (399.7 MHz, 298 K in D_2O/PBS, 4 drops of D_2O in 1 mL PBS7.4) monitoring of thiol-alkynone double reaction between 3-butyn-2-one and 2-mercaptoethanol in PBS7.4.

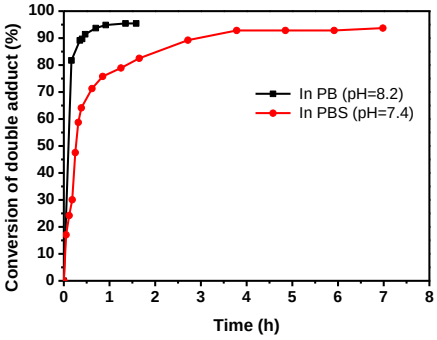

Figure S3.11. The formation of double adduct product in the thiol-alkynone double addition reaction between 3-butyn-2-one and 2-mercaptoethanol in PB8.2 and PBS7.4 over time.

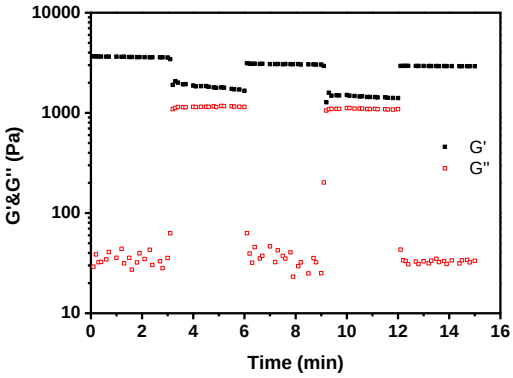

Figure S3.12. Step-strain sweep of 10 wt% Gel-PBS7.4, alternative strain switched from 1% to 300% twice then back to 1% (ω = 1 Hz, 25 °C).

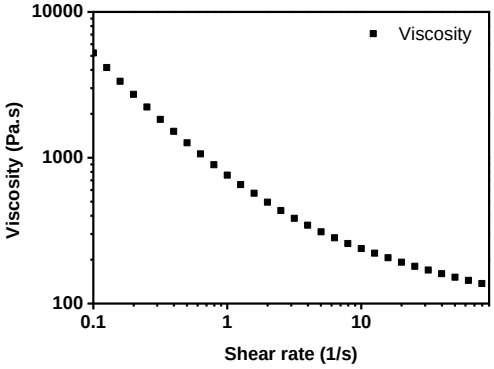

Figure S3.13. Viscosity of 10 wt% Gel-PB8.2 measured as a function of the shear rate.

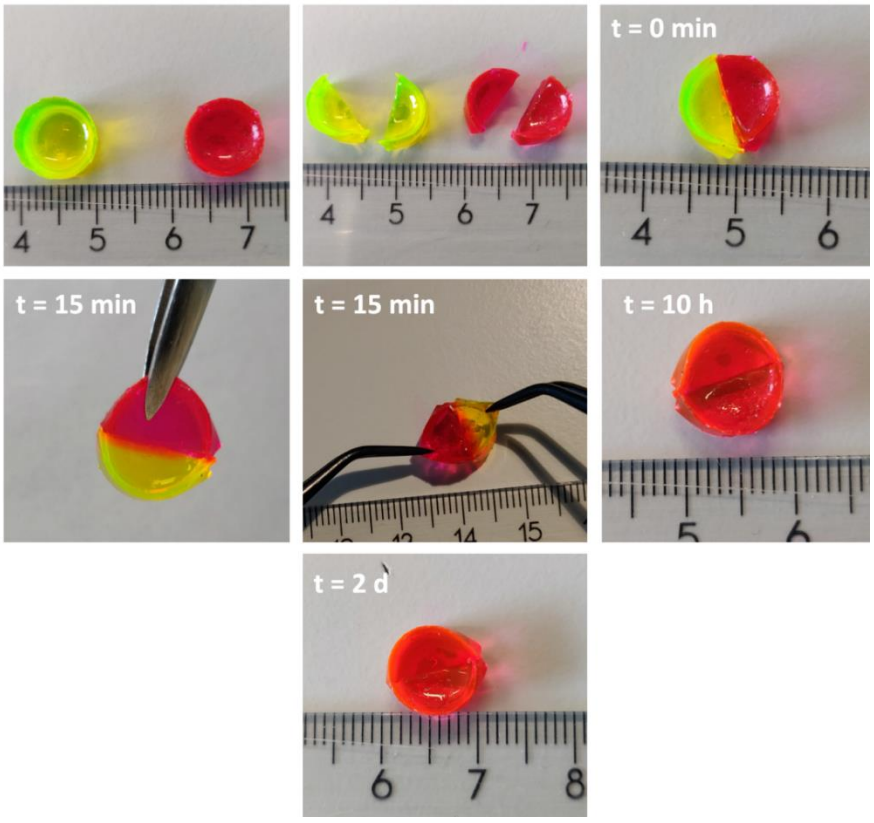

Figure S3.14. Photographs of self-healing process of 10 wt% Gel-PB8.2.

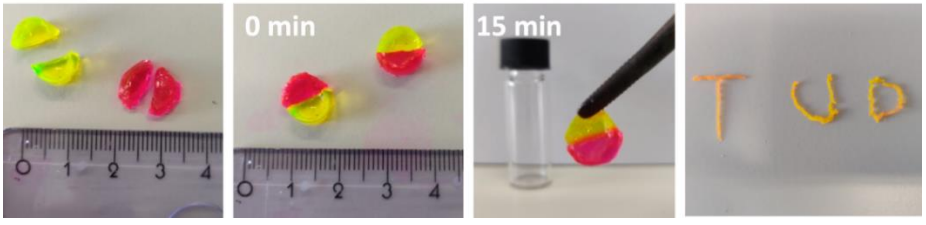

Figure S3.15. Photographs of self-healing process and injection of 10 wt% Gel-PBS7.4.

Chapter 4

A Fuel-driven Transient Polymer Hydrogel via Dynamic Thiol Double Addition

Abstract: Fuel-driven transient hydrogels gained a lot of attention in the past decades because of their autonomous dynamic and temporal programmable life-like properties. However, most fuel-driven transient hydrogels is based on noncovalent interactions, leading to an unpredictable crosslink density. In this chapter, we propose and investigate a redox-control reversible thiol-alkynone double addition. A redox-responsive hydrogel is developed by such reversible addition. In addition, a fuel-driven transient formation of thiol-alkynone double adduct can be achieved on small molecules. Although we did not apply this system in a hydrogel material, design routes are suggested in this chapter.

4.1 Introduction

Stimuli-responsive hydrogels have attracted great attention in many research groups because of their potential application in biomedical settings, for instance in tissue engineering, controlled drug delivery and as wound healing dressings.[1–4] Hydrogels can respond to external stimuli (e.g. pH, temperature, light, chemical triggers) with a functional switch causing a programmed material response (formation, destruction, stiffening, softening). Typically, the functional property of classical hydrogels will maintain a permanent stable state until another trigger is applied. Thus, two triggers sequentially delivered are required to achieve an "A-B-A" state cycle in classical hydrogels. This contrasts to autonomous dynamic and transient time-programmable properties observed in living soft tissues.[5–7] It would therefore be interesting to develop a new generation of hydrogel materials with transient properties, enabling more advanced applications in biomaterials.[8–11] Fuel-driven transient hydrogels, for example, are able to realize these temporally controlled behaviors by coupling a chemical reaction network (CRN) to hydrogel formation.[12–18] These type of dynamic hydrogels are activated by the addition of a fuel which forms a product to alter a desired property (e.g. stiffness or lifetime). Importantly, this product is unstable and spontaneously decays over time, which means that the response in lifetime change can be controlled by the reaction kinetics of the CRN. However, most fuel-driven transient hydrogels are still designed and developed based on noncovalent interactions (supramolecular hydrogels), resulting in an untuneable crosslink density.[19] Only one example of transient covalently polymeric hydrogel was constructed by a known fuel-driven CRN in recent years.[17] It would be of great interest if we can properly design a fuel driven CRN which is able to be coupled to the formation of a covalently crosslinked hydrogel.

In chapter 2, we proposed a new fuel-driven CRN utilizing redox-controlled conjugate addition and elimination which has potential to be used in transient covalent crosslinking of soft materials. However, because of side-reactivity of the cycle, operation of a full continuous cycle in one pot was not achieved. It is an important challenge to design a chemical reaction cycle that can be used for the transient formation of crosslinks in a hydrogel material.[20,21] The dynamic thiol-alkynone double addition discussed in chapter 3 is a dynamic covalent reaction which has seen increasing application in recent years.[22–25] Here, addition of a thiol to an alkynone first causes the irreversible generation of a thiol-alkynone single adduct. This single adduct can react with a second thiol to produce a thermodynamically favored thiol-alkynone double adduct in a reversible reaction. However, if an external oxidizing agent is provided to oxidize the starting thiol to disulfide, the reverse reaction can become thermodynamically favored, causing a breakage of one of the thiol-alkynone covalent bonds. Since the single thiol-alkynone addition is irreversible, the alkynone species will remain as the single adduct and not further revert to the initial alkynone. Moreover, once a reducing agent is introduced to deplete the disulfide, release of free thiols can thermodynamically drive this reaction forward, re-generating the thiol-alkynone double adduct. We would like to use this redox-controlled reversible thiol-alkynone double addition to develop a new fuel-driven transient hydrogel system. Here, we first investigated the redox-controlled reversibility of dynamic thiol-alkynone double addition on a small molecular model. Then, by applying this thiol-alkynone double addition in hydrogel formation, a redox-responsive hydrogel was created via 4-arm PEG thiol addition to 3-butyn-2-one. Next, we expanded this redox-responsive system to a transient fuel-driven system. Fuel-driven transient small molecule thiol-alkynone double addition was achieved by

addition of tris(2-carboxyethyl)phosphine (TCEP) to drive the reduction of disulfides to free thiols, favoring the formation of the thiol-alkynone double addition. Combining this with an oxidant such as H_2O_2 or O_2 to oxidize the free thiols back to disulfides leads to a transient response. Although we still did not apply this fuel driven transient system in a hydrogel material, design routes are suggested in this chapter.

4.2 Results and Discussion

4.2.1 Redox-responsive thiol-alkynone double addition on a small molecular model

To investigate redox control over thiol-alkynone single and double addition products, we first used a small molecular model (3-butyn-2-one **1** as an alkynone; β-mercaptoethanol **2** as a thiol) to monitor the thiol-alkynone single and double addition equilibrium upon action by redox agents (**Figure 4.1a**). 3-Butyn-2-one **1** can react with β-mercaptoethanol (BME) **2** once to generate a single adduct **3**. A second BME addition to the single adduct **3** produces a double adduct **4**. The redox chemistry of BME oxidation and reduction to and from its disulfide (disulfide-BME **5**) is able to tune which thiol-alkynone adduct is thermodynamically favored. Oxidation of BME **2** to disulfide-BME **5** favors formation of the single adduct **3**, leading to the cleavage of a single thiol-alkynone covalent bond in the double adduct **4**. Furthermore, this preference can be switched to the double adduct **4** by re-introduction of free BME **2** through reduction of disulfide-BME **5**. Essentially, in such a dynamic covalent system, the equilibrium position can be controlled using redox fuels.

To demonstrate the proposed redox-responsive thiol-alkynone double addition we used ^{1}H NMR spectroscopy to track the reaction of 3-butyn-2-one **1** (1 eq.) with BME **2** (2 eq.) in phosphate buffer (100 mM, pH=8.2, "PB8.2") at room temperature. This resulted in conversion of 88% of the alkynone **1** to the double adduct **4** as determined by ^{1}H NMR of the double adduct **4** peak at 2.63-2.71 ppm (**Figure 4.1b** and **Figure S4.4**). Addition of an oxidizing agent (H_2O_2, 1 eq.) resulted in a fast decay of the double adduct **4** and simultaneous formation of the single adduct **3** over time (**Figure S4.4-S4.5**). After most double adduct **4** was consumed, the addition of reducing agent (TCEP, 1 eq.) caused a dramatic increase in the conversion to the double adduct **4** (from ~6% to ~65%) in 3 hours, with a corresponding decrease of single adduct **3** (from ~63% to ~8%). The reaction cycle of BME-alkynone double addition was able to run at least 3 times by subsequent additions of H_2O_2 and TCEP over 100 hours. Unfortunately, the peak conversion to double adduct **4** upon adding TCEP in these reversible cycles decreased from 65% to 53% then to 38%. This decrease is likely due to the known side reaction between TCEP and the single adduct **3**.[26]

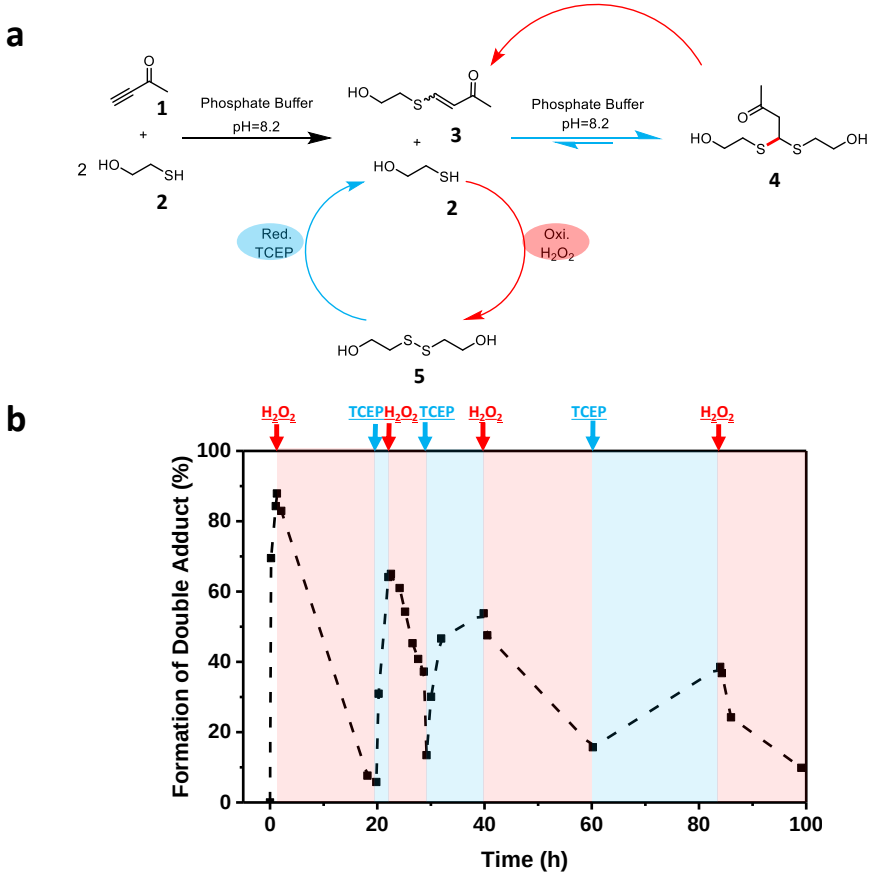

Figure 4.1. Small molecule demonstration of redox-responsive thiol-alkynone double addition. (a) Schematic representation of redox-responsive thiol-alkynone double addition between 3-butyn-2-one **1** and BME **2** in PB8.2 reversibly controlled by H_2O_2 and TCEP. (b) The conversion of 3-butyn-2-one **1** to double adduct **4** from the reaction between 3-butyn-2-one **1** (1 eq.) and BME **2** (2 eq.) in PB8.2 as monitored by ^{1}H NMR (the double adduct has characteristic peaks at 2.63-2.71 ppm). Conversion is controlled by addition of H_2O_2 and TCEP (each time 1eq.) over time after initial formation of a majority of double adduct species. The red area indicates that after adding H_2O_2, the conversion of double adduct **4** decreased with time. The blue area indicates that after adding TCEP, the conversion of double adduct **4** increased with time.

4.2.2 Redox-responsive hydrogel via thiol-alkynone double addition

After the model test of H_2O_2-TCEP responsive thiol-alkynone double addition, we applied this dynamic reaction to hydrogel formation and decomposition upon interaction with redox stimuli. The hydrogel was synthesized by crosslinking 4-arm-PEG thiol with 3-butyn-2-one via thiol-alkynone double addition (**Figure 4.2a**). Upon mixing 4-arm PEG thiol (thiol groups is 2 eq.) and 3-butyn-2-one (1 eq.) in a 1.5 mL glass vial at room temperature, a disc-shaped hydrogel (thickness: 4 mm; diameter: 9 mm) formed in half an hour. After this disc-shaped hydrogel was transferred into a square-shaped container, it converted to a flowing polymer

solution in 1 day by adding H_2O_2 in PB8.2 solution (0.75 eq. to thiol group in 4-arm PEG thiol). Addition of TCEP (0.38 eq.) to the solution later resulted in the reformation of a square-shaped hydrogel (3mm × 10mm × 10mm) in 5 days (**Figure S4.6**). We chose 0.75 eq. of H_2O_2 and 0.38 eq. of TCEP (half amount with respect to H_2O_2) because the amount of TCEP added will influence the reformation of hydrogel. When the amount of TCEP is above 0.5 eq., the hydrogel will not be reformed probably due to the side-reaction (Michael addition) between TCEP and the single adduct. To support these qualitative results, rheological testing was also performed. A new hydrogel was first formed on the Peltier plate of rheometer by mixing 4-arm PEG thiol and 3-butyn-2-one, with successful gelation demonstrated by a crossover of the storage modulus (G') and the loss modulus (G") within 30 minutes (**Figure 4.2b**).

After the storage modulus (G') reached equilibrium (7.2×10^3 Pa) at 90 min, H_2O_2 (0.75 eq.) was added on the top surface of the hydrogel (thickness: ~1 mm; diameter: 40 mm). This resulted in an obvious decrease of the storage modulus (G') (from 4.5×10^3 Pa to 0.7×10^3 Pa) over 6 hours, as observed in a rheological time sweep, suggesting that crosslinks in the hydrogel were broken resulting from the addition of H_2O_2. Note that the decrease of G' from 7.2×10^3 Pa to 3.8×10^3 Pa immediately after addition of H_2O_2 may be caused by the operation of raising the geometry for oxidant addition. Interestingly, a small increase of G' during the first 4 mins of the oxidation process can be observed, probably resulting from hydrogel self-healing against the damage caused during rheometer geometry opening. Addition of TCEP (0.38 eq.) at 6 hours after addition of H_2O_2 initially caused the complete collapse of hydrogel, followed by the reformation of the hydrogel, indicated by the time sweep measurement. The reason for collapse of the hydrogel after adding TCEP may be that TCEP initially cleaved any disulfide bonds acting as additional crosslinks in the hydrogel network after the previous oxidation process. The subsequent reformation of the hydrogel results from the reformation of thiol-alkynone double adducts in the network.

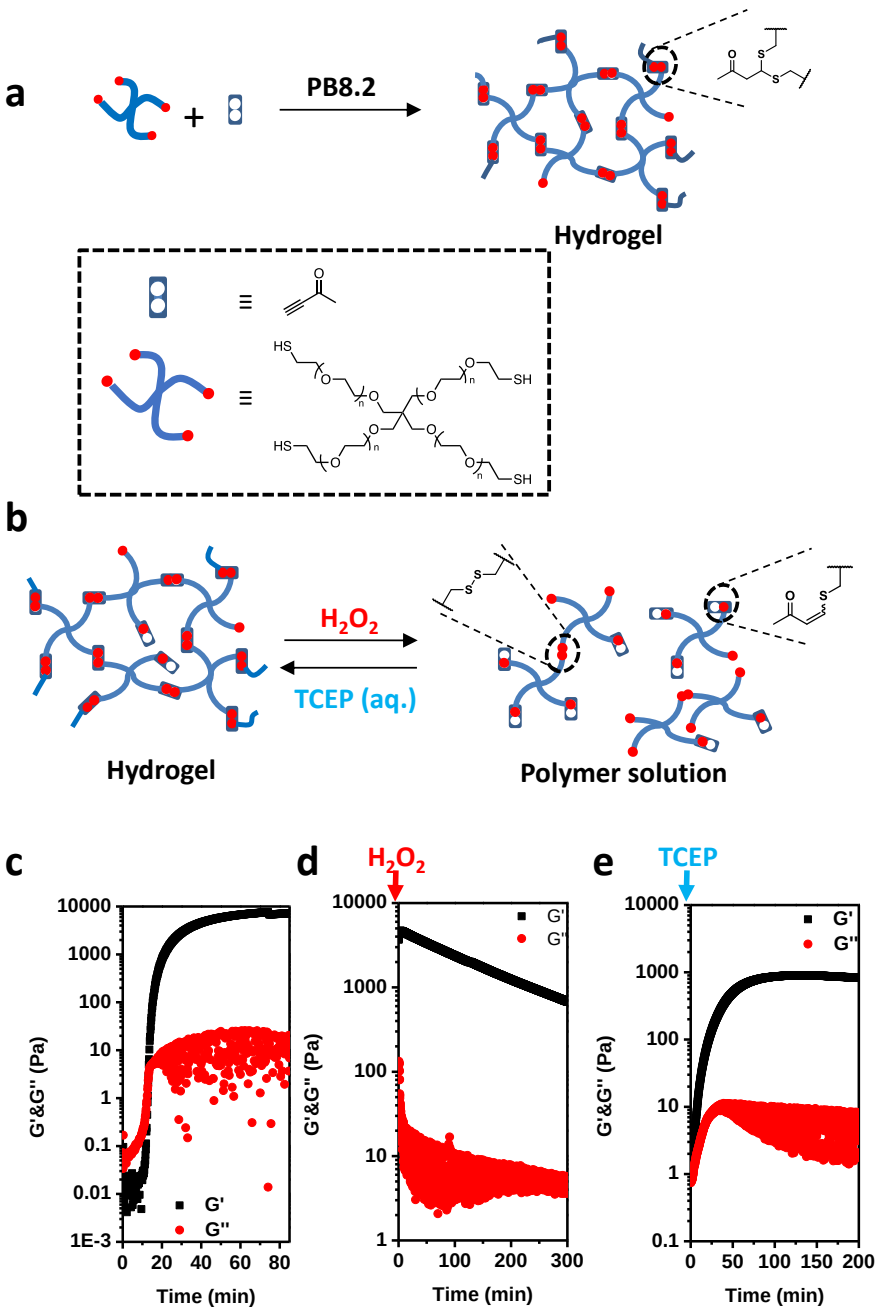

Figure 4.2. Redox-responsive hydrogel formation and collapse via redox-controlled thiol-alkynone double addition. Schematic representation of redox-responsive hydrogel to polymer solution process: (a) hydrogel formation by crosslinking a tetra thiol star polymer with 3-butyn-3-one; (b) hydrogel degradation to polymer solution by addition of H_2O_2 to break the thiol-alkynone double adduct crosslinks

and form non-crosslinking thiol-alkynone single adduct. Crosslinks are then reformed by addition of TCEP to regenerate the double adduct species. (c) Time sweep measurement of the gelation process for a 10 wt% hydrogel by combining 4-arm PEG thiol (thiols group is 2 eq.) and an alkynone (1 eq.) (γ = 1%, ω = 1 Hz, 25 ˚C). (d) Time sweep measurement of the degradation process for a 10 wt% hydrogel after adding H_2O_2 (0.75 eq.) on the top of hydrogel (γ = 1%, ω = 1 Hz, 25 ˚C). (e) Time sweep measurement for the reformation process of a 10 wt% hydrogel after adding TCEP (0.38 eq.) on the top of hydrogel (γ = 1%, ω = 1 Hz, 25 ˚C).

4.2.3 Fuel-driven transient formation of thiol-alkynone double adduct

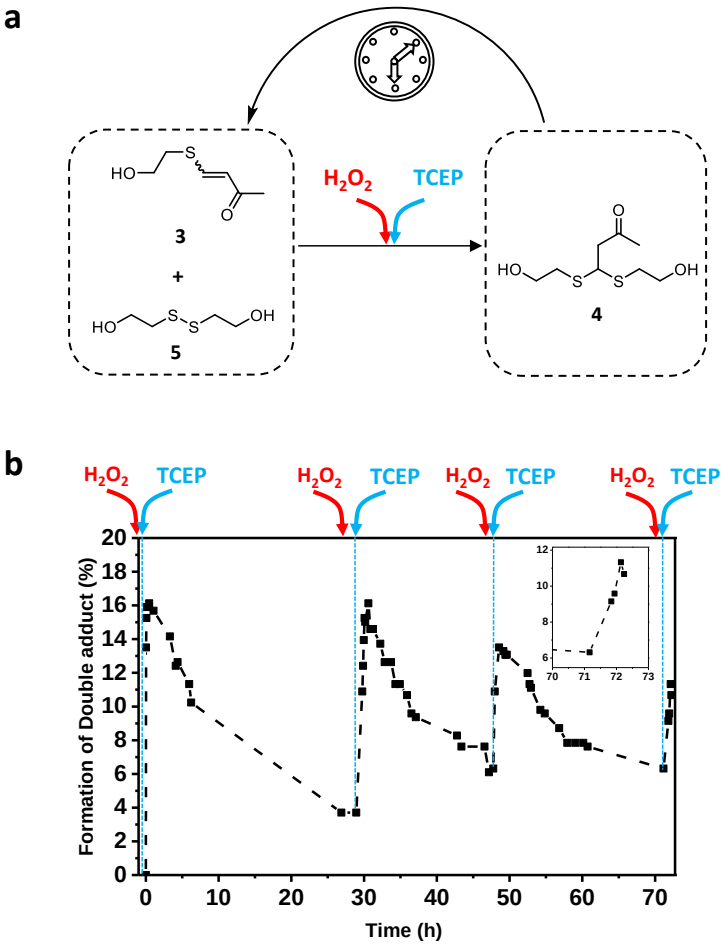

Figure 4.3. Small molecule demonstration of fuel-driven transient formation of thiol-alkynone double adduct **4** using H_2O_2 and TCEP. (a) Schematic representation of fuel-driven transient formation of double adduct **4** between single adduct **3** and disulfide-BME **5** by addition of H_2O_2 and TCEP (both 1 eq.) sequentially. (b) The conversion of single adduct **3** to double adduct **4** in the fuel-driven transient thiol-alkynone double addition between single adduct **3** (1 eq.) and disulfide-BME **5** (0.5 eq.) in PB8.2 as monitored by ^{1}H NMR over time (monitoring **4** at 2.63-2.71 ppm). After the depletion of a majority of

double adduct species, H_2O_2 and TCEP (both 1 eq.) were added sequentially, initiating a new cycle. The insert is a zoom between 70 to 73 minutes.

Based on the redox-responsive thiol-alkynone double addition, we studied a fuel-driven transient thiol-alkynone double addition system. Unlike in the above redox-responsive system where an oxidizing agent is added after generation of the double adduct **4**, the oxidizing species has to be present before generation of the double adduct **4** in a fuel-driven transient system, providing an oxidizing environment. In a system starting with predominately single adducts **3**, double adducts **4** may be generated by addition of a reducing agent (acting here a fuel). If the oxidant species is already present in the system in sufficient excess, it will eventually deplete any double adducts **4** formed over time, leading to a fuel-driven transient double adduct formation.

We began by analyzing a small molecule model, with H_2O_2 as an oxidizing agent to maintain the oxidizing environment and TCEP as a fuel. We started by mixing the single adduct **3** (1 eq.), 2-hydroxyethyl disulfide (BME-disulfide **5**) (0.5 eq.) and H_2O_2 (1 eq.) in PB8.2 at room temperature (**Figure 4.3a** and **Figure S4.7**). After addition of TCEP (1 eq.), we observed a fast increase in the conversion of the single adduct **3** to the double adduct **4** from 0% at 0 min to 16% at 24 min (**Figure 4.3b**). Subsequently, a spontaneous slow decay of the double adduct **4** occurred, reducing to 3.7 % conversion at 29 h. It should be noted that before addition of 1 eq. TCEP to trigger a second cycle, 1 eq. H_2O_2 has to be replenished, otherwise the double adduct **4** regenerated by addition of TCEP cannot be consumed over time. After addition of separate H_2O_2 and TCEP solutions, the conversion to double adduct **4** rapidly increased to 16% within 2 hours, then went down slowly to 6% after a further 17h. Probably due to the side reaction between single adduct **3** and TCEP, the highest conversion of double adduct **4** in the third and fourth cycle decreased to 14% and 11%. Regardless, we have proven that a fuel-driven transient thiol-alkynone double adduct **4** formation can be achieved by simultaneous addition of H_2O_2 and TCEP. However, three issues in this design system hinder the further hydrogel application: 1. The low conversion to double adduct **4** (16%) during the cycle is not enough to crosslink polymers to form a hydrogel network since the lowest conversion of double adduct for hydrogel formation via 4-arm thiol and alkynone is 60% at 10% solid polymer content. 2. H_2O_2 has to be refilled to maintain the oxidizing environment at the beginning of each cycle. 3. TCEP will rapidly react with H_2O_2 which causes a non-productive waste of fuel.

The previous redox partners, TCEP and H_2O_2, do not ideally meet the key requirement for fuel-driven transient systems, which is having a faster forward reaction than both the back reaction and the reaction between redox partners. Comparing to the relatively strong oxidizing agent, H_2O_2, molecular oxygen is a mild oxidizing agent which exists in the environment and has also been used in other fuel-driven systems.[27] However, oxidation of thiols by O_2 in the air is a relatively slow process, which when left unattended will probably lead to the formation a permanent hydrogel with an untuneable lifetime.[28] Using catalysis is another way to control and match reactivity of oxidation and reduction. Riboflavin, known as Vitamin B_2, is able to catalyze the oxidation of thiol by O_2.[29,30] To investigate the feasibility of TCEP-driven transient double addition, using riboflavin catalyzed oxidation by O_2, we combined 3-butyn-2-one **1** (1 eq.), BME **1** (2 eq.) and riboflavin (0.1 eq.) in a 4 mL glass vial (open to air) with continuous stirring at room temperature (**Figure 4.4a**). A 76% conversion of alkyne to double adduct **4** can be obtained after 2.5 hours, as detected by ^{1}H NMR (**Figure 4.4b** and **Figure S4.8**). Afterwards, the conversion to double adduct **4** started to

decrease autonomously over time to 24% at 61 hours. At this point addition of TCEP (0.5 eq.) led to a regeneration of the double adduct **4** to a conversion of 41% at 66 hours. This followed by another spontaneous decay of double adduct **4** to single adduct **3** (conversion reduced to ~6%). Furthermore, a second fuel-driven transient cycle was obtained by adding a second batch of TCEP (0.5 eq.) at 115 hours. In addition to riboflavin, we also tried methylene blue (another oxidation catalyst, "MB"), to catalyze the oxidation of thiols by O_2. Similar fuel-driven transient double adduct **4** formation also was achieved (**Figure S4.9** and **S4.10**). We only performed one TCEP-driven double adduct **4** formation cycle in MB catalyzed O_2 oxidation system, showing a fast regeneration of double adduct **4** upon adding TCEP (0.5 eq.) (from ~0 % at 74 hours to ~50% at 79 hours), and followed by a slow decay to 14% at 114 hours.

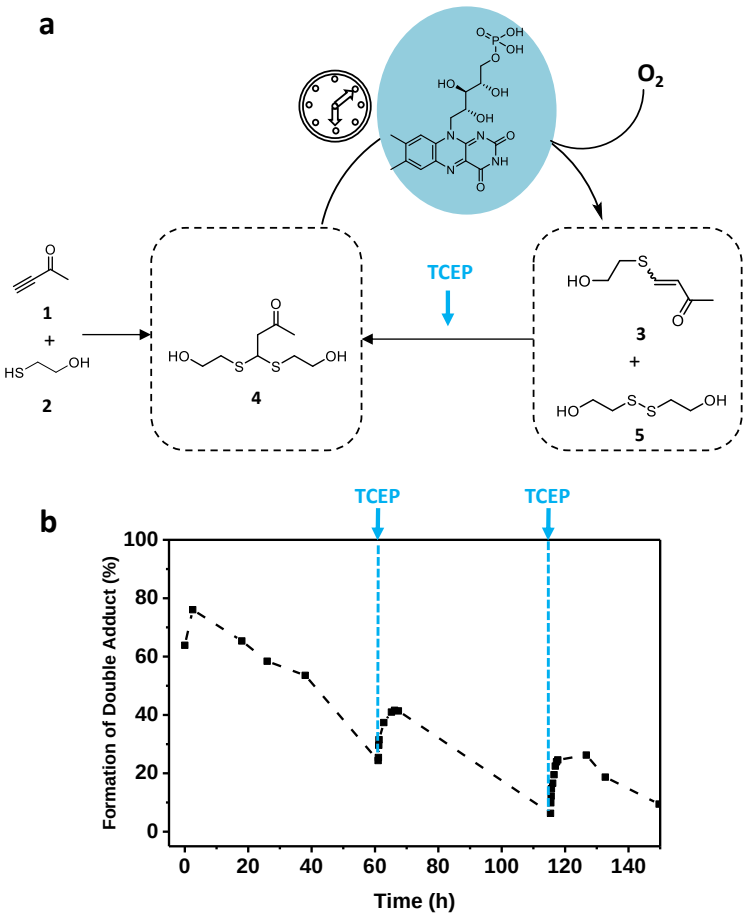

Figure 4.4. Small molecule demonstration of TCEP-driven transient formation of thiol-alkynone double adduct oxidized by O_2 under catalysis of riboflavin. (a) Schematic representation of catalyzed O_2 fuel-driven transient formation of thiol-alkynone double adduct **4**. (b) The conversion to double adduct **4** in the fuel-driven transient thiol-alkynone double addition reaction between 3-butyn-2-one **1** and BME **2** in PB8.2 over time. Consumption of double adduct **4** was achieved by an oxidation of BME **2** using O_2

under catalysis of riboflavin. Regeneration of the double adduct **4** was achieved by a reduction of disulfide-BME **5** by TCEP (0.5 eq.) acting as fuel.

4.2.4 Recommendation

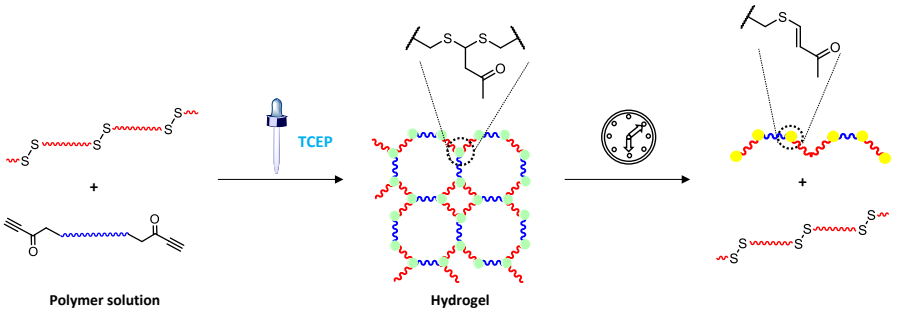

Scheme 4.1. Schematic representation of outlook for a fuel-driven transient hydrogel via thiol-alkynone double addition.

Although we tried to build a fuel-driven transient hydrogel system based on the fuel-driven transient thiol-alkynone double addition system discussed above, it was found that the previously developed redox-responsive hydrogel made from 4-arm PEG thiol and 3-butyn-2-one via thiol-alkynone double addition is not suitable for a fuel-driven transient hydrogel system. Once the double adduct bond crosslinks are broken by an oxidation process, disulfide bonds can be generated as another form of crosslinks. These additional disulfide crosslinks can maintain the system in a hydrogel state, despite the destruction of double adduct crosslinks after oxidant addition. This hinders the measurement of fuel-driven sol-gel-sol transition in such a hydrogel by rheological tests. Another strategy to form a hydrogel via thiol-alkynone double addition starts from a solution of a disulfide polymer and a bis-alkynone molecule in PB8.2 (**Scheme 4.1**). Addition of TCEP will release free thiols, and a hydrogel could then form via thiol-alkynone double addition. If there is an ideal oxidizing environment, depletion of the double adduct would lead to degradation of the hydrogel to a solution. We have attempted to synthesize a water soluble bis-alkynone molecule or polymer as shown in Scheme 1. However, we have not obtained such a bis-alkynone molecule to date, although we tested different synthetic routes.

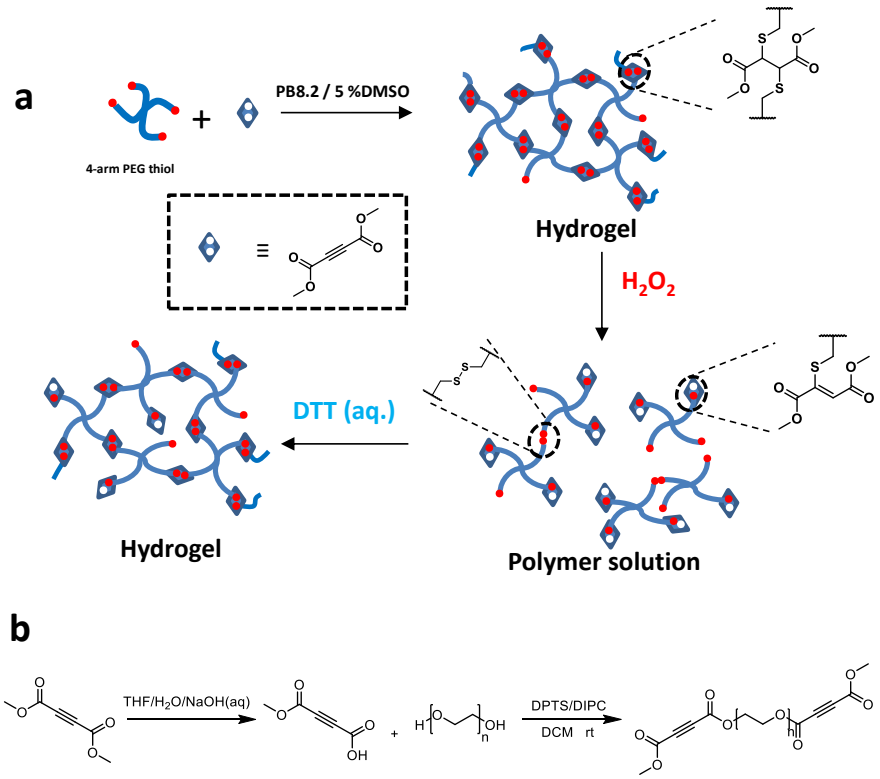

Figure 4.5. Schematic representation of redox-responsive hydrogel via thiol-dimethyl acetylenedicarboxylate (DMADC) double addition and a proposed synthetic route of a bis-DMADC crosslinker. (a) Schematic representation of redox-responsive hydrogel to polymer solution process via DMADC-thiol double addition: hydrogel formation by crosslinking a tetra thiol star polymer with the DMADC; hydrogel decomposition to polymer solution by adding H_2O_2; hydrogel reformation by adding DTT (dithiothreitol). (b) the proposed synthetic route of the water soluble bis-DMADC molecule. Abbreviations: THF= tetrahydrofuran; DPTS= 4-(dimethylamino) pyridinium-4-toluenesulfonate; DIPC= diisopropylcarbodiimide; DCM=dichloromethane.

Besides alkynones, we found that another candidate can also be used in a fuel driven thiol-double addition system. Dimethyl acetylenedicarboxylate (DMADC) can react with two thiols under the same conditions as the alkynone-double addition reaction. Additionally the DMADC-thiol double adducts are also unstable under oxidizing conditions and degrade to the single adducts.[31] We have successfully formed a hydrogel by crosslinking 4-arm PEG thiol with DMADC and demonstrated hydrogel degradation by addition of H_2O_2 and hydrogel reformation by addition of DTT (dithiothreitol) (**Figure 4.5a**). After tests of redox-reversibility of hydrogel via DMADC-thiol double addition, we proposed a synthetic plan for water soluble bis-DMADC molecule (**Figure 4.5b**). Once such a water soluble bis-DMADC molecule is synthesized, we could test this for fuel driven transient hydrogelation.

4.3 Conclusions

In summary, we proposed a strategy to develop a new fuel-driven transient polymeric hydrogel by a redox-responsive and dynamic thiol-alkynone double addition reaction. A fuel-driven transient system was developed step-by-step from a small molecule model to a hydrogel material. We investigated these systems using both a simple redox stimuli responsive process and a fuel driven transient process. We first confirmed that the equilibrium of the thiol-alkynone double addition reaction can be responsive to redox agents (H_2O_2 and TCEP). Then a redox-responsive hydrogel formed from 4-arm-PEG thiol and an alkynone was checked by reshape experiments and rheological analysis. Next, we used two different oxidizing methods (H_2O_2 or O_2 in air under catalysis of riboflavin or methylene blue) to obtain TCEP-driven transient formation of double adduct. The final fuel-driven transient polymer hydrogel is still under development.

4.4 References

(1) Stuart, M. A. C.; Huck, W. T. S.; Genzer, J.; Müller, M.; Ober, C.; Stamm, M.; Sukhorukov, G. B.; Szleifer, I.; Tsukruk, V. V.; Urban, M.; Winnik, F.; Zauscher, S.; Luzinov, I.; Minko, S. Emerging Applications of Stimuli-Responsive Polymer Materials. *Nat. Mater.* **2010**, *9*, 101–113.

(2) Yu, S.; Wang, C.; Yu, J.; Wang, J.; Lu, Y.; Zhang, Y.; Zhang, X.; Hu, Q.; Sun, W.; He, C.; Chen, X.; Gu, Z. Injectable Bioresponsive Gel Depot for Enhanced Immune Checkpoint Blockade. *Adv. Mater.* **2018**, *30*, 1–8.

(3) Shi, Q.; Liu, H.; Tang, D.; Li, Y.; Li, X. J.; Xu, F. Bioactuators Based on Stimulus-Responsive Hydrogels and Their Emerging Biomedical Applications. *NPG Asia Mater.* **2019**, *11*, 64.

(4) Ding, M.; Jing, L.; Yang, H.; Machnicki, C. E.; Fu, X.; Li, K.; Wong, I. Y.; Chen, P. Y. Multifunctional Soft Machines Based on Stimuli-Responsive Hydrogels: From Freestanding Hydrogels to Smart Integrated Systems. *Mater. Today Adv.* **2020**, *8,* 100088.

(5) Heinen, L.; Walther, A. Celebrating Soft Matter's 10th Anniversary: Approaches to Program the Time Domain of Self-Assemblies. *Soft Matter* **2015**, *11*, 7857–7866.

(6) Walther, A. Viewpoint: From Responsive to Adaptive and Interactive Materials and Materials Systems: A Roadmap. *Adv. Mater.* **2020**, *32*, 1–10.

(7) Jain, A.; Dhiman, S.; Dhayani, A.; Vemula, P. K.; George, S. J. Chemical Fuel-Driven Living and Transient Supramolecular Polymerization. *Nat. Commun.* **2019**, *10* (1), 1–9.

(8) Etxeberria, A.; Ruiz-Mirazo, K. The Challenging Biology of Transients: A View from the Perspective of Autonomy. *EMBO Rep.* **2009**, *10*, 33–36.

(9) Du, X.; Zhou, J.; Shi, J.; Xu, B. Supramolecular Hydrogelators and Hydrogels: From Soft Matter to Molecular Biomaterials. *Chem. Rev.* **2015**, *115*, 13165–13307.

(10) Lorenz, J. S.; Schnauß, J.; Glaser, M.; Sajfutdinow, M.; Schuldt, C.; Käs, J. A.; Smith, D. M. Synthetic Transient Crosslinks Program the Mechanics of Soft, Biopolymer-Based Materials. *Adv. Mater.* **2018**, *30*, 1–8.

(11) Rüegg, M.; Blum, R.; Boero, G.; Brugger, J. Biodegradable Frequency-Selective Magnesium Radio-Frequency Microresonators for Transient Biomedical Implants. *Adv. Funct. Mater.* **2019**, 1903051.

(12) Boekhoven, J.; Brizard, A. M.; Kowlgi, K. N.; Koper, G. J. M.; Eelkema, R.; van Esch, J. H. Dissipative Self-Assembly of a Molecular Gelator by Using a Chemical Fuel. *Angew. Chem. Int. Ed.* **2010**, *49*, 4825–4828.

(13) Boekhoven, J.; Hendriksen, W. E.; Koper, G. J. M.; Eelkema, R.; Esch, J. H. Van. Transient Self-Assembly of Active Materials Fueled by a Chemical Reaction. *Science.* **2015**, *349*, 1075.

(14) Heuser, T.; Weyandt, E.; Walther, A. Biocatalytic Feedback-Driven Temporal Programming of Self-Regulating Peptide Hydrogels. *Angew. Chemie Int. Ed.* **2015**, *54*, 13258–13262.

(15) Pappas, C. G.; Sasselli, I. R.; Ulijn, R. V. Biocatalytic Pathway Selection in Transient Tripeptide Nanostructures. *Angew. Chemie Int. Ed.* **2015**, *54*, 8119–8123.

(16) Tena-Solsona, M.; Rieß, B.; Grötsch, R. K.; Löhrer, F. C.; Wanzke, C.; Käsdorf, B.; Bausch, A. R.; Müller-Buschbaum, P.; Lieleg, O.; Boekhoven, J. Non-Equilibrium Dissipative Supramolecular Materials with a Tunable Lifetime. *Nat. Commun.* **2017**, *8*, 1–8.

(17) Zhang, B.; Jayalath, I. M.; Ke, J.; Sparks, J. L.; Hartley, C. S.; Konkolewicz, D. Chemically Fueled Covalent Crosslinking of Polymer Materials. *Chem. Commun.* **2019**, *55*, 2086–2089.

(18) Mondal, S.; Podder, D.; Nandi, S. K.; Roy Chowdhury, S.; Haldar, D. Acid-Responsive Fibrillation and Urease-Assisted Defibrillation of Phenylalanine: A Transient Supramolecular Hydrogel. *Soft Matter* **2020**, 10115–10121.

(19) Eelkema, Rienk, and A. P. Pros and Cons: Supramolecular or Macromolecular: What Is Best for Functional Hydrogels with Advanced Properties? *Adv. Mater.* **2020**, 201906012.

(20) Singh, N.; Formon, G. J. M.; De Piccoli, S.; Hermans, T. M. Devising Synthetic Reaction Cycles for Dissipative Nonequilibrium Self-Assembly. *Adv. Mater.* **2020**, *32*, 1906834..

(21) Rieß, B.; Grötsch, R. K.; Boekhoven, J. The Design of Dissipative Molecular Assemblies Driven by Chemical Reaction Cycles. *Chem* **2020**, *6* , 552–578.

(22) Shiu, H. Y.; Chan, T. C.; Ho, C. M.; Liu, Y.; Wong, M. K.; Che, C. M. Electron-Deficient Alkynes as Cleavable Reagents for the Modification of Cysteine-Containlng Peptides in Aqueous Medium. *Chem. - A Eur. J.* **2009**, *15*, 3839–3850.

(23) Joshi, G.; Anslyn, E. V. Dynamic Thiol Exchange with β-Sulfido-α,β-Unsaturated Carbonyl Compounds and Dithianes. *Org. Lett* **2012**, *14*, 4714–4717.

(24) Matysiak, B. M.; Nowak, P.; Cvrtila, I.; Pappas, C.; Liu, B.; Komaromy, D.; Otto, S. Antiparallel Dynamic Covalent Chemistries. *J. Am. Chem. Soc.* **2017***, 139,* 6744-6751.

(25) Van Herck, N.; Maes, D.; Unal, K.; Guerre, M.; Winne, J. M.; Prez, F. E. Du. Covalent Adaptable Networks with Tunable Exchange Rates Based on Reversible Thiol-Yne Cross-Linking. *Angew. Chem. Int. Ed.* **2019***, 9,* 3609-3617.

(26) Kantner, T.; Watts, A. G. Characterization of Reactions between Water-Soluble Trialkylphosphines and Thiol Alkylating Reagents: Implications for Protein-Conjugation Reactions. *Bioconjug. Chem.* **2016**, *27*, 2400–2406.

(27) Leira-Iglesias, J.; Tassoni, A.; Adachi, T.; Stich, M.; Hermans, T. M. Oscillations, Travelling Fronts and Patterns in a Supramolecular System. *Nat. Nanotechnol.* **2018**, *13*, 1021–1027.

(28) Murahashi, S. I.; Zhang, D.; Iida, H.; Miyawaki, T.; Uenaka, M.; Murano, K.; Meguro, K. Flavin-Catalyzed Aerobic Oxidation of Sulfides and Thiols with Formic Acid/Triethylamine. *Chem. Commun.* **2014**, *50*, 10295–10298.

(29) Ohkado, R.; Ishikawa, T.; Iida, H. Flavin-Iodine Coupled Organocatalysis for the Aerobic Oxidative Direct Sulfenylation of Indoles with Thiols under Mild Conditions. *Green Chem.* **2018**, *20*, 984–988.

(30) Wayne Holden, J.; Main, L. The Kinetics and Mechanism of the Oxidation of Mercaptoethanol by Riboflavin. *Aust. J. Chem.* **1977**, *30* 1387–1391.

(31) Daglar, O.; Gungor, B.; Guric, G.; Gunay, U. S.; Hizal, G.; Tunca, U.; Durmaz, H. Rapid Hyperbranched Polythioether Synthesis Through Thiol-Michael Addition Reaction. *J. Polym. Sci.* **2020**, *58*, 824–830.

4.5 Supplementary information

4.5.1. Materials and Measurements

NMR spectra were recorded on an Agilent-400 MR DD2 (399.7 MHz for ^{1}H and 100.5 MHz for ^{13}C) at 298 K. The rheological measurements were performed using a rheometer (AR G2, TA instruments) equipped with a steel plate-and-plate geometry of 40 mm in diameter and equipped with a hexadecane trap. Thiol terminated 4-arm poly (ethylene glycol) (PEG10k-4-SH, Mw = 10 000, Đ ≤ 1.05) was purchased from JenKem Technology (USA). 3-Butyn-2-one, tris (2-carboxyethyl) phosphine hydrochloride, dimethylacetylene dicarboxylate, dithiothreitol were purchased from Fluorochem ltd. β-Mercaptoethanol, dimethyl sulfone, triazabicyclodecene,1,4-diazabicyclo[2.2.2]octane, trimethylamine, 2-hydroxyethyl disulfide, methylene blue, sodium phosphate (monobasic, anhydrous), sodium phosphate (dibasic), 3-(trimethylsilyl)-1-propanesulfonic acid sodium salt were purchased from Sigma Aldrich. Phosphate buffer solution (100 mM, pH = 8.2; 'PB8.2') was prepared by sodium phosphate (monobasic, anhydrous) and sodium phosphate (dibasic). All compounds and solvents were used as received without further purification. The technical solvents were purchased from VWR and the reagent grade solvents were purchased from Sigma Aldrich. Riboflavin 5'-monophosphate sodium salt was purchased from TCI Europe. All rheological tests were carried out at 25 ˚C and all other tests were carried out at room temperature.

4.5.2. Experimental Method

Synthesis of the single adduct 3

1 **2** **3**

3-Butyn-2-one (690 μL, 8.81 mmol, 1 eq.), β-mercaptoethanol (618 μL, 8.81 mmol, 1 eq., "BME") and 4 drops of triethylamine was added into 40 mL dichloromethane. The solution was stirring at room temperature 3 hours. Then the solution was washed by distilled water (1 × 50 mL) and brine (2 × 50 mL). The organic layer was dried over by $MgSO_4$ and the solvent was evaporated in vacuo. The obtained crude compound was purified by flash column chromatography (silica gel, ethyl acetate: petroleum ether =8:1) to obtain the yellow liquid (780 mg, yield: 60%).^{1}H NMR (399.7 MHz, DMSO-d_6) δ 7.83 (d, J = 15.6 Hz, 1H), 6.11 (d, J = 15.6 Hz, 1H), 5.01 (t, J = 5.4 Hz, 1H), 3.61 (d, J = 5.8 Hz, 2H), 2.97 (t, J = 6.4 Hz, 2H), 2.16 (s, 3H). ^{13}C NMR (100.5 MHz, 298 K in DMSO-d_6) δ 194.65, 148.36, 124.29, 59.95, 34.72, 27.26.

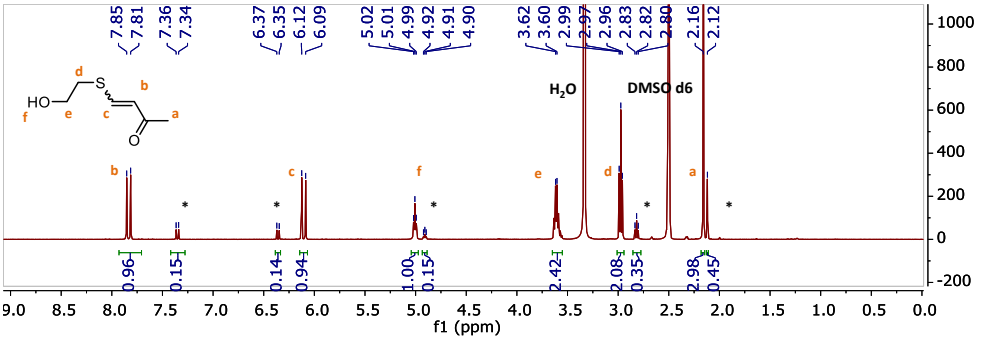

Figure S4.1. [1]H-NMR (399.7 MHz, 298 K in DMSO-d_6) spectrum of the single adduct **3**.

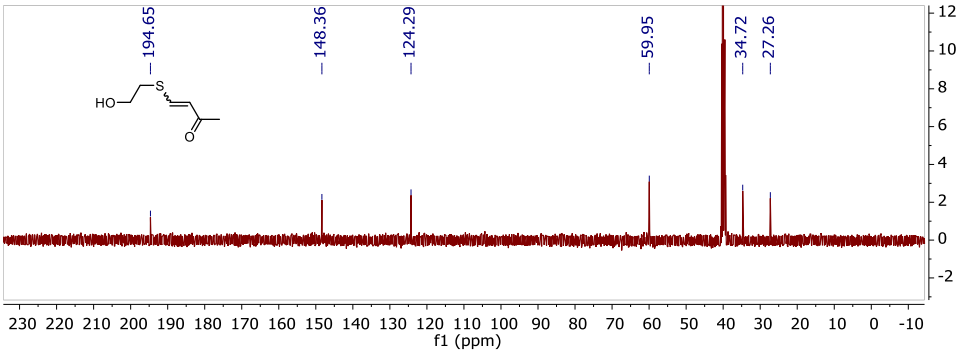

Figure S4.2. [13]C NMR (100.5 MHz, 298 K in DMSO-d_6) spectrum of the single adduct **3.**

Synthesis of the double adduct 4

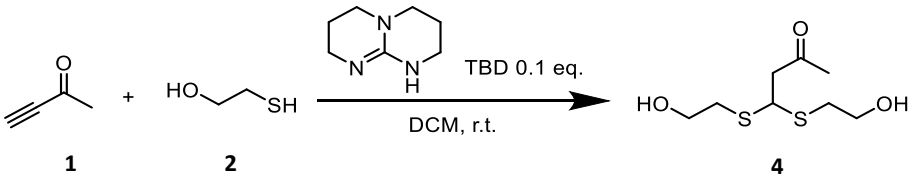

3-Butyn-2-one (230 µL, 2.94 mmol, 1 eq.), β-mercaptoethanol (412 µL, 5.87 mmol, 2 eq.) and triazabicyclodecene (41 mg, 0.0294 mmol, 0.1 eq.) was added into 40 mL dichloromethane. The solution was stirred at room temperature overnight. Then the solvent was evaporated in vacuo. The obtained crude compound was purified by flash column chromatography (silica gel, silica gel, ethyl acetate: petroleum ether =8:1) to obtain a transparent oil (143 mg, yield: 22%).[1]H NMR (399.7 MHz, DMSO-d_6) δ 4.83 (s, 2H), 4.40 (s, 1H), 3.55 (s, 4H), 2.90 (d, *J* = 7.2 Hz, 2H), 2.68 (s, 4H), 2.12 (s, 3H).

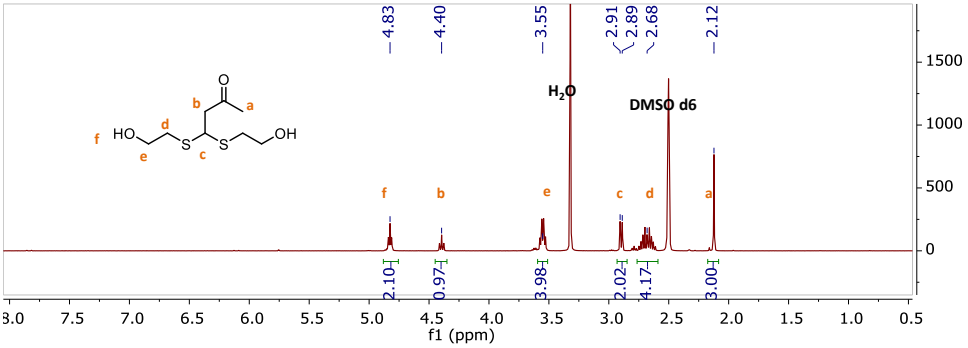

Figure S4.3. ^{1}H-NMR (399.7 MHz, 298 K in DMSO-d_6) spectrum of the double adduct **4**.

Small molecular model study of redox-responsive thiol-alkynone double addition

The aim of this study is to prove the feasibility of redox-controlled thiol-alkynone double addition by adding an oxidizing agent (H_2O_2) and a reducing agent (TCEP). The solution of the oxidant (H_2O_2) and reductant (TCEP) were made fresh for each addition and used within 1 h. 3-Butyn-2-one (3.4 µL, 0.0441 mmol, 1 eq.), β-mercaptoethanol (6.2 µL, 0.0882 mmol, 2 eq.) was added into a 4 mL glass vial containing 890 µL phosphate buffer solution (100 mM, pH=8.2; 'PB8.2') and 100 µL D_2O. Methyl sulfone (1.4 mg in 10 µL PB8.2) was added to the mixture as internal standard. The vial was vortexed to ensure thorough mixing. Then 600 µL of the mixture was transferred to an NMR tube, followed by monitoring the thiol-alkynone reaction by ^{1}H-NMR. After each measurement, the solution was transferred back to the vial. H_2O_2 PB8.2 solution (4.5 µL in 45.5 µL, 0.0441 mmol, 1 eq.) or TCEP PB8.2 solution (12.6 mg in 600 µL, adjusted to to pH = 8.2 by 1M NaOH solution, 0.0441 mmol, 1 eq.) was added into the vial at different time points.

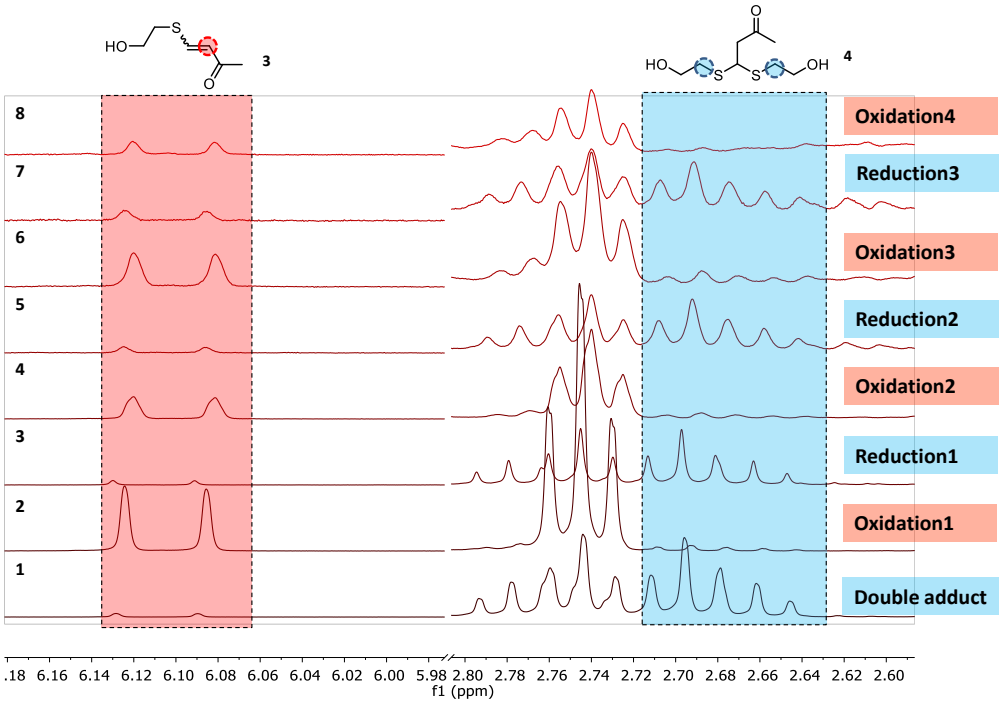

Figure S4.4. ^{1}H-NMR (399.7 MHz, 298 K in D_2O / PB8.2=1:9) monitoring of the redox-responsive thiol-alkynone double addition between 3-butyn-2-one **1** and BME **2** in PB8.2 reversibly controlled by H_2O_2 and TCEP. Spectrum 1 shows that the double adduct was generated after mixing 3-butyn-2-one **1** and BME **2**. Spectrum 2, 4, 6 show after the first, second, third and fourth time of addition of H_2O_2, the double adduct **4** was converted to the single adduct **3**. Spectrum 3, 5, 7 show after the first, second and third time of addition of TCEP, the single adduct **3** was converted to the double adduct **4**.

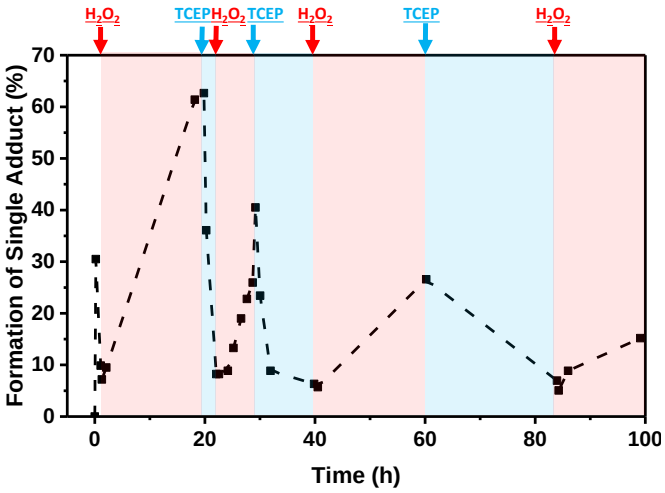

Figure S4.5. The conversion of double adduct to single adduct in the thiol-alkynone double addition reaction between 3-butyn-2-one **1** and BME **2** in PB8.2 controlled by adding H_2O_2 and TCEP over time. The red area indicates that after adding H_2O_2, the conversion of the single adduct **3** increased with time. The blue area indicates that after adding TCEP, the conversion of the single adduct **3** decreased with time.

Redox-responsive hydrogel via thiol-alkynone double addition

4-arm PEG thiol (50 mg) was dissolved in 150 µL PB8.2 as PEG-thiol solution. 3-butyn-2-one (7.8 µL) was dissolved in 1 mL PB8.2 as alkynone solution. A transparent colorless disc-shaped hydrogel was obtained by mixing 150 µL PEG-thiol solution (50 mg polymer in 150 µL) and 100 µL alkynone solution (0.78 µL in 100 µL) in a glass vial at room temperature. The total polymer concentration is 10 wt % and the ratio of alkynone to thiol groups is 1:2. After around 30 min, a hydrogel (thickness: 4 mm; diameter: 9 mm) was formed and transferred to a square-shaped container (8-well cell culture plate). Then H_2O_2 PB8.2 solution (3.1 µL in 47 µL, 0.3 M, 0.75 eq. to thiol group in 4-arm PEG thiol polymer) was adding on the top of the hydrogel. The container was closed by a glass slide and kept in a moist environment. The hydrogel/solution was gently touched by a glass stick to test for any sol-gel transition every half day. After around 24 hours, the hydrogel had decomposed to solution completely. Then TCEP PB8.2 solution (4.3 mg in 100 µL, adjusted to pH=8.2 by 1M NaOH solution, 0.38 eq. to thiol group in 4-arm PEG thiol polymer) was adding into the solution, stirred using a glass rod to ensure thorough mixing. After 5 days, a squared-shaped hydrogel (3mm × 10mm × 10mm) had formed which was cut and taken out of the container.

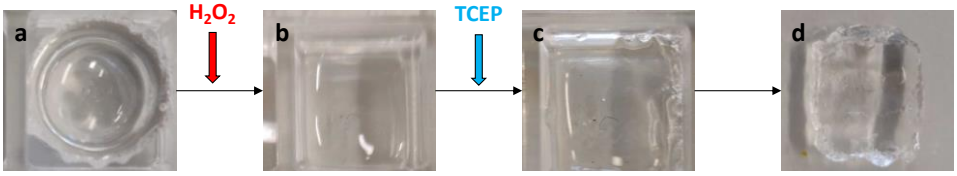

Figure S4.6. Photographs of redox-responsive hydrogel via thiol-alkynone double addition triggered by redox agents (H_2O_2 and TCEP). (a) A disc-shape hydrogel in a square container at 0 h. (b) The disc-shaped hydrogel was completely decomposed to a solution at 24 hours after adding H_2O_2. (c) The solution converted to a square-shaped hydrogel at 5 days after adding TCEP. (d) The square-shaped hydrogel can be taken out of the container.

Rheological measurements of redox-responsive hydrogels

Thiol-alkynone double addition hydrogels were prepared as described above, at 10 wt% in PB8.2. After mixing PEG thiol solution and alkynone solution, 0.7 mL of the sample was positioned on the rheometer plate. Time sweep measurements were performed at a fixed strain (γ = 1%) and frequency (ω =6.28 rad/s = 1 Hz). After storage modulus (G') reached equilibrium state, the upper-geometry was raised and H_2O_2 PB8.2 solution (4.3 µL in 46, 0.4 M, 0.75 eq. to thiol group in 4-arm PEG thiol polymer) was adding on the top of hydrogel. The upper-geometry was lowered until normal force to 0 ± 0.1 N and a time sweep measurement was performed using previous parameters. After 6 hours, the upper-geometry was raised and TCEP PB solution (6.0 mg in 100 µL, adjusted to pH=8.2 by 1M NaOH solution, 0.38 eq. to thiol group in 4-arm PEG thiol polymer) was adding on the top of the

semi-hydrogel. The upper-geometry was lowered until normal force to 0 ± 0.1 N and a time sweep measurement was performed using previous parameters.

Fuel-driven transient BME-alkynone double adduct formation by H_2O_2 and TCEP

The single adduct **3** (6.04 mg, 0.0413 mmol, 1 eq.), 2-hydroxyethyl disulfide **5** (2.5 µL, 0.0207 mmol, 0.5 eq.), 3-(trimethylsilyl)-1-propanesulfonic acid sodium salt (0.9 mg, internal standard) and H_2O_2 PB8.2 solution (4.2 µL in 46 µL, 0.4 M, 1 eq.) was adding to 850 µL PB8.2 and 100 µL D_2O. Then TCEP PB solution (11.84 mg in 600 µL, adjusted to pH=8.2 by 1M NaOH solution, 1 eq.) was added into mixture immediately. The mixture solution was transferred into an NMR tube and the reaction was monitored by ^{1}H NMR.

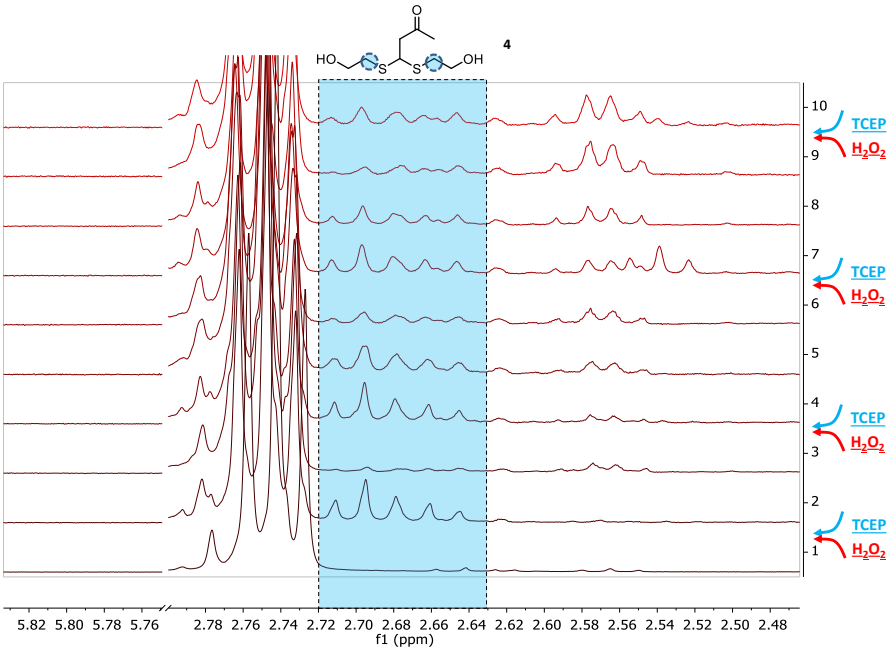

Figure S4.7. ^{1}H-NMR (399.7 MHz, 298 K in D_2O/PB8.2 = 1:9) monitoring of a fuel-driven transient formation of double adduct **4** between single adduct **3** and disulfide-BME **5** by addition of H_2O_2 and TCEP (both 1 eq.) sequentially. Specturm1 shows that the double adduct **4** is not present in the solution at the starting point. Spectrum 2, 4, 7 and 10 show that after adding separate H_2O_2 and TCEP, the double adduct **4** was generated. Spectrum 3, 5, 6, 7, 8 and 9 show that after generation of the double adduct **4** by adding separate H_2O_2 and TCEP, the double adduct **4** started to be consumed.

TCEP-driven transient formation of thiol-alkynone double adduct oxidized by O_2 catalyzed by riboflavin

3-Butyn-2-one (3.4 µL, 0.0441 mmol, 1 eq.), β-mercaptoethanol (6.2 µL, 0.0882 mmol, 2 eq.), methyl sulfone (1.4 mg, internal standard) and riboflavin 5'-monophosphate (2.3 mg 0.0044mmol, 0.1 eq.) were added to a 4 mL glass vial containing 900 µL PB8.2 and 100 µL D_2O. Then the mixture was transferred to an NMR tube to monitor the conversion of the double adduct **4** generation by ^{1}H NMR. Once each NMR measurement was done, the

solution was transferred back to the vial. The solution was stirring in a glass vial (4 mL, diameter=15 mm) open to air to ensure a sufficient oxygen concentration. TCEP PB solution (6.2 mg in 500 µL, adjusted to pH=8.2 by 1M NaOH solution, 0.5 eq.) was added into mixture at time point 61 hour and 115 hours. The weight of mixture solution and vial was recorded after each time measurement and distilled water was added to keep the concentration constant.

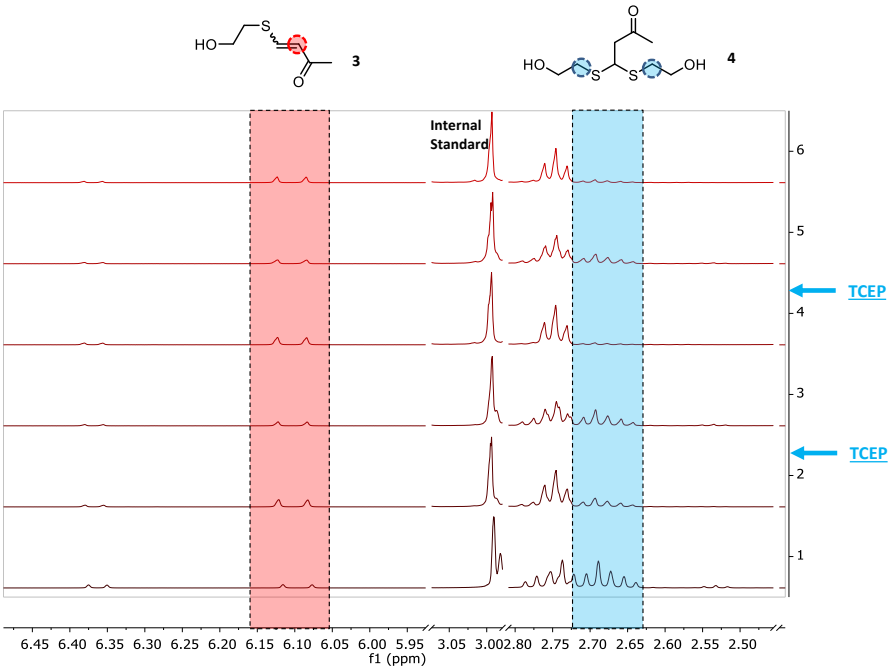

Figure S4.8. ^{1}H-NMR (399.7 MHz, 298 K in D_2O/PB8.2=1:9) monitoring of the TCEP-driven transient formation of thiol-alkynone double adduct using riboflavin catalyzed oxidation by O_2. Specturm1 shows that the double adduct **4** was generated after mixing 3-butyn-2-one **1** and BME **2**. Spectrum 3 and 5 show that after adding TCEP, the double adduct **4** was generated. Spectrum 2, 4, 8 and 6 show that after generation of the double adduct **4** by adding TCEP, the double adduct **4** was consumed over time.

TCEP-driven transient formation of thiol-alkynone double adduct oxidized by O_2 catalyzed by methylene blue

3-Butyn-2-one (3.4 µL, 0.0441 mmol, 1 eq.), β-mercaptoethanol (6.2 µL, 0.0882 mmol, 2 eq.), methyl sulfone (1.4 mg, internal standard) and methylene blue (0.7 mg in 10 µL PB8.2, 0.0022 mmol, 0.5 eq.) were added to a 4 mL glass vial containing 890 µL PB8.2 and 100 µL D_2O. Then the mixture was transferred to an NMR tube to monitor the conversion of the double adduct **4** generation by ^{1}H NMR. Once each NMR measurement was done, the solution was transferred back to the vial. The solution was stirring in a glass vial (4 mL, diameter = 15 mm) opening to air to ensure a sufficient oxygen concentration. TCEP PB solution (6.2 mg in 500 µL, adjusted to pH=8.2 by 1M NaOH solution, 0.5 eq.) was added into mixture after 74 hours. The weight of mixture solution and vial was recorded after each

time measurement and distilled water was added to keep the concentration constant. The light in the fumehood was always kept on when this experiment was running.

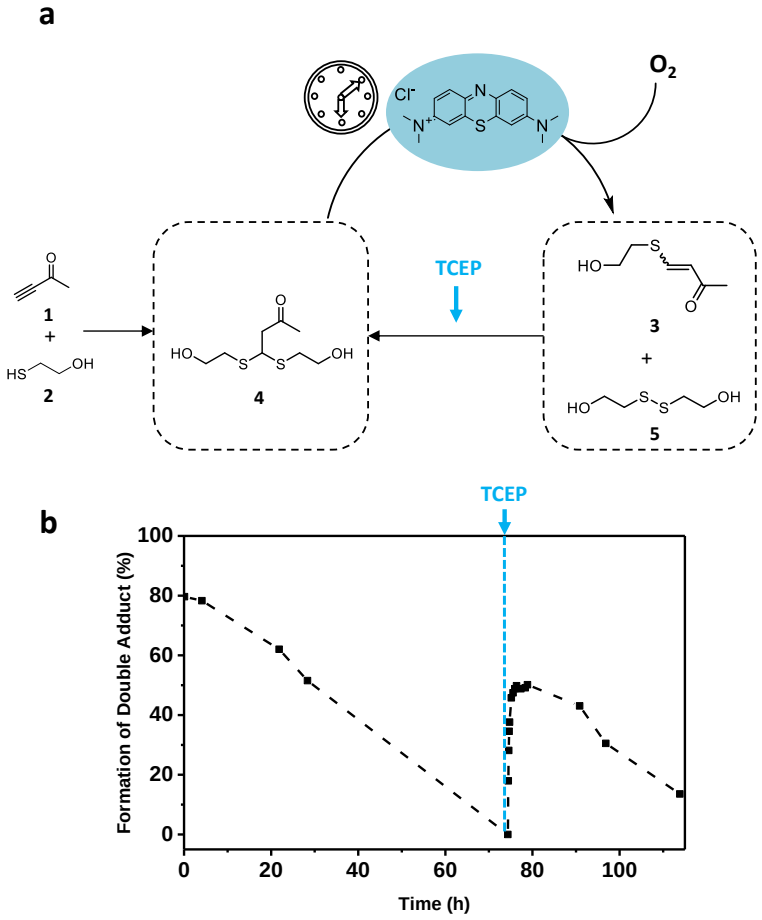

Figure S4.9. Small molecule demonstration of TCEP-driven transient formation of thiol-alkynone double adduct oxidized by O_2 under catalysis of methylene blue. (a) Schematic representation of catalyzed O_2 fuel-driven transient formation of the double adduct **4**. (b) The conversion to the adduct product **4** over time in the TCEP-driven transient thiol-alkynone double addition reaction between 3-butyn-2-one **1** and BME **2** in PB8.2 oxidized by O_2 under catalysis of methylene blue. Consumption of the double adduct **4** was achieved by an oxidation of BME **2** using O_2 under catalysis of methylene blue. Regeneration of the double adduct **4** was achieved by a reduction of disulfide-BME **5** by TCEP (0.5 eq.) acting as fuel.

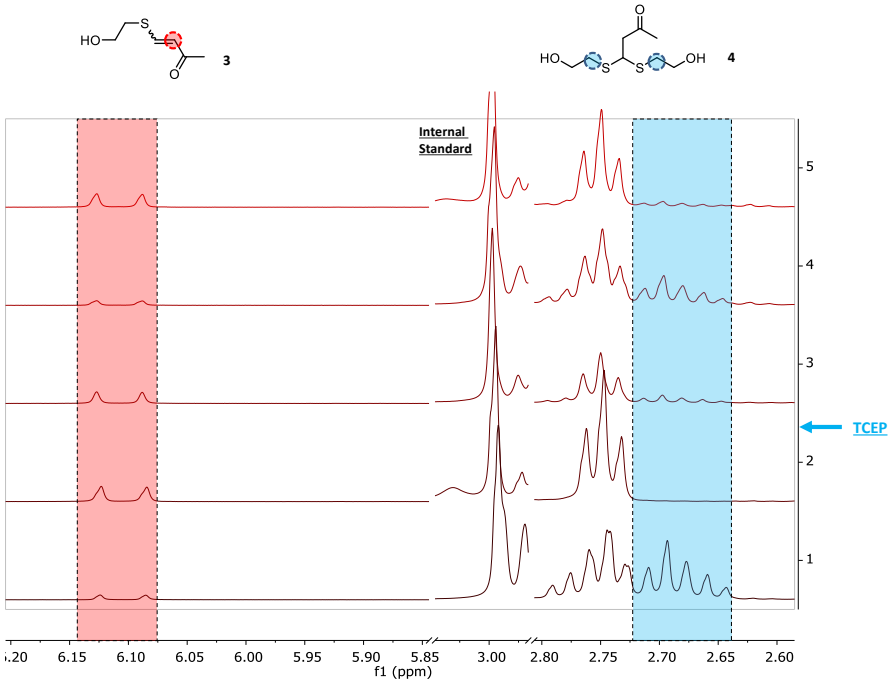

Figure S4.10. ^{1}H-NMR (399.7 MHz, 298 K in D_2O/PB8.2=1:9) monitoring of TCEP-driven transient formation of thiol-alkynone double adduct oxidized by O_2 under catalysis of methylene blue. Spectrum 1 shows that the double adduct **4** was generated after mixing 3-butyn-2-one **1** and BME **2**. Spectrum 3 and 4 show that after adding TCEP, the double adduct **4** was generated. Spectrum 2 and 5 show that after generation of the double adduct **4** by adding TCEP, the double adduct **4** was consumed.

Gel-sol transition test of redox-responsive thiol-DMADC double addition hydrogel using H_2O_2 and DTT

4-arm PEG thiol (20 mg) was dissolved in 190 μL PB8.2 as PEG-thiol solution. Dimethyl acetylenedicarboxylate (4.9 μL, 'DMADC') was dissolved in 0.1 mL DMSO to make a DMADC solution. A transparent colorless disc-shaped hydrogel was obtained in 10 seconds by mixing 190 μL PEG-thiol solution (20 mg polymer in 190 μL) and 100 μL DMADC solution (0.49 μL in 100 μL) in a glass vial at room temperature. The total solid concentration is 10 wt % and the ratio of DMADC to thiol groups is 1:2. Then H_2O_2 PB8.2 solution (40.9 μL, 9.8 M, 50 eq. to thiol group in 4-arm PEG thiol polymer) was adding on the top of hydrogel in the vial. The gel-sol transition was monitored by vial-inversion every hour. After around 10 h, the hydrogel had decomposed to solution completely. Then dithiothreitol (DTT) PB solution (27.3 mg in 20 μL PB8.2, 20 eq. to thiol group in 4-arm PEG thiol polymer) was added to the solution and the vial was shaken to ensure thorough mixing. The hydrogel would be reformed in 10 seconds checked by vial inversion.

Chapter 5

Dynamic hydrogels via thiol-vinyl sulfone crosslinking

Abstract: In this chapter**,** we show coupling and decoupling reactions of thiols to an azanorbornadiene bromo sulfone. A self-healing injectable hydrogel is prepared using such sulfone to crosslink a 4-arm-PEG thiol. In addition, glutathione-triggered dye release from the hydrogel shows that this hydrogel is capable of being a delivery vehicle for controlled drug release.

5.1 Introduction

Self-healing hydrogels are smart soft materials that are capable of autonomous recovery upon damage and regaining their integrity, offering remarkable potential for some biomedical applications such as wound healing dressings, tissue engineering and drug delivery.[1–3] Especially as a drug carrier, self-healing hydrogels are able to be injected at the disease location, leading to a more efficient delivery of drugs compared to oral administration and intravenous injection.[4–6] Moreover, as several specific physiological signals exist in the tumor microenvironment, signal-responsive degradation is an important property for self-healing hydrogels to target drug release in a controlled fashion.[7] Such hydrogels can be constructed using noncovalent bonds and dynamic covalent bonds. However, many of the physical hydrogels made by noncovalent bonds are too weak to be load-bearing and some dynamic covalent reactions require harsh conditions (for example, high temperature) to achieve a reversible process, hindering the application of such self-healing hydrogels.[8] In addition, expensive and complicated synthetic procedures for the precursors of self-healing hydrogel will limit their preparation and further clinical application.[9–11] Thus, a new type of dynamic covalent chemistry, not only allowing operation under mild conditions but also being capable of formation and signal-triggered disintegration would be in demand for the development of self-healing hydrogels for biomedical applications.

Norbornadiene derivatives with electron withdrawing substituents can also serve as Michael acceptors to couple thiol and amine groups.[12–14] In recent years the retro-Diels-Alder (rDA) reaction of thiol-coupled norbornadiene derivatives enabled the use of norbornadiene as a cleavable linker in bioconjugation to proteins or in degradable hydrogels (**Scheme 5.1a**).[15–17] However, retro-Diels-Alder cleavage of thiolated norbornadiene does not release the original thiol, limiting their application in triggered release from polymer drug conjugates. Anslyn and co-coworkers reported Meldrum's acid derivative **2** as Michael acceptor that can couple thiols or amines and decouple by a chemical trigger to release the original thiols or amines under mild conditions (**Scheme 5.1b**).[18,19] Based on this coupling and decoupling chemistry, applications like optical sensing, vitrimers, degradable polymers and hydrogels have been reported so far.[20–22] However, the synthesis of such Meldrum's acid derivative **2** requires severely toxic compounds, such as methyl iodide and carbon disulfide, which may hinder their further application. Besides the two coupling and release approaches described above, the Bernardes group recently found that azanorbornadiene bromo sulfone **3** can couple two thiols and then go through an rDA reaction to produce a bis-thiolated vinyl sulfone product **5** (**Scheme 5.1c**).[23] This bis-thiolated vinyl sulfone product **5** could be also a potential crosslinker to form hydrogels or polymer networks. In the current chapter, we investigate the dynamic nature of bis-thiolated vinyl sulfone product **5** and its application as a crosslinker in hydrogel networks. This bis-thiolated vinyl sulfone product is essentially similar functionality as Meldrum's acid derivative **2,** but can be synthesized through a much more benign process. We demonstrate that azanorbornadiene bromo sulfone **3** can conjugate with two thiols, followed by an rDA reaction to generate bis-thiolated vinyl sulfone **5,** which allows the release of the original thiol triggered by dithiothreitol (DTT) (**Scheme 5.1c**). Moreover, we formed a hydrogel using azanorbornadiene bromo sulfone **3** crosslinking a 4-arm polyethylene glycol (PEG) tetra-thiol under ambient conditions. Such hydrogels show tunable mechanical properties by varying the concentration of precursors, self-healing properties upon damage, and are injectable. In the end, glutathione-triggered controlled

release of a dye (FITC) from these hydrogels demonstrates the potential for application in controlled drug delivery.

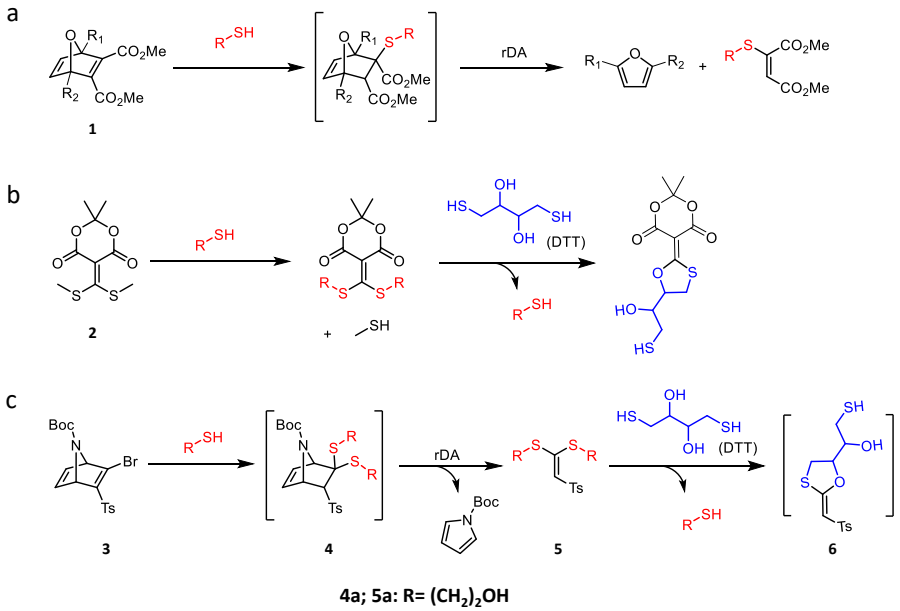

Scheme 5.1. Examples of thiol conjugate additions by electron-deficient norbornadienes and Meldrum's acid derivative as Michael acceptors. (a) Thiol-triggered retro-Diels−Alder cleavage reactions of oxanorbornadienes **1**. (b) The coupling of a thiol using Meldrum's acid derivative **2** and the decoupling of thiol using dithiothreitol (DTT). (c) Reaction of azanorbornadiene bromo sulfone **3** with thiol following a spontaneous retro-Diels-Alder (rDA) reaction to bis-thiolated vinyl sulfone **5** and the proposed release of the initial thiol from **5** triggered by dithiothreitol (DTT).

5.2 Results and Discussion

Azanorbornadiene bromo sulfone **3** was synthesized according to a previously reported method.[23] Although an intermediate in the synthesis of sulfone **3**, p-tolyl 2-bromoethynyl sulfone **S1,** is also a Michael acceptor that can conjugate two thiols, we found that a too fast reaction between bromoethynyl sulfone **S1** and thiol leads to heterogeneous hydrogel formation, which is undesired (**Scheme S1**). In this research, we focus on azanorbornadiene bromo sulfone **3** to avoid the fast reactions. First, we investigated the viability of coupling and decoupling of thiols by using a small molecule model test with β-mercaptoethanol (BME) as the thiol and DTT as the decoupling agent. After mixing sulfone **3** and 3 equivalents BME in phosphate buffer (100 mM phosphate, pH = 8.2; "PB8.2") with 50% dimethyl sulfoxide (DMSO) as a cosolvent at room temperature, bis-thiolated vinyl sulfone **5a** can be generated with 100% conversion after 15.5 hours. We also monitored the progress of thiol conjugation reactions using ^{1}H NMR spectroscopy (**Figure S5.5**). The first thiol conjugation reaction is completed in 10 minutes, indicated by the rapid disappearance of sulfone **3** together with appearance of the single BME conjugation product **S2**. Next, a fast spontaneous retro-Diels-Alder (rDA) reaction following the second BME conjugation caused that we were only able to

observe bis-thiolated vinyl sulfone **5a** but not the intermediate **4a** (**Scheme 5.1c** and **Figure S5.5**). Because of the poor solubility of sulfone **3** in water, we had to use a minimum of 50% DMSO in such model test. It was found that more DMSO (67%) in the solvent will decrease the reactivity between sulfone **3** and BME, leading to only 14% conversion to sulfone **5a** after 43 hours (**Figure S5.6**). Furthermore, we demonstrated the deconjugation of thiol between isolated sulfone **5a** with DTT (10 eq.). ^{1}H NMR monitoring shows the consumption of sulfone **5a** together with release of free BME and further oxidation of BME to disulfide, after the excess DTT is depleted (**Figure S5.7**). After the addition of DTT, sulfone **5a** decreased from 100% at the moment of DTT addition, to 4% after 21.5 hours (**Figure S5.8**).

We investigated the formation of hydrogels using azanorbornadiene bromo sulfone **3** to crosslink 4-arm PEG thiol in 40% DMSO/PB8.2 at room temperature (**Figure 5.1a**). A transparent, colorless hydrogel (4 wt% polymer content and 1:2 ratio of crosslinker and thiols) formed 140 min after mixing a sulfone **3** DMSO solution (1.5 mg in 176 µL, 20 mM) with a 4-arm PEG thiol PB 8.2 solution (17.6 mg polymer in 264 µL, 6.7 wt%) in a glass vial at room temperature, checked by the vial-inversion method (**Figure S5.9**). Rheological time sweep also indicated hydrogel formation after mixing the two solutions, showing the storage modulus (G') surpassing the loss modulus (G") at ~120 min and a G' of 3.2×10^2 Pa with a tan δ (G"/G') of 1.3×10^{-2} at ~5.6 hours (**Figure 5.1b**). No remaining sulfone **3** was observed in the ^{1}H NMR spectrum after 7 min of mixing the solutions. The reaction progress of single thiol-sulfone adduct and bis-thiolated vinyl sulfone during gel formation is consistent with the small molecule model test, confirmed by ^{1}H NMR monitoring and the tube-inversion method (**Figure S5.10**). A hydrogel formed in an NMR tube at ~2.5 hours with the formation of bis-thiolated vinyl sulfone surpassing 28%. We also observed the formation of disulfide bonds during gel formation, which could be considered as additional crosslinking next to bis-thiolated vinyl sulfone crosslinking in the gel. Next, we confirmed degradation of these hydrogels triggered by DTT using ^{1}H NMR monitoring. After addition of DTT (54.4 mg DTT in 50 µL PB8.2 solution, 120 eq. to thiol groups) on the top of formed gel in the NMR tube, the hydrogel decomposed to solution at 4.6 hours checked by tube-inversion method. ^{1}H NMR showed that gel dissolution is concomitant with disappearance of the bis-thiolated vinyl sulfone crosslinks and single thiol-sulfone adduct (**Scheme S5.2** and **Figure S5.12**). In addition, the rheological characterization of a hydrogel with 6 wt% polymer content was also performed, showing a higher final G' of 1.7×10^3 Pa (**Figure 5.1c**). Besides of tests above at 1:2 ratio of crosslinker and thiols, we also studied hydrogel formation using less crosslinker (1:4 molar ratio of crosslinker and thiols) at 4 wt% and 6 wt%. Surprisingly, higher G' of gels at 1:4 crosslinker:thiols (8.9×10^2 Pa and 3.2×10^3 Pa, respectively) comparing to the 1:2 ratio gels were found in both 4 wt% and 6 wt% gel (**Figure 5.1c**). The 1:4 ratio of crosslinker and thiols may cause that much more unreacted thiol is left to form disulfide crosslinking in the hydrogel. To investigate how disulfide crosslinking influences the mechanic properties of gels, a control experiment was performed to measure a hydrogel crosslinked only by disulfide bonds. We first measured a time sweep of gelation of 4-arm PEG thiol in 40% DMSO/PB8.2 solution on the rheometer. Although G' surpassed G" at ~15 minutes during time sweep, gelation only took place at the edge of the rheometer disk and the center of the disk was still in a liquid or semi-gel state ~380 minutes. Such heterogeneous gelation may result from insufficient air oxidation of 4-arm PEG thiol or poor diffusion characteristics. In the end, the time sweep of the 6 wt% disulfide hydrogel shows a lower final G' of 1.2×10^3 Pa than both 1:2 and 1:4 crosslinker:thiols ratio of 6 wt% gel (**Figure S5.15**). Probably the combination of crosslinking by thiolated vinyl sulfone and disulfide at 1:4 crosslinker:thiols

enhanced the crosslink density compared to the thiolated vinyl sulfone crosslinks at 1:2 crosslinker:thiols or only disulfide crosslinks.

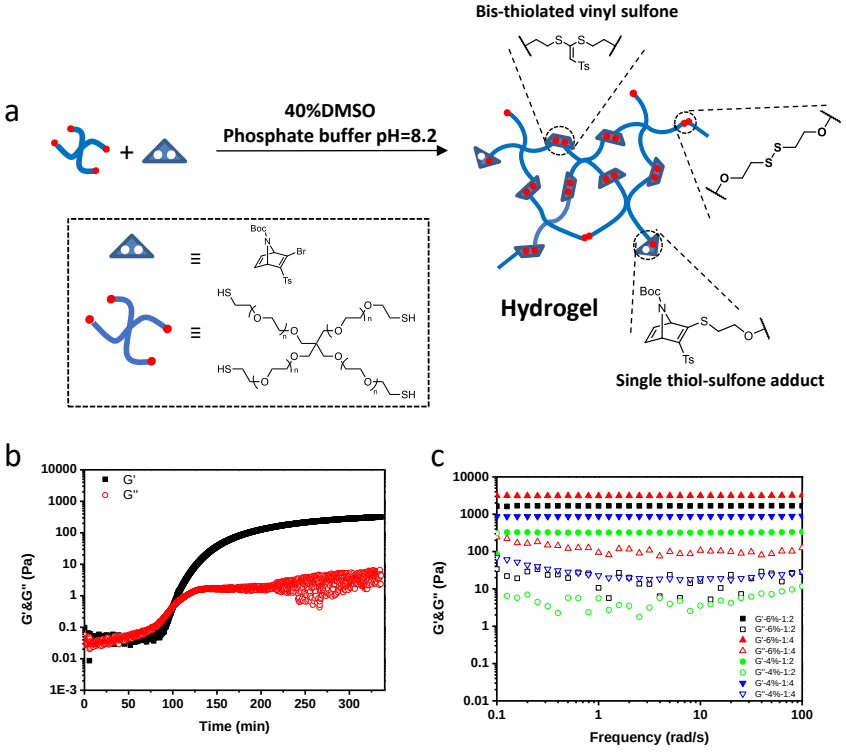

Figure 5.1. Formation of hydrogel via reactions between thiol and sulfone **3** and their rheological properties. (a) Schematic presentation of hydrogel formation by crosslinking 4-arm PEG thiol with azanorbornadiene bromo sulfone **3**. (b) Time sweep measurement of the gelation process of a 4 wt% hydrogel at 1:2 ratio of crosslinker and thiol groups (γ = 1%, ω = 1 Hz, 25 °C). (c) Frequency sweeps of the hydrogels with 4 wt% at 1:2 and 1:4 ratio of crosslinker with thiol groups and 6wt% at 1:2 and 1:4 ratio of crosslinker with thiol groups (γ = 1%, ω = 100-0.1 rad/s, 25 °C).

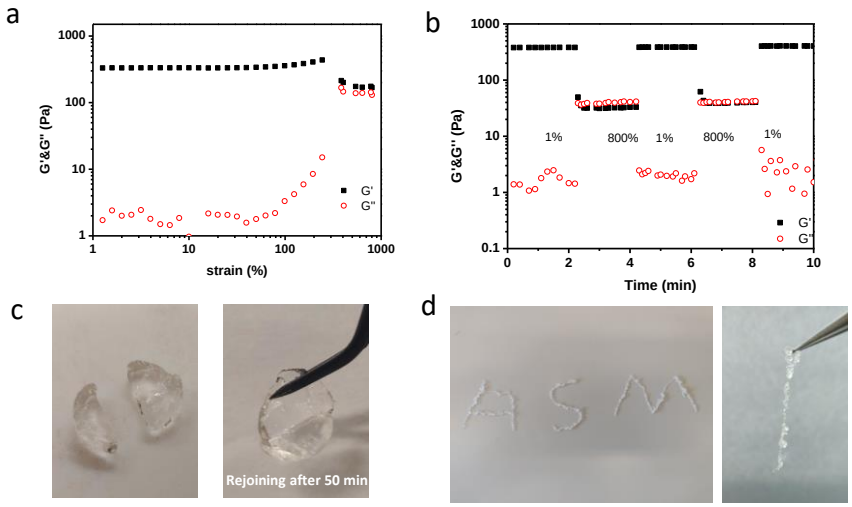

Figure 5.2. Self-healing and injectable properties of hydrogels. (a) Strain sweep of 4 wt% thiol-vinyl sulfone gel. (b) Step strain measurement of 4 wt% thiol-vinyl sulfone gel, strain is switched from 1% to 800% to 1%, for two cycles. (c) Macroscopic 4 wt% thiol-vinyl sulfone gel (thickness: 4 mm; diameter: 9 mm). A gel cylinder was made and cut in half using a scalpel, and then two halves were pressed together. After 50 min, the two parts had adhered and could hold their own weight. (d) Gel injection: a 4 wt % thiol-vinyl sulfone gel was able to press through a 20G needle by hand, leading to a 0.6 ± 0.2 mm diameter strip-shaped hydrogel.

We first investigated the self-healing capability of a 4 wt% gel by rheological measurements and macroscopic tests. In the rheometer, the storage modulus of the gel reached its equilibrium value (3.2×10^2 Pa) after 330 min. Then a strain sweep was carried out to determine the critical strain to destroy the hydrogel network. Although we did not observe the crossover point of G' and G", decrease of G' and increase of G" can be seen and their value became much closer (~2.0×10^2 Pa) after a strain over 300% was applied (**Figure 5.2a**). Next we performed continuous step change of the strain between 1% and 800% to estimate the self-healing property of the hydrogel. As can be seen in **Figure 5.2b**, a substantially decrease of G' from 3.8×10^2 Pa to 40 Pa and increase of tan δ to 1 occurred when an 800% strain was applied to the hydrogel, suggesting mechanical failure of the hydrogel although the hydrogel did not collapse to solution completely. After 2 minutes of applying 800% strain to the hydrogel, upon return to 1% strain G' immediately recovered to its initial value and a tan δ < 1, suggesting a fast healing of hydrogel after damage. In addition, this self-healing process is reproducible upon another strain cycle from 1% to 800% then to 1%. Besides the 4 wt% gel at 1:2 crosslinker:thiols, 4 wt% gel at 1:4 crosslinker:thiols and 6 wt% gel at 1:2 crosslinker:thiols also showed the self-healing property in step strain sweep measurements (**Figure S5.13-S5.15**). The strain sweep of 6 wt% gel at 1:4 crosslinker:thiols could not be performed because the gel was squeezed out of the upper-geometry plate of the rheometer when a large strain was applied. Next, a macroscopic self-healing test was performed by rejoining two pieces of half-disk shaped gels. As shown in **Figure 5.2c**, a disk shaped hydrogel was cut into two equal halves using a scalpel and reconnected together at the cut face. After ~50 minutes, the two halves of gel

had rejoined together and could be lifted using a tweezer. Furthermore, we demonstrated the injectability of a 4 wt% hydrogel by extruding the gel through a 20G syringe needle (**Figure 5.2d**). After injection, the gel recovers instantly and can be lifted using a tweezer. We wrote macroscopic letters using gel extrusion (**Figure 5.2d**).

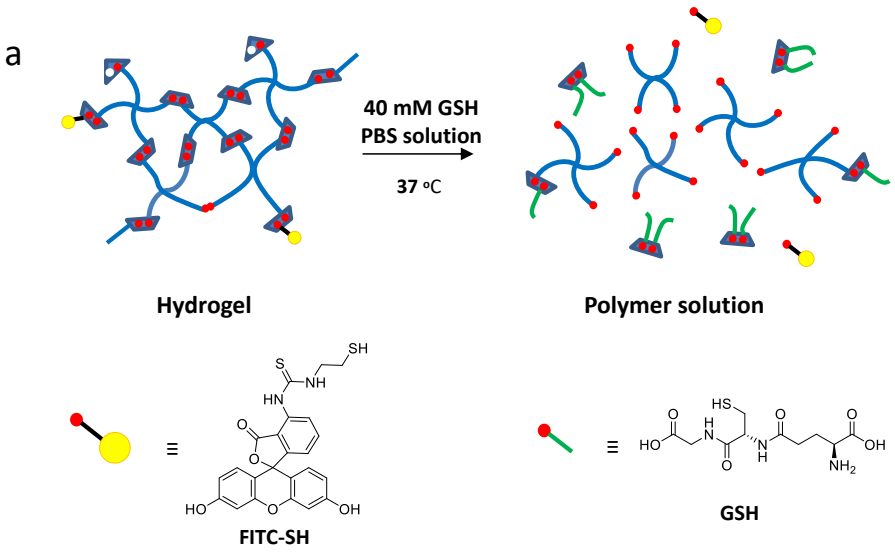

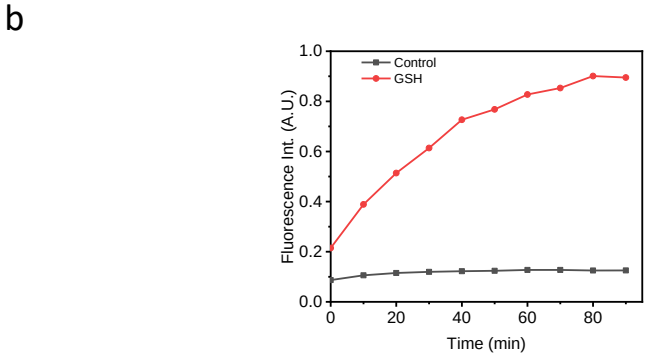

Figure 5.3. FITC-thiol-containing thiol-vinyl sulfone hydrogel for release test triggered by glutathione (GSH). (a) Schematic presentation of FITC-containing hydrogel degradation triggered by GSH. (b) The FITC –thiol release profile of the 4 wt% thiol-vinyl sulfone gel in 40 mM GSH PBS solution and of the 4 wt% thiol-vinyl sulfone gel in only PBS solution.

Glutathione (GSH) is the most abundant thiol in mammalian cells and it can have an increased concentration in tumor tissue.[7] We investigated the release of FITC-thiol dye from thiol-vinyl sulfone hydrogel triggered by GSH. Briefly, GSH phosphate buffered saline (PBS) solution (1 mL, 40 mM GSH) was added on the top of FITC loaded 4 wt% thiol-vinyl sulfone hydrogel and incubated at 37 ˚C. The hydrogel degraded to solution completely at 80 minutes to release whole dye (**Figure 5.3b**). As control experiments, release behavior of FITC was studied using an FITC-loaded hydrogel without GSH trigger (1 mL PBS). Only

14% FITC released in control sample compared with GSH triggered one at 120 mins. Here we demonstrate that GSH can trigger a faster release of dye in hydrogel than the non-triggered control.

5.3 Conclusion

In a summary, we developed a degradable self-healing injectable hydrogel using the easy synthesized small molecule azanorbornadiene bromo sulfone **3** as a crosslinker. We first used of sulfone **3**, BME and DTT as small molecule models, to demonstrate the addition-elimination processes in 50% DMSO/PB8.2 at room temperature. After addition of two BMEs to sulfone **3**, a bis-thiolated vinyl sulfone **5a** will be generated by a spontaneous retro-Diels-Alder reaction, allowing a decoupling triggered by DTT to release the original BMEs. We illustrated the facile preparation of hydrogels with tunable mechanical properties. The dynamic nature of bis-thiolated vinyl sulfone endows the hydrogel with self-healing and injectable properties, demonstrated by rheological measurements, macroscopic self-healing and injection tests. GSH-triggered release of FITC from the hydrogel also suggested that this hydrogel is able to deliver drugs in a controllable way.

5.4 Reference

(1) Zhang, Y. S.; Khademhosseini, A. Advances in Engineering Hydrogels. *Science.* **2017***, 356,* 3627*.*

(2) Li, J.; Mooney, D. J. Designing Hydrogels for Controlled Drug Delivery. *Nat. Rev. Mater.* **2016***, 1,* 16017.

(3) Uman, S.; Dhand, A.; Burdick, J. A. Recent Advances in Shear-Thinning and Self-Healing Hydrogels for Biomedical Applications. *J. Appl. Polym. Sci.* **2020**, *137*, 48668.

(4) Yang, L.; Li, Y.; Gou, Y.; Wang, X.; Zhao, X.; Tao, L. Improving Tumor Chemotherapy Effect Using an Injectable Self-Healing Hydrogel as Drug Carrier. *Polym. Chem.* **2017**, *8*, 5071–5076.

(5) Bhattarai, N.; Gunn, J.; Zhang, M. Chitosan-Based Hydrogels for Controlled, Localized Drug Delivery. *Adv. Drug Deliv. Rev.* **2010**, *62*, 83–99.

(6) Yu, L.; Ding, J. Injectable Hydrogels as Unique Biomedical Materials. *Chem. Soc. Rev.* **2008**, *37*, 1473–1481.

(7) Mo, R.; Gu, Z. Tumor Microenvironment and Intracellular Signal-Activated Nanomaterials for Anticancer Drug Delivery. *Mater. Today* **2016**, *19* (5), 274–283.

(8) Overstreet, D. J.; Dutta, D.; Stabenfeldt, S. E.; Vernon, B. L. Injectable Hydrogels. *J. Polym. Sci. Part B Polym. Phys.* **2012**, *50*, 881–903.

(9) Wong Po Foo, C. T. S.; Lee, J. S.; Mulyasasmita, W.; Parisi-Amon, A.; Heilshorn, S. C. Two-Component Protein-Engineered Physical Hydrogels for Cell Encapsulation. *Proc. Natl. Acad. Sci. U. S. A.* **2009**, *106*, 22067–22072.

(10) Yesilyurt, V.; Webber, M. J.; Appel, E. A.; Godwin, C.; Langer, R.; Anderson, D. G. Injectable Self-Healing Glucose-Responsive Hydrogels with PH-Regulated Mechanical Properties. *Adv. Mater.* **2016**, *28*, 86–91.

(11) Wu, D.; Wang, W.; Diaz-Dussan, D.; Peng, Y. Y.; Chen, Y.; Narain, R.; Hall, D. G. In Situ Forming, Dual-Crosslink Network, Self-Healing Hydrogel Enabled by a Bioorthogonal Nopoldiol-Benzoxaborolate Click Reaction with a Wide PH Range. *Chem. Mater.* **2019**. *31*, 4092-4102

(12) Hong, V.; Kislukhin, A. A.; Finn, M. G. Thiol-Selective Fluorogenic Probes for Labeling and Release. *J. Am. Chem. Soc.* **2009**, *131*, 9986–9994.

(13) Kislukhin, A. A.; Higginson, C. J.; Hong, V. P.; Finn, M. G. Degradable Conjugates from Oxanorbornadiene Reagents. *J. Am. Chem. Soc.* **2012**, *134*, 6491–6497.

(14) Gil De Montes, E.; Jiménez-Moreno, E.; Oliveira, B. L.; Navo, C. D.; Cal, P. M. S. D.; Jiménez-Osés, G.; Robina, I.; Moreno-Vargas, A. J.; Bernardes, G. J. L. Azabicyclic Vinyl Sulfones for Residue-Specific Dual Protein Labelling. *Chem. Sci.* **2019**, *10*, 4515–4522.

(15) Higginson, C. J.; Kim, S. Y.; Peláez-Fernández, M.; Fernández-Nieves, A.; Finn, M. G. Modular Degradable Hydrogels Based on Thiol-Reactive Oxanorbornadiene Linkers. *J. Am. Chem. Soc.* **2015**, *137*, 4984–4987.

(16) Fell, J. S.; Lopez, S. A.; Higginson, C. J.; Finn, M. G.; Houk, K. N. Theoretical Analysis of the Retro-Diels-Alder Reactivity of Oxanorbornadiene Thiol and Amine Adducts. *Org. Lett.* **2017**, *19*, 4504–4507.

(17) De Pascalis, L.; Tekkam, S.; Finn, M. G. Azanorbornadienes as Thiol-Reactive Cleavable Linkers. *Org. Lett.* **2020**, *22*, 6248–6251.

(18) Diehl, K. L.; Kolesnichenko, I. V.; Robotham, S. A.; Bachman, J. L.; Zhong, Y.; Brodbelt, J. S.; Anslyn, E. V. Click and Chemically Triggered Declick Reactions through Reversible Amine and Thiol Coupling via a Conjugate Acceptor. *Nat. Chem.* **2016**, *8*, 968–973.

(19) Meadows, M. K.; Sun, X.; Kolesnichenko, I. V.; Hinson, C. M.; Johnson, K. A.; Anslyn, E. V. Mechanistic Studies of a "Declick" Reaction. *Chem. Sci.* **2019**, *10*, 8817–8824.

(20) Sun, X.; Anslyn, E. V. An Auto-Inductive Cascade for the Optical Sensing of Thiols in Aqueous Media: Application in the Detection of a VX Nerve Agent Mimic. *Angew. Chem. Int. Ed.* **2017**, *56*, 9522–9526.

(21) Sun, X.; Chwatko, M.; Lee, D. H.; Bachman, J. L.; Reuther, J. F.; Lynd, N. A.; Anslyn, E. V. Chemically Triggered Synthesis, Remodeling, and Degradation of Soft Materials. *J. Am. Chem. Soc.* **2020**, *142*, 3913–3922.

(22) El-Zaatari, B. M.; Ishibashi, J. S. A.; Kalow, J. A. Cross-Linker Control of Vitrimer Flow. *Polym. Chem.* **2020**, *11*, 5339-5345.

(23) Gil de Montes, E.; Istrate, A.; Navo, C. D.; Jiménez-Moreno, E.; Hoyt, E. A.; Corzana, F.; Robina, I.; Jiménez-Osés, G.; Moreno-Vargas, A. J.; Bernardes, G. J. L. Stable Pyrrole-Linked Bioconjugates through Tetrazine-Triggered Azanorbornadiene Fragmentation. *Angew. Chem. Int. Ed.* **2020***, 132,* 6255-6259.

5.5 Supplementary information

5.5.1. Materials and Measurements

NMR spectra were recorded on an Agilent-400 MR DD2 (399.7 MHz for ^{1}H and 100.5 MHz for ^{13}C) at 298 K. The rheological measurements were performed using a rheometer (AR G2, TA instruments) equipped with a steel plate-and-plate geometry of 40 mm in diameter and equipped with a hexadecane trap. The cumulative release of dye was measured using the fluorescence channel of a JASCO J-815 CD spectrometer. The hydrogel for cumulative release of dye was incubated using an Eppendorf Thermomixer C. Thiol terminated 4-arm poly (ethylene glycol) (PEG10k-4-SH, M_w = 10 000, Đ ≤ 1.05) was purchased from JenKem Technology (USA). Dithiothreitol was purchased from Fluorochem ltd. β-Mercaptoethanol (BME), sodium phosphate (monobasic, anhydrous), sodium phosphate (dibasic), 3-(trimethylsilyl)-1-propanesulfonic acid sodium salt, p-tolyl (2-trimethylsilyl) ethynyl sulfone, N-Boc-pyrrole, silver nitrate, and glutathione were purchased from Sigma Aldrich. N-bromosuccinimide was purchased from Thermo Fisher. Phosphate buffer solution (100 mM, pH=8.2; 'PB8.2') was prepared using sodium phosphate (monobasic, anhydrous) and sodium phosphate (dibasic). All compounds and solvents were used as received without further purification. The technical solvents were purchased from VWR and the reagent grade solvents were purchased from Sigma Aldrich. All rheological tests were carried out at 25 ˚C and all other tests were carried out at room temperature. p-Tolyl 2-bromoethynyl sulfone and azanorbornadiene bromo sulfone was synthesized according to methods in previous literature.[1]

5.5.2. Experimental Method

Gelation test using 4-arm PEG thiol crosslinked by p-Tolyl 2-bromoethynyl sulfone S1

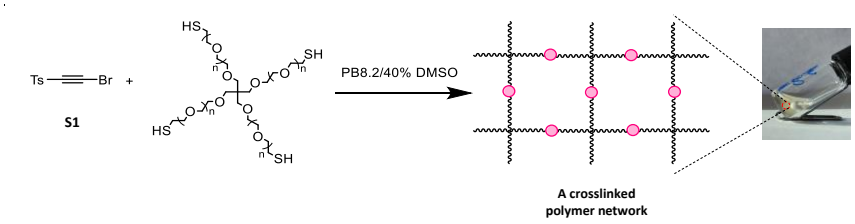

Scheme S5.1. Schematic presentation of formation of a crosslinked polymer network using 4-arm PEG thiol crosslinked by p-Tolyl 2-bromoethynyl sulfone **S1**

p-Tolyl 2-bromoethynyl sulfone **S1** is an intermediate compound in the synthesis of azanorbornadiene bromo vinyl sulfone **3**. Such 2-bromoethynyl sulfone **S1** is also a Michael acceptor that is capable to conjugate two thiols together. We first investigated the feasibility of gelation using 4-arm PEG thiol crosslinked by p-Tolyl 2-bromoethynyl sulfone **S1**. 4-arm PEG thiol (25 mg) was dissolved in 150 µL phosphate buffer solution (pH=8.2, 100 mM, "PB8.2") as a PEG-thiol solution. p-Tolyl 2-bromoethynyl sulfone **S1** (1.6 mg) was dissolved in 100 µL DMSO as a crosslinker solution. The crosslinker solution was added dropwise into the PEG-thiol solution. We found that a small piece of yellow gel was formed immediately only in the area where the droplet of the crosslinker solution and the surface of thiol solution were mixed.

Synthesis of the single BME conjugation product S2

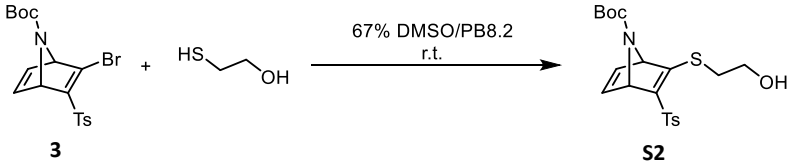

To a solution of azanorbornadiene bromo sulfone **3** (82.9 mg, 0.194 mmol, 1 eq.) in DMSO (10 mL), a solution of β-mercaptoethanol (27.4 µL, 0.389 mmol, 2 eq.) in phosphate buffer solution (pH=8.2, 100 mM, 5 mL) was added and the mixture was stirred overnight at room temperature. Then, the solvent was removed by freeze-drying. 10 mL ethyl acetate was added to the solid mixture and the solution was filtered to remove any buffer salts. The solvent was evaporated in vacuo. The obtained crude compound was purified by flash column chromatography (silica gel, ethyl acetate: petroleum ether =2:1) to obtain a yellow liquid (45 mg, yield: 54%). ^{1}H NMR (399.7 MHz, DMSO-d$_6$) δ 7.62 (d, J = 7.7 Hz, 2H), 7.36 (d, J = 7.7 Hz, 2H), 6.86 (s, 2H), 5.45 (s, 1H), 5.18 (s, 1H), 3.62 (m, 4H), 3.09 (m, 5H), 2.73 (s, 1H), 2.30 (s, 3H), 1.08 (s, 9H).

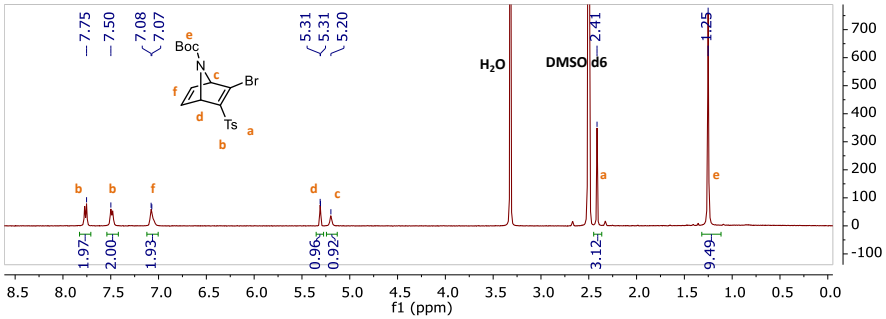

Figure S5.1. ^{1}H-NMR (399.7 MHz, 298 K in DMSO-d$_6$) spectrum of Azanorbornadiene bromo vinyl sulfone **3**.

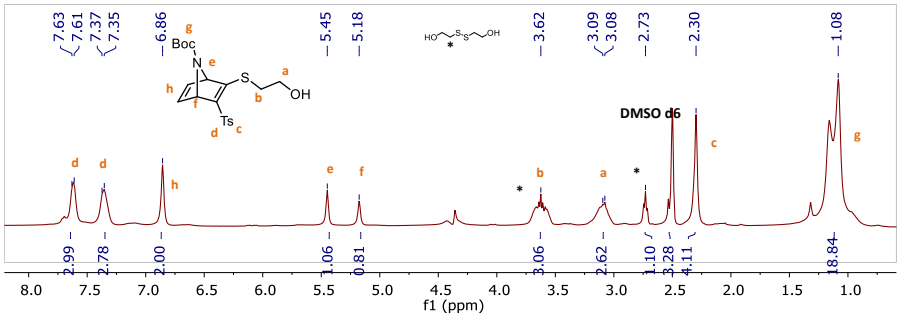

Figure S5.2. ^{1}H-NMR (399.7 MHz, 298 K in DMSO-d$_6$) spectrum of the single BME conjugation product **S2**.

Synthesis of bis-thiolated vinyl sulfone product 5a

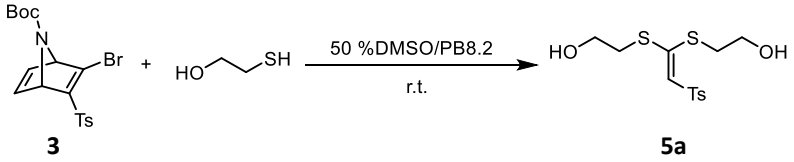

To a solution of azanorbornadiene bromo sulfone **3** (100.8 mg, 0.236 mmol, 1 eq.) in DMSO (6 mL), a solution of β-mercaptoethanol (37 µL, 0.389 mmol, 2 eq.) in phosphate buffer solution (pH=8.2, 100 mM, 6 mL) was added and the mixture was stirred overnight at room temperature. Then, the solvent was removed by freeze-drying. 10 mL ethyl acetate was added to the solid mixture and the solution was filtered to remove any buffer salts. The solvent was evaporated in vacuo. The obtained crude compound was purified by flash column chromatography (silica gel, ethyl acetate: petroleum ether =2:1) to obtain a white powder (54.2 mg, yield: 69%). ^{1}H NMR (399.7 MHz, DMSO-d_6) δ 7.81 (d, J = 8.1 Hz, 2H), 7.41 (d, J = 8.0 Hz, 2H), 6.49 (s, 1H), 3.57 (s, 2H), 3.33 (s, 2H), 3.06 (s, 2H), 2.98 (s, 2H), 2.40 (s, 3H). ^{13}C NMR (100.5 MHz, 298 K in DMSO-d_6), δ 156.53, 144.07, 139.65, 129.92, 127.57, 119.82, 60.37, 58.84, 36.75, 35.02, 21.52.

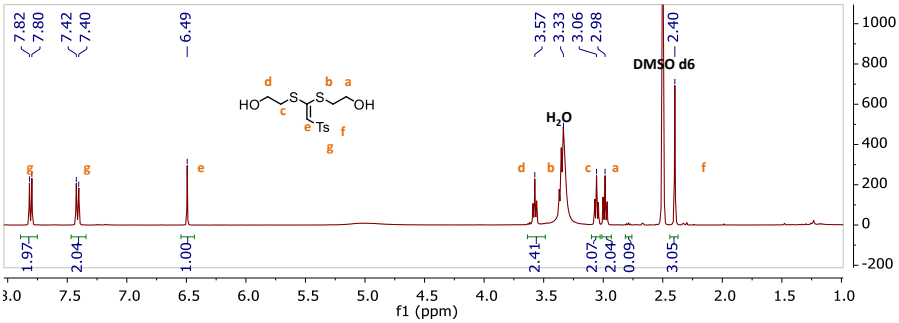

Figure S5.3. ^{1}H-NMR (399.7 MHz, 298 K in DMSO-d_6) spectrum of bis-thiolated vinyl sulfone product **5a**.

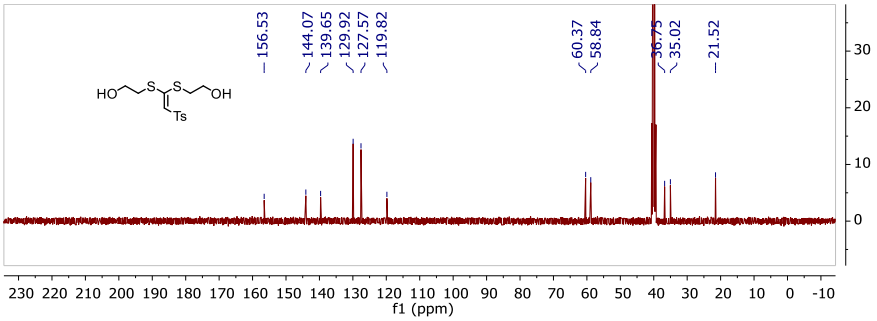

Figure S.54. ^{13}C NMR (100.5 MHz, 298 K in DMSO-d_6) spectrum of bis-thiolated vinyl sulfone product **5a.**

Reactivity studies of reaction between azanorbornadiene bromo sulfone 3 and BME in 67% DMSO/PB8.2 and 50% DMSO/PB8.2 by ^{1}H NMR

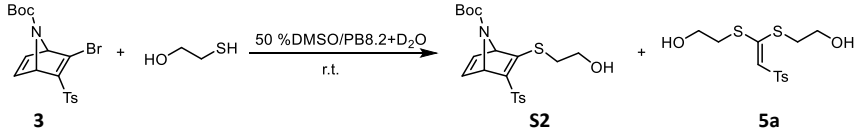

To a solution of azanorbornadiene bromo sulfone **3** (1.8 mg, 0.004 mmol, 1 eq.) in DMSO-d_6 (0.31 mL), a solution of β-mercaptoethanol (0.87 µL, 0.012 mmol, 3 eq.) in PB8.2 (0.24mL) and D_2O (0.05 mL) was added and the reaction between azanorbornadiene **3** and BME was monitored at room temperature. 3-(trimethylsilyl)-1-propanesulfonic acid sodium salt (DSS) (0.5 mg) was added as internal standard. The reaction was allowed to proceed for 16 h. The product structure was confirmed by ^{1}H-NMR.

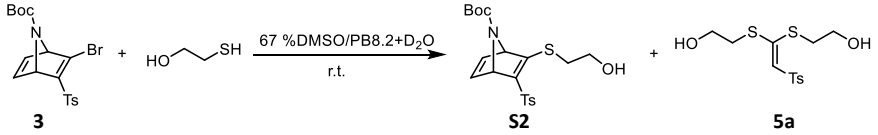

To a solution of azanorbornadiene bromo sulfone **3** (3.5 mg, 0.008 mmol, 1 eq.) in DMSO-d_6 (400 µL), a solution of β-mercaptoethanol (1.7 µL, 0.025 mmol, 3 eq.) in PB8.2 (150 µL) and D_2O (50 µL) was added and the reaction between azanorbornadiene **3** and BME was monitored at room temperature. DSS (0.5 mg) was added as internal standard. The reaction was allowed to proceed for 43 h. The product was confirmed by ^{1}H-NMR.

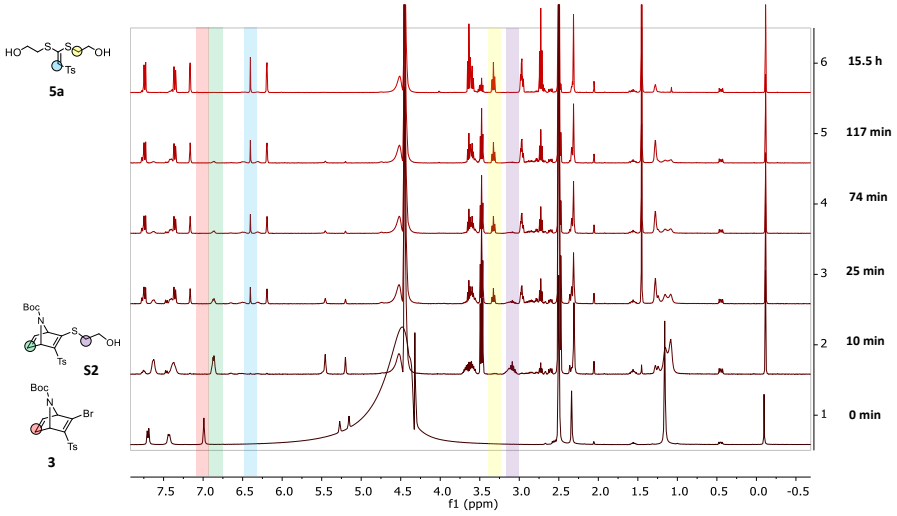

Figure S5.5. ^{1}H-NMR (399.7 MHz, 298 K in 50%DMSO/(PB8.2+D_2O) spectra of reaction between azanorbornadiene bromo sulfone **3** and β-mercaptoethanol at room temperature. Spectrum 1 shows that only azanorbornadiene bromo sulfone **3** (1.8 mg, 0.004 mmol, 1 eq) was in the solution at t = 0 min. Spectrum 2 to Spectrum 6 show the mixture at different time points after adding β-mercaptoethanol

(0.87 µL, 0.012 mmol, 3 eq.) into the solution. Red highlight represents the characteristic peak of the azanorbornadiene bromo sulfone **3**. Green and purple highlights represent the characteristic peak of **S2**. Blue and yellow highlights represent the characteristic peaks of **5a**.

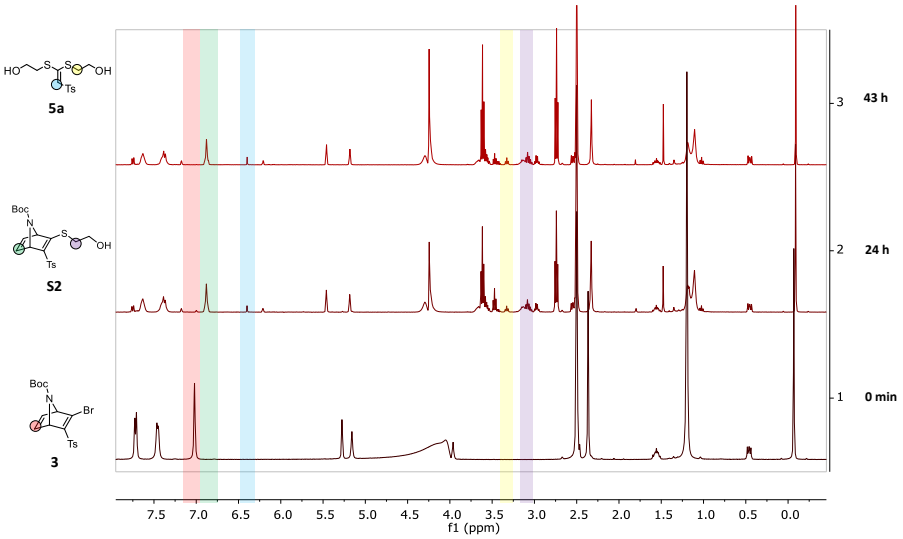

Figure S5.6. ^{1}H-NMR (399.7 MHz, 298 K in 67%DMSO/ (PB8.2+D_2O) spectra of the reaction between azanorbornadiene bromo sulfone **3** and β-mercaptoethanol at room temperature. Spectrum 1 shows that only a Azanorbornadiene bromo sulfone **3** (3.5 mg, 0.008 mmol, 1 eq.) was in the solution at t = 0 min. Spectrum 2 and Spectrum 3 show the mixture at different time points after adding β-mercaptoethanol (1.7 µL, 0.025 mmol, 3 eq.) into the solution. Red highlight represents the characteristic peak of azanorbornadiene bromo sulfone **3**. Green and purple highlights represent the characteristic peaks of **S2**. Blue and yellow highlights represent the characteristic peaks of **5a**.

Kinetic traces of reaction between Bis-BME-vinyl sulfone product and DTT by ^{1}H NMR

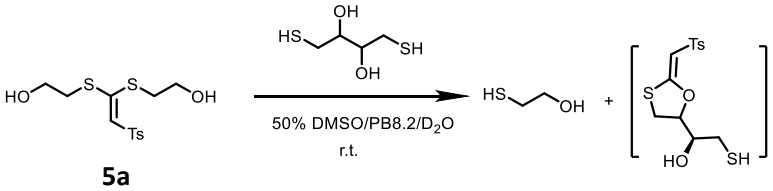

Bis-thiolated vinyl sulfone product **5a** (3.0 mg, 0.009 mmol, 1 eq.) was dissolved in an NMR tube containing a solution of DMSO-d_6 (500 µL), PB8.2 (440 µL) and D_2O (50 µL). DSS (0.5 mg) was added as an internal standard. After the first ^{1}H NMR spectrum was measured (t = 0 min), DTT (13.9 mg, 0.09 mmol, 10 eq.) was added into the solution immediately. The ^{1}H NMR spectra were recorded over time at room temperature until the reaction reached equilibrium.

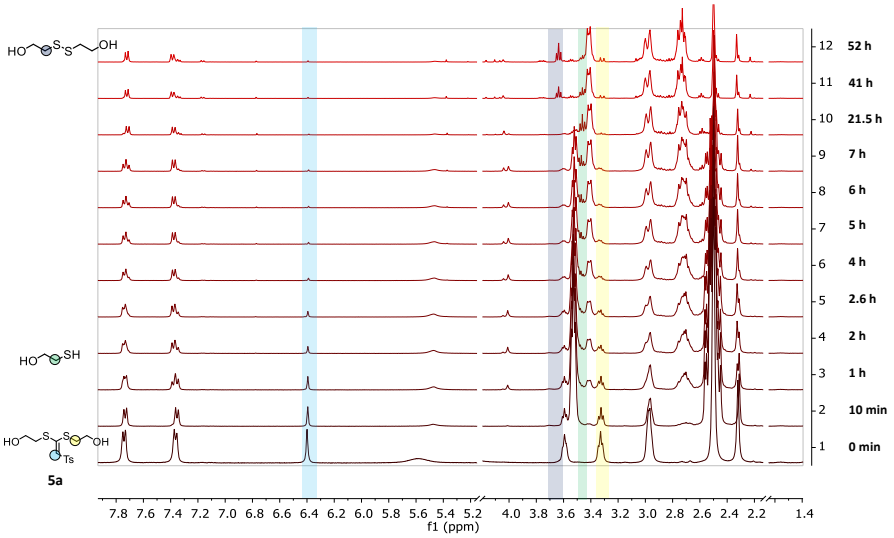

Figure S5.7. ^{1}H-NMR (399.7 MHz, 298 K in 50%DMSO/(PB8.2+D_2O) spectra of reaction between bis-thiolated vinyl sulfone product **5a** and DTT at room temperature. Spectrum 1 shows that only **5a** (3.0 mg, 0.009 mmol, 1 eq) was in the solution at t = 0 min. Spectrum 2 to Spectrum 12 show the mixture at different time points after adding DTT (13.9 mg, 0.09 mmol, 10 eq.) into the solution. Green highlights represent the characteristic peaks of BME. Blue and yellow highlights represent the characteristic peaks of **5a**. Grey highlight represents the characteristic peak of oxidized 2-mercaptoethanol.

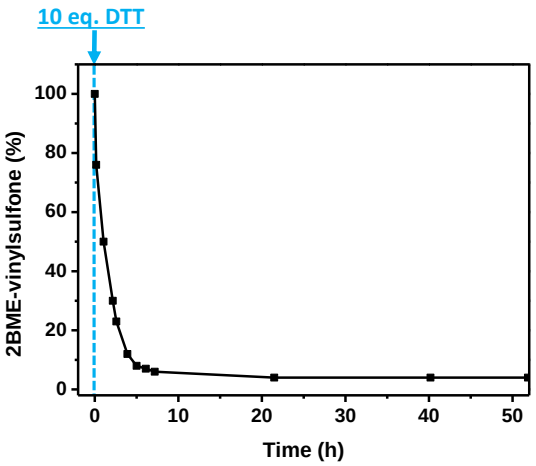

Figure S5.8. The degradation monitoring of bis-thiolated vinyl sulfone product **5a** by adding DTT in solution of 50%DMSO/ (PB8.2+D_2O) over time.

Preparation of hydrogel via thiol-vinyl sulfone crosslinking

Hydrogels were prepared by a mixing procedure. 4-arm PEG thiol (17.6 mg) was dissolved in 264 µL PB8.2 as PEG-thiol solution. Azanorbornadiene bromo sulfone **3** (1.5 mg) was

dissolved in 176 µL DMSO as crosslinker solution. A transparent colorless hydrogel was obtained by mixing 264 µL PEG-thiol solution (17.6 mg polymer in 264 µL, 6.7 wt %) and 176 µL crosslinker solution (1.5 mg in 176 µL, 20 mM) in a glass vial at room temperature. Starting from these amounts, the total solid concentration is 4 wt % and the ratio of crosslinker to thiol groups is 1:2 unless specified otherwise.

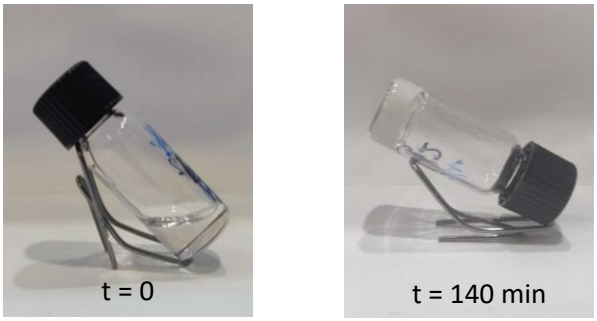

Figure S5.9. A solution of thiol polymer and azanorbornadiene bromo sulfone **3** in 40% DMSO/PB8.2, at the start of the gelling process (left) and after 140 min (right), when a transparent gel has formed.

Kinetic traces of gelation process between 4-arm PEG thiol and Azanorbornadiene bromo sulfone 3 by ^{1}H NMR

4-arm PEG thiol (23.9 mg, 0.0024 mmol, and 4% total polymer concentration) was dissolved in 309 µL PB8.2 and 50 µL D_2O as PEG-thiol solution. Azanorbornadiene bromo sulfone **3** (2.0 mg, 0.0047 mmol, 2 eq. to thiol groups in 4-arm PEG) was dissolved in 239 µL DMSO-d_6. Two solutions were mixed in a glass NMR tube at room temperature. DSS (1 mg) was added as the internal standard. The reaction during hydrogel formation was monitored by ^{1}H NMR at room temperature. The hydrogel formation was tested by the tube-inversion method after each NMR measurement.

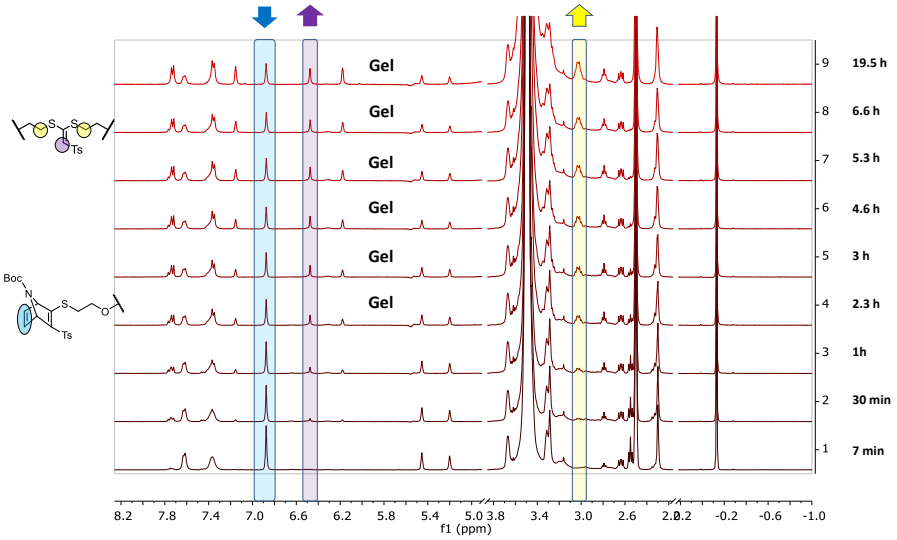

Figure S5.10. ^{1}H-NMR (399.7 MHz, 298 K in 40%DMSO/ (PB8.2+D_2O) monitoring of reaction during bis-thiolated vinyl sulfone hydrogel formation by azanorbornadiene bromo sulfone **3** and 4-arm PEG thiol at room temperature. Blue highlight represents the characteristic peak of single thiol- sulfone adduct group. Purple and yellow highlights represent the characteristic peaks of bis-thiolated vinyl sulfone product group.

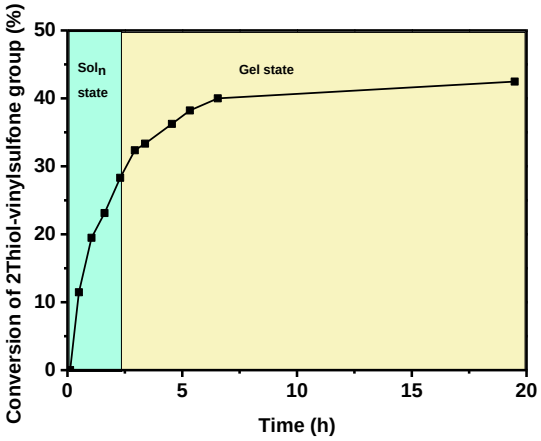

Figure S5.11. The conversion of bis-thiolated vinyl sulfone product group during bis-thiolated vinyl sulfone hydrogel formation between azanorbornadiene bromo sulfone **3** and 4-arm PEG thiol at room temperature. The conversion of bis-thiolated vinyl sulfone product group is calculated based on the integration of the alkene protons of bis-thiolated vinyl sulfone product by ^{1}H NMR. The gel-sol transition is determined by vial inversion method. The methyl signal of sodium trimethylsilylpropanesulfonate was set as the internal standard. The cyan area in the graph indicates that the sample is in solution state. The yellow area indicates that the sample is in the hydrogel state.

^{1}H NMR kinetic traces of the hydrogel degradation process

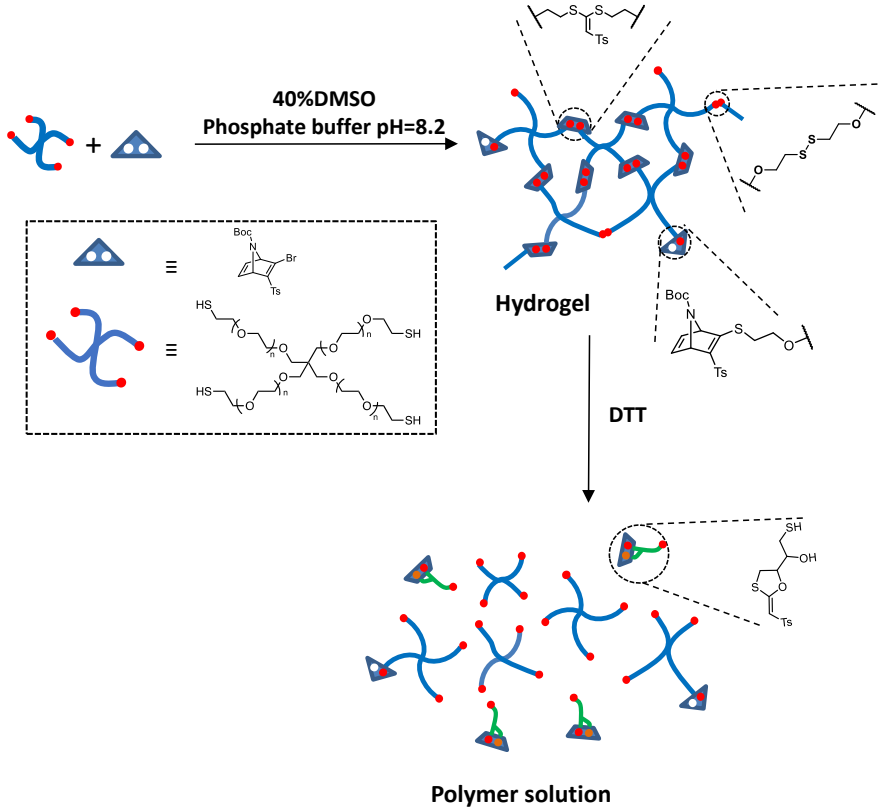

Scheme S5.2. The decomposition of bis-thiolated-vinyl sulfone hydrogel triggered by DTT

4-arm PEG thiol (29.3 mg, 0.0059 mmol, 4% total polymer concentration) was dissolved in 441 µL PB8.2 and 50 µL D_2O as PEG-thiol solution. Azanorbornadiene bromo sulfone **3** (2.5 mg, 0.0029 mmol, 2 eq. to thiol groups in 4-arm PEG) was dissolved in 292 µL DMSO-d_6. Two solutions were mixed in a glass NMR tube at room temperature. DSS (1 mg) was added as the internal standard. DTT PB8.2 solution (54.4 mg in 50 µL PB8.2, 0.35 mmol, 120 eq. to thiol groups in 4-arm PEG) was added on the top of hydrogel in NMR tube. The reaction during hydrogel formation and degradation was monitored by ^{1}H NMR at room temperature. Hydrogel formation and degradation were tested by the tube-inversion method after each NMR measurement.

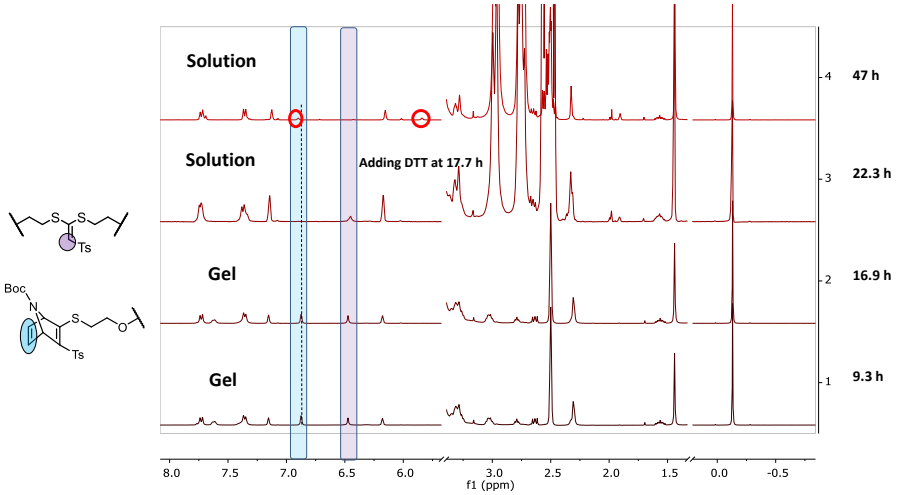

Figure S5.12. ^{1}H-NMR (399.7 MHz, 298 K in 40%DMSO/(PB8.2+D_2O) monitoring of reaction during formation of bis-thiolated vinyl sulfone hydrogel by azanorbornadiene bromo sulfone **3** and 4-arm PEG thiol and degradation of hydrogel by adding DTT on the top of hydrogel in NMR tube at room temperature. Blue highlight represents the characteristic peak of single thiol-Azanorbornadiene bromo vinyl sulfone adduct group. Purple highlight represents the characteristic peak of bis-thiolated vinyl sulfone product group. Red circle in spectrum 4 (the top one) indicated a new peak, possibly from the DTT adduct.

Rheological measurements of hydrogels

Bisthiolated-vinyl sulfone hydrogels were prepared as described above, at 4 wt% polymer concentration and 1:2 ratio azanorbornadiene bromo sulfone/ thiol (Gel-4%-1:2). After mixing PEG thiol solution and azanorbornadiene bromo sulfone 3 solution, 0.7 mL of the sample was positioned on the rheometer plate. Time sweep measurements were performed at fixed strain (γ = 1%) and frequency (ω = 6.28 rad/s = 1 Hz). Frequency sweep measurements were performed from 0.1 to 100 rad/s at fixed strain (γ = 1%). All frequency sweeps were measured after the storage modulus (G') reached an equilibrium state. All rheology measurements described above were performed in the linear viscoelastic region. The modulus of hydrogels was measured under strain sweep from 1 to 1000% strain at a fixed frequency (ω = 6.28 rad/s). Continuous step strain measurements were measured at fixed frequency (ω = 6.28 rad/s). Oscillatory strains were switched from 1% strain to subsequent 800% strain with 1 minute for every strain period. Besides for Gel-4%-1:2, the same rheological measurements were also performed at 4 wt% polymer concentration and 1:4 ratio azanorbornadiene bromo sulfone/thiol (Gel-4%-1:4); 6 wt% polymer concentration and 1:2 ratio azanorbornadiene bromo sulfone/ thiol (Gel-6%-1:2); 6 wt% polymer concentration and 1:4 ratio azanorbornadiene bromo sulfone/thiol (Gel-6%-1:4). 6 wt% Disulfide hydrogel was prepared by mixing 4-arm PEG thiol PB8.2 solution (42 mg in 420 µL, 0.004 mmol) and DMSO (280 µL) in 4 mL glass vial. Then the sample was positioned on the rheometer plate to perform the same rheological tests with bis-thiolated vinyl sulfone hydrogels.

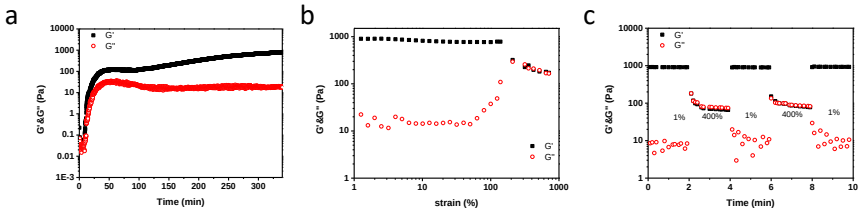

Figure S5.13. Rheological sweep measurements of 4 wt% bisthiol-vinyl sulfone hydrogel at 1:4 crosslinker: thiol ratio (ω = 1 Hz). a) Time sweep measurements (γ = 1%); b) Strain sweep measurements; c) Step-strain sweep, alternative strain switched from 1% to 400% twice then back to 1%.

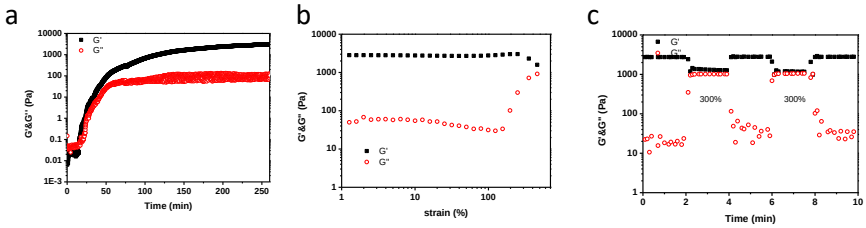

Figure S5.14. Rheological sweep measurements of 6 wt% bisthiol-vinyl sulfone hydrogel at 1:2 crosslinker: thiol ratio (ω = 1 Hz). a) Time sweep measurements (γ = 1%); b) Strain sweep measurements; c) Step-strain sweep, alternative strain switched from 1% to 300% twice then back to 1%.

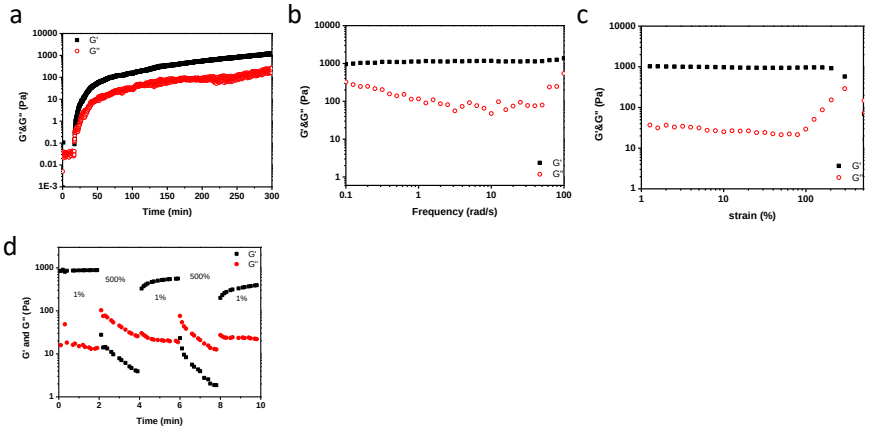

Figure S5.15. Rheological sweep measurements of 6 wt% disulfide hydrogel. a) Time sweep measurements (γ = 1%, ω = 1 Hz); b) Frequency sweep measurement (γ = 1%, ω = 0.1-100 Hz); c) Strain sweep measurements; d) Step-strain sweep, alternative strain switched from 1% to 500% twice then back to 1%.

Macroscopic self-healing and injectable test of hydrogels

A disk-shaped bis-thiolated vinyl sulfone hydrogel (thickness: 4 mm; diameter: 9 mm) was prepared as described above. The total polymer concentration is 4 wt % and the ratio of crosslinker to thiol groups is 1:2. After formation, the hydrogel was cut into two equal pieces using a scalpel. The two hydrogel pieces were pressed together and kept in a moist environment for 50 mintues. Healing of the hydrogel was checked by manually lifting the combined gel using tweezers. Afterwards, this healed hydrogel was cut to 4 equal pieces using a scalpel. Then a piece of hydrogel was put in a syringe (1 mL volume; 0.5 inner diameter) using a tweezer and syringe plunger, and subsequently injected through a 20G needle using manual force.

Cumulative release of thiol-labeled FITC dye

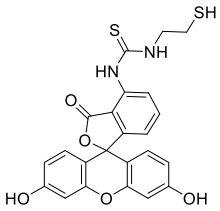

FITC-SH

Thiol labelled fluorescein derivative (FITC-SH) was synthesized following a literature procedure.[2] (**Figure S5.16**) 4-arm PEG thiol (14.00 mg, 0.0014 mmol) was dissolved in 175 µL PB8.2 as PEG-thiol solution. Azanorbornadiene bromo sulfone (1.2 mg, 0.0028 mmol) was dissolved in 170 µL DMSO as crosslinker solution. FITC-SH (1.3 mg) was dissolved in 506 µL DMSO as dye stock solution. First 5.0 µL dye stock solution (2.8×10^{-5} mmol FITC-SH) were mixed with crosslinker solution (1 eq.) in a 1.5 mL glass vial at room temperature. This step is to ensure that FITC-SH react with crosslinker by single thiol conjugation. Then PEG-thiol stock solution was added into solution. After the vial was vortexed 5 min, two 100 µL solution was transferred into two 1.5 mL Eppendorf vials as control hydrogel and GSH hydrogel. The Eppendorf vial was wrapped by aluminum foil and left standing for 15 hours. Gelation in the Eppendorf vial was confirmed by vial-inversion method. PBS solution (5 x 1 mL) was adding on top of the hydrogel and removed immediately to wash the hydrogel. 1 mL 40 mM glutathione (GSH) PBS solution (pH =7.4 adjusted using 1 M NaOH solution) was added on top of the GSH hydrogel and 1 mL PBS solution was added on the top of control hydrogel. The release system was kept in a 37 ˚C incubator. At predetermined time points, aliquots of the supernatant (150 µL) were taken out for determination of the amount of released FITC-SH and replaced with the same volume of PBS. Fluorescence was measured at λ_{ex} = 495 nm and λ_{em} = 515 nm in a fluorescence quartz cuvette.

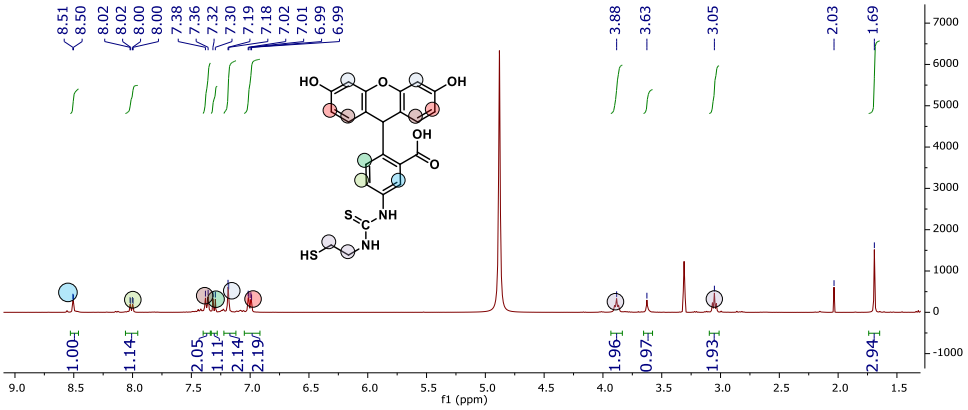

Figure S5.16. ^{1}H-NMR (399.7 MHz, 298 K in MeOD) spectrum of FITC-SH.

Reference

(1) Gil de Montes, E.; Istrate, A.; Navo, C. D.; Jiménez-Moreno, E.; Hoyt, E. A.; Corzana, F.; Robina, I.; Jiménez-Osés, G.; Moreno-Vargas, A. J.; Bernardes, G. J. L. Stable Pyrrole-Linked Bioconjugates through Tetrazine-Triggered Azanorbornadiene Fragmentation. *Angew. Chem. Int. Ed*. **2020**, *132*, 6255-6259.

(2) Li, L.; Li, J.; Du, X.; Welle, A.; Grunze, M.; Trapp, O.; Levkin, P. A. Direct UV-Induced Functionalization of Surface Hydroxy Groups by Thiol-Ol Chemistry. *Angew. Chem. Int. Ed*. **2014**, *53*, 3835–3839..

Summary

Dynamic hydrogels have attracted much attention as the reversible nature of their crosslinks provides many useful and fascinating type of dynamic behaviour. Such dynamic behaviour includes network remodelling, self-healing and programmed or responsive gel-sol transitions, which can be used in tissue engineering, controlled drug release and wound dressings. However, addressing the dynamic nature of these reversible crosslinks often requires catalysts or harsh conditions. Therefore, development of new dynamic hydrogels that allow exchange processes under ambient conditions is desirable.

Common living systems have adaptive functions which can respond to external stimuli in a controlled way, exhibiting promising properties including programmed lifetime, adaptive mechanical properties and communication. As those systems often are maintained outside of equilibrium, it is difficult to apply similar concepts in conventional synthetic materials. A few examples of fuel-driven transient supramolecular hydrogels have been developed. However, supramolecular hydrogels always show unpredictable crosslink density, which may hinder further application. It is therefore interesting to develop a fuel-driven covalent polymeric hydrogel system with transiently controlled crosslinking.

In this thesis, we examine the development of fuel-driven transient covalently crosslinked polymer hydrogels via reversible thiol conjugate additions. Although the final aim is not fully achieved, two classes of dynamic hydrogels and several useful concepts have been developed along the way.

In Chapter 2, we investigate a novel chemical reaction network for fuel-driven transient formation of covalent bonds, based on redox-controlled conjugate addition and elimination chemistry. Although the full cycle cannot operate in a single system because of substantial side reactivity, the bond formation, breaking and regeneration process can be realized by separate reactions. Overall, this proposed chemical reaction network may have potential to be applied in the formation of soft materials with transient properties.

In Chapter 3, we move to the investigation of a different reversible thiol conjugate addition, the thiol-alkynone double addition, which is used in the construction of a self-healing injectable hydrogel. Such dynamic hydrogels can be generated by crosslinking a four-arm polyethylene glycol (PEG) tetra-thiol with an alkynone via thiol-alkynone double addition. The mechanical properties of the obtained hydrogels can be easily tuned by varying the concentrations of the network components. These hydrogels are self-healing, shear thinning, and can be injected through a medical syringe needle after which they spontaneously reform a gel. Importantly, these hydrogels exhibit dynamic viscoelastic behavior and biocompatibility, showing great potential in biomedical applications.

In Chapter 4, we study a different chemical reaction network, involving a redox-controlled reversible thiol-alkynone double addition. We propose a strategy to develop a new fuel-driven transient covalently crosslinked hydrogel using such a dynamic double addition. The investigations start from a small molecule model and then move to a hydrogel material. First we demonstrate the reversibility of the thiol-alkynone double addition using redox agents (H_2O_2 and TCEP). Based on that model, a redox-responsive hydrogel forms by crosslinking a 4-arm-PEG thiol with alkynone. Next, TCEP-driven transient formation of thiol-alkynone double adducts is achieved by two different oxidizing methods (H_2O_2 or O_2 in air under

catalysis of riboflavin or methylene blue). After final synthesis of a bis-alkyne polymer, we propose to achieve fuel-driven transient formation of hydrogels in the future.

Finally, in Chapter 5 we apply a thiol-azanorbornadiene derivative coupling reaction into hydrogel formation to prepare a degradable self-healing hydrogel. After coupling two thiols into an azanorbornadiene bromo sulfone reagent, a retro-Diels−Alder (rDA) reaction will occur spontaneously to give a bias-thiolated vinyl sulfone product. We find that such bis-thiolated vinyl sulfone product can be triggered by DTT to release the original thiols. Then a self-healing injectable hydrogel is prepared using the azanorbornadiene bromo sulfone to crosslink a 4-arm-PEG thiol. In the end, glutathione-triggered dye release from the hydrogel also shows that this hydrogel is able to deliver drugs in a controllable approach.

In conclusion, in this thesis we propose a series of reversible thiol conjugate additions for the construction of new dynamic hydrogels. Although the fuel driven transient hydrogel is still under development, several new dynamic hydrogels, such as redox-responsive hydrogel, degradable hydrogels, and self-healing injectable hydrogels have been successfully developed based on reversible thiol conjugate additions, also showing potential for biomedical applications.

Samenvatting

Dynamische hydrogelen hebben veel aandacht getrokken omdat het reversibele karakter van de crosslinks veel nuttige en fascinerende processen met een dynamische aard mogelijk maakt. Dergelijke dynamische processen omvatten het herstructureren van netwerken, zelf herstellend vermogen en geprogrammeerde of responsieve gel-sol overgangen. Deze processen kunnen worden ingezet bij weefselmanipulatie, gecontroleerde afgifte van geneesmiddelen en in wondverband. Veelal, zijn katalysatoren of zeer reactieve reagentia nodig om de hydrogel crosslinks van een dynamisch karakter te voorzien. Daarom is de ontwikkeling van nieuwe hydrogelen welke operationeel zijn onder standaard omstandigheden en een dynamisch karakter hebben wat resulteert in uitwisselingsprocessen, wenselijk

Veel voorkomende levende systemen hebben adaptieve functies die op gecontroleerde wijze kunnen reageren op externe prikkels, waarbij zij veelbelovende eigenschappen vertonen, zoals een geprogrammeerde levensduur, adaptieve mechanische eigenschappen en communicatie. Aangezien deze systemen vaak ‘uit evenwicht’ werken, is het moeilijk om soortgelijke systemen te bewerkstelligen in conventionele synthetische materialen. Er zijn enkele voorbeelden van transiente supramoleculaire hydrogelen ontwikkeld welke gevoed worden door een substraat (brandstof). Echter, supramoleculaire hydrogelen hebben altijd een onvoorspelbare crosslink dichtheid wat verdere toepassing kan belemmeren. Het is daarom interessant om een substraat-gedreven covalent polymeer hydrogel systeem met transient gecontroleerde crosslinks te ontwikkelen.

In dit proefschrift onderzoeken we de ontwikkeling van brandstof-gedreven transient covalent gebonden polymeer hydrogelen via reversibele thiol conjugaten. Hoewel het einddoel niet volledig is bereikt, zijn er gedurende dit onderzoek twee typen dynamische hydrogelen en verschillende bruikbare concepten ontwikkeld.

In hoofdstuk 2 onderzoeken we een nieuw chemisch reactienetwerk voor brandstof-gedreven transiente vorming van covalente bindingen, gebaseerd op redox-gecontroleerde conjugaat additie en eliminatie chemie. Hoewel de volledige cyclus niet werkt binnen 1 systeem vanwege significante zijreacties, kunnen de afzonderlijke componenten als het vormen en breken van covalente bindingen en het regeneratieproces wel in afzonderlijke reacties worden gerealiseerd. Het in hoofdstuk 2 voorgestelde chemische reactienetwerk kan mogelijk worden toegepast als applicatie in zachte materialen met dynamische eigenschappen.

In hoofdstuk 3 gaan we over op het onderzoek van een andere reversibele thiol conjugaat additie, namelijk de thiol-alkynon dubbele additie welke gebruikt wordt bij de constructie van een zelf herstellende injecteerbare hydrogel. Dergelijke dynamische hydrogels kunnen worden gegenereerd door een vierarmige polyethyleenglycol (PEG) tetra-thiol te reageren met een alkynon via thiol-alkynon-dubbeladditie. De mechanische eigenschappen van de hydrogelen kunnen gemakkelijk worden afgestemd door de concentraties van de afzonderlijke netwerkcomponenten te variëren. Deze hydrogelen zijn zelfhelend, shear thinning, en kunnen geïnjecteerd worden door een medische injectienaald waarna ze spontaan een gel vormen. Belangrijk is dat deze hydrogelen een dynamisch visco-elastisch

gedrag vertonen en biocompatibel zijn, dit zorgt namelijk voor groot potentieel als biomedische toepassing.

In hoofdstuk 4 bestuderen we een chemisch reactienetwerk, waarbij een redox-gecontroleerde reversibele thiol-alkynon-dubbel-additie gebuikt wordt. We stellen hier een strategie voor om een nieuw brandstof-gedreven tijdelijk covalent ge-crosslinkt hydrogel netwerk te ontwikkelen waarin we een reversibele, dubbele thiol-alkynon additie gebruiken. In dit onderzoek beginnen we met een simpel molecule model, waarna we overgaan naar een hydrogel. Eerst demonstreren we de reversibiliteit van de thiol-alkynon-dubbel-additie met behulp van redox reagentia (H2O2 en TCEP). Dit model is de basis voor een redox-responsieve hydrogel welke gevormd wordt door een 4-arm-PEG thiol te crosslinken met een alkynon. Vervolgens wordt een TCEP-gedreven tijdelijke vorming van thiol-alkynon dubbele adducten gedemonstreerd gebruikmakende van twee verschillende oxidatiemethoden (H2O2 of O2 in lucht gekatalyseerd door riboflavine of methyleenblauw). Na de uiteindelijke synthese van een bis-alkyne polymeer, stellen we voor om in de toekomst brandstof-gedreven transiënte vorming van hydrogels te bereiken.

Tenslotte, in hoofdstuk 5 passen we een thiol-azanorbornadieen derivaat koppelingsreactie toe in hydrogel vorming om een afbreekbare zelf-helende hydrogel te bereiden. Na koppeling van twee thiolen in een azanorbornadieen bromo sulfon reagens, zal een retro-Diels-Alder (rDA) reactie spontaan optreden om een bi-thiolated vinyl sulfon product te geven. Wij hebben vastgesteld dat dergelijke bi-gediolateerd vinylsulfonproduct kan worden getriggerd door DTT waarmee de oorspronkelijke thiolen vrijkomen. Vervolgens wordt een zelfhelende injecteerbare hydrogel gemaakt door azanorbornadiene bromo sulfon te crosslinken met 4-arm-PEG thiol. In dit onderzoek laten we zien dat we met een glutathion getriggerde event de afgifte van een kleurstof uit de hydrogel kunnen controleren en daarmee tonen we aan dat deze hydrogel ook gebruikt kan worden om geneesmiddelen controleert af te leveren.

Concluderend demonstreren we in dit proefschrift een serie van reversibele thiolconjugaten voor, waarmee we nieuwe dynamische hydrogelen kunnen maken. Hoewel de brandstof gedreven transiënte hydrogel nog in ontwikkeling is, zijn verschillende nieuwe dynamische hydrogelen, zoals redox-responsieve hydrogelen, degradeerbare hydrogelen en zelfhelende injecteerbare hydrogelen met succes ontwikkeld op basis van reversibele thiolconjugaten, welke ook potentieel hebben in biomedische toepassingen.

Acknowledgements

I still remember the first day of my PhD when I came to office D2.260 as a newest member of ASM. Many people came and left in past years, now I became the oldest member in D2.260. It likes a montage movie when I try to recall all the moments I spend with all people in my PhD period. I would like to thanks all of you whom I met in past five years. It is my luck that I get support and help from you.

First of all, I would like to thank my supervisor and promotor, Rienk. Thank you for giving me the opportunity to do this PhD research. I still remember what a rookie I was when I just started here. You are always very patient to give me guidance and advice. I learned a lot from discussion with you, not only about research skills but also how to communicate more efficiently. Thanks a lot for helping me check and correct my writing. I cannot handle my PhD without your help. Jan, thanks to be my co-promotor. You always have many critical questions in our group meeting. Stephen Picken, It was a nice experience to explore our new rheometer with you. Thanks for arranging our new rheometer. Eduardo, you can always came up with some points which I cannot think of. Thanks for the discussion about rheological part of my hydrogels. Ger, Laura, Wolter, we didn't talk too much, but thanks for your questions and suggestions in ASM group meeting.

Furthermore, I would like to thank the committee members, Justin, Sijbren, Hans, Sander, Evgeny and Atsushi for reading and assessing my thesis. Thanks to my PhD research funding, Chinese Scholarship Council (CSC) and a consolidator grant from the European Research Council (ERC).

Next, I would like to thanks other staff members in our Building 58. Ben, thanks for your advices about my rheological measurements. You are always cheerful. Enjoy your retirement! Marcel, thanks for organizing Sinterklaas eve in the first year of my PhD. Your tips about organizing labcleaning was helpful. Xiaohui, thanks for inviting us to you home. It is good to listen your story in Germany and the Netherlands before. Stephen Eustace, thanks a lot for your advice about my NMR measurements. I won't be surprised if you can speak Chinese someday. Lars, Sietse and Duco, thanks for your help about arrangement in our labs and also checking my safety sheets. Veby, you are a great mother. Thanks for helping me deal with my extension issue. Els, Caroline, Louw and Tony, thanks for your help!

I also would like to acknowledge my lovely colleges. Fanny, you always keep smiling. Thanks for your help at the beginning of my PhD. Susan, you are always very kind and patient to give me advices about my research and everything in our labs. Many encourage from you makes me more confident. Many thanks! Guotai, you have a lot of good ideas and critical questions about research. Thanks a lot for many discussions when I felt struggling with my experiments. Benjamin (Benji), you are the man who accompanied me through my whole PhD life. It was a nice experience to travel Italy (Milan, Venice and Lecce) with you! Tobias, you are always very calm no matter what happened. Also, nice BBQ and Limoncello from you. Thanks for organizing ASM afterwork activity. Peggy, our passionate officemate. Thanks for research discussion and advice from you. Irene, I am sure that you can make your molecules and catalysis in the end. Our chat about Italian and Chinese food had much fun! Michelle, I cannot believe how you can make your PhD so fast. Good luck with your new career. Reece, Thanks for assisting me revise my texts. You polymer advices are always

valuable. Cansel, it is hard to see that you are not smiling. Good luck! Yongjun, Congrats to become a father this year. Thanks for discussion about polymers. Kai, Yiming and Qian, Thanks for helping me a lot in my first two years of PhD. The experience you shared about research and life are super helpful. Tomasz, my boardgame buddy, your passion about sports, instruments and boardgame impressed me. Thanks for inviting me to your boardgame party! Suellen, you are the another one staying in our office very late. I was happy when you are showing your nice polymer photos to me. Hendrik, I hope I can teach you more “interesting” Chinese words in the future. Thanks for nice chatting with you. Matija, just where to find you when it’s drinking time. It’s nice to chat with you about Chinese and Croatia football. Vasu, the best singer in Chemists, Thanks for share your experience of PhD. Zhenyu, you are always kind to everyone. Good luck with your work. Serhii, you are always very calm and wise in our every activities. It’s nice to chat with you. Angie, hope you can also defence your PhD soon. Elmira, it was nice to exchange story about Chinese and Iran traditions. Good luck. Emma, Thank you for hosting Sinterklaas eve in your house. Good wishes to you and your family. Sarah, you are always showing up when it’s party or drinking time. Good luck with your PhD. Fan Hu, Good luck to your new postdoc. Ardeshir, Frank, Sander, Vincent, Mariano, Jos, Sahil, Anand, Mark, Zilong, Riming, Kui, Yucheng and Jianwu, It is nice to meet you. Thanks for nice chatting. Yu Wang, Jianan, Juncheng, Bohang, Wenjun, Chuncheng and Kaiqiao, it was very happy to play Avalon or football with you at Friday. All the best! Georgy, although you are not in our ASM, I can always get a lot valuable inputs about synthetic and analytic chemistry from you. Thanks a lot. I believe that you will become a PI soon.

Additionally, I would like to thanks my students. Marziye, it’s great you made our dex-hydrogel in the end. I can always learn a lot from supervising you. Hope you have a good future. LO1 student, Emmelien, Erik, Jurian, Kayeu, we have lots of fun together. Thanks!

Cong, Xiuxiu, Yong, Jian, Yandong, Weibo, Lizhou, Chengteng, Jinjin, Senlei, Haopeng and Xiang, I have lots of good memories with you about dinner and travelling. You makes my free time much more colourful. Thanks a lot!

最后， 感谢我的父母和姐姐。是你们一直以来的支持和鼓励让我求学更有动力！

About the Author

Bowen Fan was born on 11th November 1990 in Jining, China. In 2013, he obtained his Bachelor degree in Chemical Engineering and Technology at China University of Mining and Technology. The same year he started his Master degree at the same university. His master project was focused on developing new self-oscillating gels with different ruthenium(II) catalysts grafted by acrylamide groups. After obtaining his Master degree in 2016, he started his Ph.D. supervised by Dr. Rienk Eelkema with the topic of dynamic polymer hydrogels through reversible thiol conjugate addition crosslinks at Delft University of Technology funded by China Scholarship Council (CSC).

List of Publications

1. **B. Fan**, K. Zhang, Q. Liu, R. Eelkema, "Self-Healing Injectable Polymer Hydrogel via Dynamic Thiol-Alkynone Double Addition Cross-Links" *ACS Macro Lett.* **2020**, *9*, 776–780.

2. **B. Fan**, Y. Men, S. A. P. Rossum, G. Li, R. Eelkema, "A Fuel Driven Chemical Reaction Network Based on Conjugate Addition and Elimination Chemistry" *ChemSystemsChem* **2020**, *2*, 2–5.

3. M. P. van der Helm, C.-L. Wang, **B. Fan**, M. Macchione, E. Mendes, R. Eelkema, "Organocatalytic Control over a Fuel‐driven Transient Esterification Network" Angew. Chem. Int. Ed. **2020**, *132*, 20785–20792.

4. F. Trausel, **B. Fan**, S. A. P. van Rossum, J. H. van Esch, R. Eelkema, "Aniline Catalysed Hydrazone Formation Reactions Show a Large Variation in Reaction Rates and Catalytic Effects" *Adv. Synth. Catal.* **2018**, *360*, 2571–2576.

5. L. Ren, **B. Fan**, Q. Gao, Y. Zhao, H. Luo, Y. Xia, X. Lu, I. R. Epstein, "Experimental, Numerical, and Mechanistic Analysis of the Nonmonotonic Relationship between Oscillatory Frequency and Photointensity for the Photosensitive Belousov-Zhabotinsky Oscillator" *Chaos*. **2015**, *25,* 064607.

6. **B. Fan**, R. Eelkema, "A Fuel-driven transient polymer hydrogel via dynamic thiol double addition" In preparation.

7. **B. Fan**, G. Li, G. Bernardes, R. Eelkema, "Dynamic hydrogels via thiol-vinyl sulfone crosslinking" In preparation.